THE UNIVERSITY OF ASTON IN BIRMINGHAM

"A study of the properties and applications of electrostatic charged particle oscillators".

Thesis submitted for the degree of

Doctor of Philosophy

by

Wrenford John Thatcher

Physics Department

February, 1970.

Acknowledgements

I would like to thank my Supervisor, Dr. R.K. Fitch, and Mr. T. Mulvey, the Project Advisor, for their continual advice, encouragement and assistance during the course of this work. My thanks are also due to Dr. A.H. McIlraith of the Division of Inorganic and Metallic Structures at the National Physical Laboratory, whose help has been invaluable.

I also wish to acknowledge the financial support of the Ministry of Technology and in particular Dr. J. Dyson, Superintendent of the Division of Optical Metrology at the National Physical Laboratory, for supporting the research in its early stages; and the Division of Inorganic and Metallic Structures for its continued support throughout the project.

Finally I would like to thank Mr. K. Bowcock, Acting Director of the computer centre, for help with the numerical analysis, and Mrs. R. Finch for her patience with the typing.

Synopsis

This investigation originated from work by Dr. A.H. McIlraith of the National Physical Laboratory who, in 1966, described a new type of charged particle oscillator. This makes use of two equal cylindrical electrodes to constrain the particles in such a way that they follow extremely long oscillatory paths between the electrodes under the influence of an electrostatic field alone. The object of this work has been to study the principle of the oscillator in detail and to investigate its properties and applications.

Any device which is capable of creating long electron trajectories has potential application in the field of ultra high vacuum technology. It was therefore considered that a critical review of the problems associated with the production and measurement of ultra high vacuum was relevant in the initial stages of the work.

The oscillator has been applied with a considerable degree of success as a high energy electrostatic ion source. This offers several advantages over existing ion sources. It can be operated at much lower pressures without the need of a magnetic field. The oscillator principle has also been applied as a thermionic ionization gauge and has been compared with other ionization gauges to pressures as low as 5×10^{-11} torr. This

new gauge exhibited a number of advantages over most of the existing gauges. Finally the oscillator has been used in an evaporation ion pump and has exhibited fairly high pumping speeds for argon gas relative to those for nitrogen.

This investigation supports the original work of Dr. A.H. McIlraith and shows that his proposed oscillator has considerable potential in the fields of vacuum technology and electron physics.

Index

CHAPTER 1.

THE PRODUCTION AND MEASUREMENT OF ULTRA HIGH VACUUM

1.1 Introduction

Since 1950 there has been a steady growth of the application of ultra high vacuum in universities, research establishments and industry. It is now commonplace for experiments to be carried out at pressures of 10^{-9} torr or less. However, while there is very little difficulty in obtaining such low pressures, there is still considerable need for improvement, not only in the ultimate vacuum which can be achieved, but also in the methods of obtaining and measuring it.

1.2. Attainment of Ultra High Vacuum

1.2.1. Fundamental considerations

The ultimate pressure, P_u, which can be obtained in a high vacuum system can be defined by the equation

$$P_u = \frac{Q_T}{S_T} \qquad \ldots\ldots\ldots\ldots\ldots (1)$$

where

Q_T = Total gas influx in torr litres per second

S_T = Total rate of removal of gas in litres per second.

In order that P_u should be small then, either the total gas influx should be made as small as possible, or the rate of removal of the gases made extremely high. Since S_T is mainly dependent on the size and type of vacuum pump used, it is apparent that if Q_T is regarded as constant it is necessary to produce a large change in the pump speed in order to produce a significant change in P_u. On the other hand Q_T is dependent on several factors, for example, influx due to leaks Q_L, gas diffusion through chamber walls Q_D outgassing from surfaces within the system Q_o and back diffusion of gases from the pump Q_P. It is normally possible to increase the pumping speed in a vacuum system by only 2 or 3 orders of magnitude, therefore if very low pressures are required it is necessary to design and process the system in order that Q_T should be reduced. This is normally achieved by constructing the system from materials such as stainless steel and glass which can be outgassed at relatively high temperatures. By paying such attention to the processing of the system it is possible to reduce Q_T to less than 10^{-12} torr litres per second.

It is clear that U.H.V. may be regarded as an extension of general high vacuum techniques. Since the vacuum pumps used to produce U.H.V. affect both Q_T as well at S_T it is necessary to consider the general principles of each type of pump applied to U.H.V. production.

1.2.2. Diffusion Pumps

It is now thought probable, that many workers making use of high vacuum in the 1930's - e.g. Anderson [1] - were in fact

obtaining pressures of better than 10^{-8} torr with diffusion pumps.

While diffusion pumps have a number of advantages such as simplicity, robustness and short cycling times, they also have a number of disadvantages. These include such phenomena as backstreaming, back diffusion and, depending on the pump fluid, back migration. These factors all contribute to the size of Q_T. In order to attain a low ultimate pressure P_u it is necessary to use suitable cold traps and baffles as described for example by Pirani and Yarwood [2]. The application of such traps and baffles also reduces the pump speed, but in spite of this pressures of 10^{-10} torr and less have been obtained using such a system.

1.2.3. Sublimation and Getter ion pumps

The diffusion pump relies on the removal of gas from the vacuum system as explained in 1.2.2. An alternative method of producing low pressures is to cause the residual gases in the system to react with or diffuse into a suitable clean metal surface. Such a process has, for example, been used with getters, in order to maintain high vacuum in valves and electron tubes. Metals such as barium or titanium can remove residual gases in a process known as sorption. The process of sorbing gas atoms by an active metal is known as gettering. In general there are three ways in which a gas or vapour can be taken up by a metal surface. The solid surface may react chemically with the gas - this is the process of chemisorption upon which the idea of gettering is based. Alternatively the gas atoms may be condensed as a layer on the fresh metal surface which is the process of adsorption, or they may bury themselves deep into

the metal, which is known as absorption.

Most of the active gases are pumped by chemisorption, as shown by Holland and Harte [3] and Holland [4], but the inert gases do not combine with the getter material in this way. In order to remove the inert gases it is necessary to ionize the gas atoms and accelerate them towards the getter surface. The ions are either pumped at the cathode by the process of ion burial or pumped at the anode according to the energetic neutrals hypothesis of Jepsen [5]. The necessity of ionizing the gas atoms has given rise to a family of pumps known as ion pumps. These are often used in conjunction with a type of pump which getters only the active gases, called a sublimation pump. Ion pumps have high speeds for the active gases although the speeds for the inert gases are often as low as 10% of the nitrogen speeds. However using this type of pump with a U.H.V. system enables the gas influx to be reduced since there is no back diffusion from ion pumps apart from the so called argon instability which can be partly overcome by the use of a third electrode or a slotted cathode. With U.H.V. systems the gas influx can also be reduced by baking the system, including the pumps. While this process reduces the subsequent outgassing of the system it also causes the release of hydrogen from the getter material as shown by Stout and Gibbons [6] and so the process of limiting the gas influx by baking also has its own limitations.

All the commercial ion pumps work on the same principle, that of driving ionized gases to a fresh clean metal surface, which can then getter the gas. In order that the pump should remove

gas at as fast a rate as possible it is important that a sufficiently large number of ions should be produced and that the ionization of the gas atoms should be carried out as efficiently as possible. This problem is exactly the same as the problem of measuring the gas pressure. In most cases high ionizing efficiency is achieved by constraining the ionizing electrons into long spiral paths using strong magnetic fields. By increasing the electron path in this way the probability of an electron making an ionizing collision is increased. One exception to the use of magnetic fields is the radial field electrostatic ion pump. This type of pump works on a principle first described by Gabor [7] in which electrons are injected into a radial electrostatic field between two concentric cylinders. Electrons follow long orbiting trajectories about the central cylinder. Development of the 'orb-ion' pumps followed the original work of Herb [8] and Herb et al [9] on the development of evapor-ion and sputter-ion pumps at the University of Wisconsin. They have been subsequently investigated by other workers among them Bills [10], Denison [11], Douglas et al [12] and Maliakal et al [13]. The radial field pump has the advantage of being magnetic field free and therefore has potential application in the field of electron and ion optics, where freedom from magnetic fields is often required.

1.2.4. Cryogenic pumps

There remains one family of pump that does not rely on the ionization of gas atoms in the presence of electrostatic or magnetic fields. The last decade has seen the emergence of the cryopump, which, operating usually at liquid helium temperatures,

condense the gas atoms from the vapour phase and holds them in the liquid phase thus producing very low pressures. The principles of the cryogenic pump have been described in the literature for example by Steinherz and Redhead [14]. Cryopump systems generally are rather bulky and expensive to maintain since they require a continuous supply of liquid helium, and this may be a reason why their potential has not been exploited.

1.3. The Measurement of Ultra High Vacuum

1.3.1. Fundamental Considerations

In many ways the problems of measuring the degree of ultra high vacuum are related to the problems of production. There are two main points to be considered. Firstly the calibration of instruments capable of measuring very low pressures, and secondly the effect of such measuring instruments on the system.

U.H.V. measurement is limited to the use of ionization gauges because no other type of gauge exists which is capable of measuring pressures in the ultra high vacuum region. Ion gauges are not absolute in the sense that a McLeod gauge or Knudsen gauge is, and so they have to be calibrated either against a suitable standard such as the McLeod, or by using a gas flow technique. Carr [15] for example, describes some of the problems arising from McLeod calibration work and the subsequent advantages of the gas flow technique. Using the technique of Carr [15] Fletcher and Watts [16] have described a practical precison gauge calibration system currently in use at the research laboratories of Edwards High Vacuum, International, Ltd. The limits of an ion gauge depend

very much on their geometry and mode of action e.g. whether they are thermionic or cold cathode ion gauges. In general the high and low pressure limits of an ion gauge are set when the ion current recorded at the collector is no longer linearly dependent with pressure. Furthermore the collector current of any ion gauge depends upon the average ionization cross-section of the residual gases contained within the system. Consequently, pressures recorded by ion gauges are critically dependent on residual gas composition.

The second point to be considered is the effect of the gauge, not only on the vacuum itself, but on experiments being conducted within the vacuum system. All ion gauges are capable of outgassing and causing dissociation of gas molecules. Consequently, the ion gauge may well be the factor which limits the production of a better vacuum. Conversely the efficient production, and collection, of ions in an ion gauge means that an ion gauge may have a pump speed of typically 0.2 litres/sec depending on the gauge geometry. Thus it can be seen that the efficient production of ions, while desirable for more accurate pressure measurement, is also a method of pumping the gas as described in section 1.2.3. In spite of their limitations total pressure measuring ion gauges continue to be widely used although increasing attention is being paid to the use of partial pressure measurement. In order to look more closely at the difficulties associated with total pressure measuring ion gauges it is necessary to define the sensitivities firstly of the cold cathode ion gauges as:-

$$S = \frac{i_p}{p} \quad \text{amp torr}^{-1} \quad \ldots\ldots\ldots\ldots (2)$$

when i_p is the collector current in amps and p is the total gas pressure in torr; and as

$$S = \frac{i_p}{p.i_e} \text{ torr}^{-1} \quad \ldots\ldots\ldots\ldots (3)$$

for thermionic ion gauges

when

i_e = primary electron current in amps.

1.3.2. Low Sensitivity Gauges

This group includes the thermionic ion gauge and also the many variations of the inverted thermionic gauge first described by Bayard and Alpert [17] in 1950. These gauges make use of an ionizing current of electrons which are released from a hot filament and oscillate through an open cylindrical grid. During the course of oscillation they ionize neutral gas atoms and molecules by collision, and the positive ion current produced is dependent upon the total gas pressure within the device. Leck [18] pointed out that the high pressure limit of any thermionic ion gauge is reached when the secondary currents caused by ion bombardment and gas ionisation approach the same order of magnitude as i_e of equation (3). For the conventionally arranged ion gauge this limits pressure measurement to about 10^{-2} torr at the high pressure end of the scale. However, the main interest in the ion gauge has centred on the lowest pressure it can measure, since there are an adequate number of gauges capable of measuring pressures in the range of 10 torr to 10^{-6} torr. The conventional thermionic ion gauge has a low pressure limit resulting from the emission of soft X-rays from the grid being collected by the ion collector. In order to reduce the collection of X-rays

Bayard and Alpert [17] designed an inverted thermionic ion gauge with reduced collector area, which will henceforth be referred to as the B.A. gauge.

The B.A. gauge has been extensively reviewed in the literature. Cobic Leck and Carter [19] for example have investigated the bistable operation of the B.A. gauge and discuss gas evolution from the walls of a glass envelope, and the effect of an electron accelerator potential of greater than 250 volts on the wall potentials. Freytag and Schram [20] have investigated the effect of variation of the physical dimensions of the B.A. gauge while Comsa [21] has investigated the collection of energetic ions.

Main interest however centres on the low pressure limit of the B.A. gauge. Because the gauge is only able to constrain ionizing electrons so that they follow only a short path before being collected, the sensitivity of the B.A. gauge is only about 10 torr^{-1}. This means that it is necessary to use rather large primary electron currents in order to produce a sufficiently large positive ion current. This large primary current gives rise to a low pressure limit dictated not only by X-ray collection from the grid but also due to positive ion desorption from the grid as shown by Lawson [22], Hartman [23,24] and Redhead [25].

In order to overcome this fundamental limitation it is either necessary to increase the sensitivity and hence reduce the primary current, or devise some means so that the residual currents are not collected. Various methods using the latter choice have been devised in the last decade. These have been reviewed by

Steckelmacher [26], and include remote collector gauges such as the bent beam gauge of Helmer and Hayward [27] and the extractor gauge of Redhead [28], suppression of the emission of photo-electrons from the ion collector e.g. as in the suppressor gauge of Schuemann [29], and the modulation of the collector current as in the modulator gauge of Redhead [30]. It appears that while these variations of the B.A. gauge are simple, robust and entirely electrostatic, their low pressure limit is about 10^{-13} torr depending on the geometrical arrangement used, because of their low sensitivity. For this reason attention has been focussed in more recent years on those gauges which have large electron paths and hence increased sensitivity.

1.3.3. High Sensitivity Gauges using Magnetic Fields

The presence of a magnetic field causes electrons with a component of velocity perpendicular to the field to perform spiral paths about the field axis. By this means the total path length of any charged particle can be greatly increased. The probability of an electron performing an ionizing collison is therefore greatly enhanced in the presence of a magnetic field. Any gauge with an increased electron path therefore has a higher sensitivity and in the case of a thermionic ion gauge, can be operated at very much lower emission currents with subsequently less problems of outgassing, pumping at the filament, X-ray production and ion desorption from the anodes.

Several ion gauges make use of a magnetic field in order to increase the electrons ionizing path. Perhaps the best known of these is the Penning ion gauge. First described by Penning [31]

as a cold cathode ion gauge, it makes use of crossed electrostatic and magnetic fields. Improvement of the structure of the anode, for example by Young and Hessian [32], who have also incorporated a trigger to enable the discharge to be struck or re-established at low pressures, has lead to cold cathode gauges capable of reading pressures as low as 10^{-12} torr.

Another cold cathode ion gauge, the cold cathode magnetron, has been described by Redhead [33] and the design, performance and operation of various forms of magnetron have been reviewed by Barnes, Gaines and Kees [34]. The outstanding advantage of these cold cathode ion gauges is the absence of a filament and the consequent absence of X-ray limitations although the low pressure limit may be set by field emission. Cold cathode gauges still cause outgassing, pumping, ion desorption and dissociation of gas molecules. One other disadvantage is the fact that the ion current-pressure characteristics of the cold cathode magnetrons and Penning gauges are non linear at low pressures.

The magnetron has also been developed in the form of a thermionic ion gauge e.g. by Lafferty [35] who describes a gauge with the electron path length so much increased over that of the B.A. gauge that the sensitivity is a factor of 10^5 larger.

A fundamental limitation exists with the magnetic ion gauges and that is the presence of strong magnetic fields, typically 0.1 $Wb/_m^2$, needed to give long electron trajectories. On account of these disadvantages the electrostatic radial field gauges based on the idea proposed by Gabor [7] appear to be very attractive.

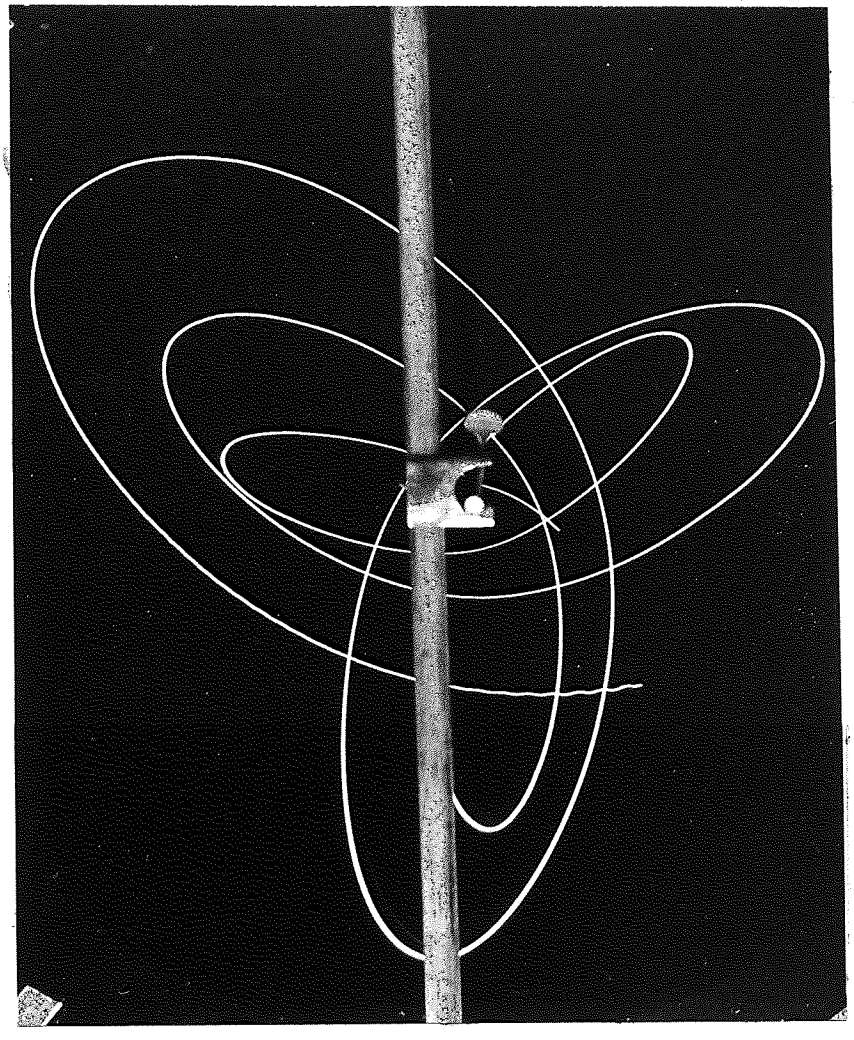

Figure 1

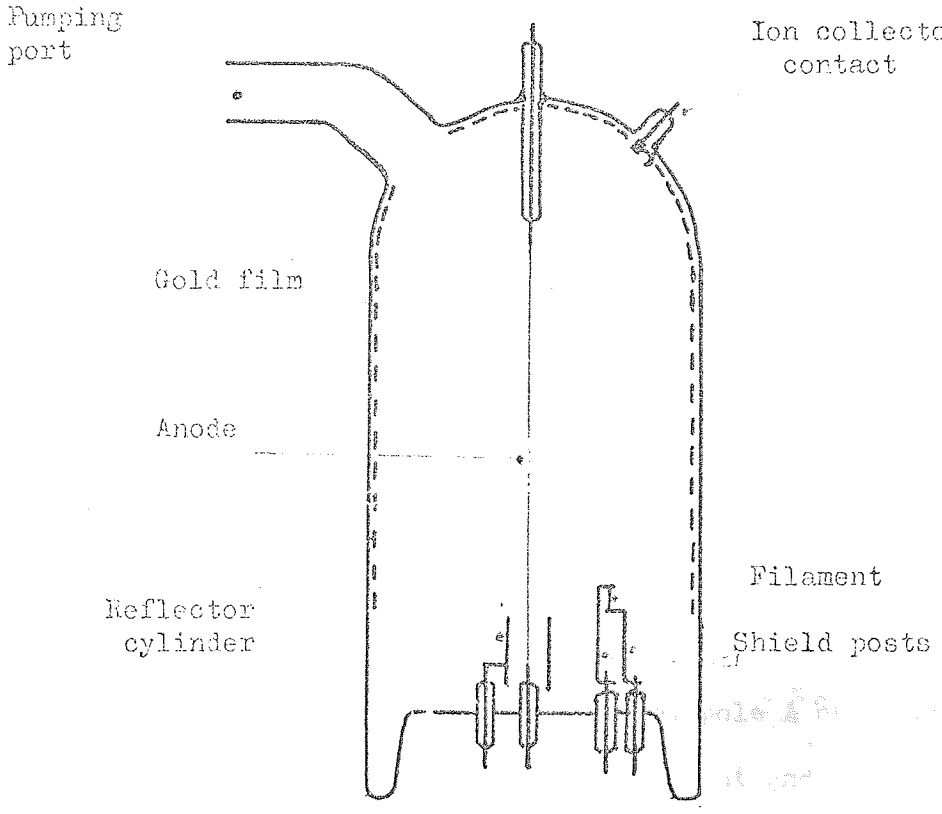
Pumping port
Ion collector contact
Gold film
Anode
Filament
Reflector cylinder
Shield posts

Figure 2

1.3.4. High Sensitivity Gauges using Electrostatic Fields

In 1963 Hooverman [36] derived the mathematical expression for a radial field with a single central pole and has shown that a charged particle with angular momentum in such a field is capable of performing an orbiting type of motion about the central pole. According to Hooverman such a particle should be capable of travelling an extremely long path. A typical trajectory simulated on a rubber model analogue is shown in Figure 1, which was kindly supplied by Dr. A.H. McIlraith at the National Physical Laboratories.

The first experimental devices making use of a radial electrostatic field in order to obtain long electron paths were described by Herb, Pauly and Fisher [37]. Figure 2 shows the geometrical arrangement used by these workers. Electrons were ejected from a filament F and prevented from reaching the central pole A by means of shield posts S placed directly between the filament and central anode. The application of a suitable bias potential V_B to the filament causes a potential disturbance such that the electrons are ejected tangentally to the anode which is held at a few hundred volts above earth potential.

The orbiting electrons are eventually collected by the anode, but travel a very long path before this happens. Positive ions produced by electron collisions with the neutral gas atoms contained in the cylinder are accelerated towards the outer cylinder, the magnitude of this ion current being a measure of the total gas pressure. The electrons leave the filament and potential disturbance at all angles and directions. Most of the electrons drift axially

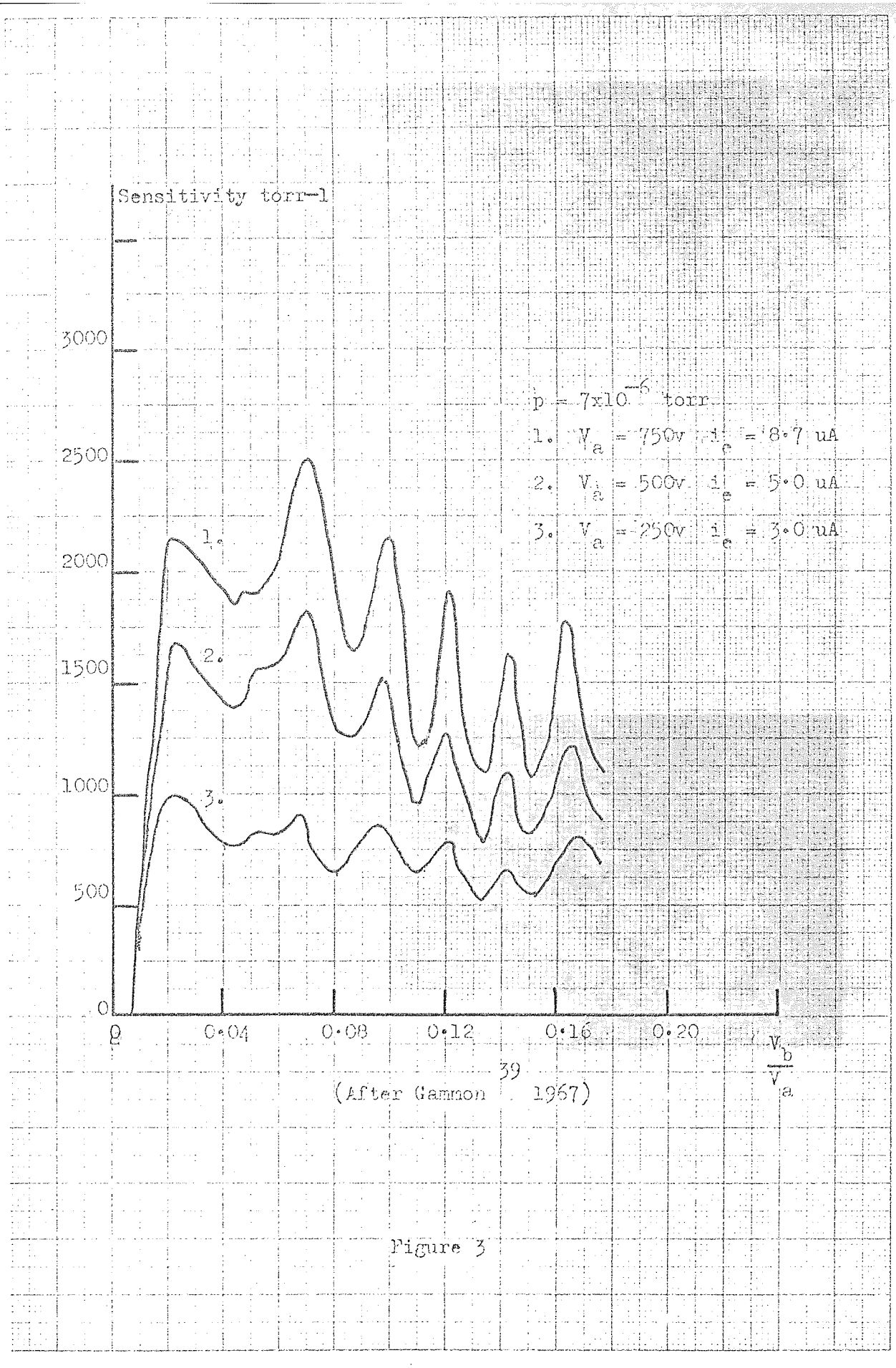

(After Gammon [39] 1967)

Figure 3

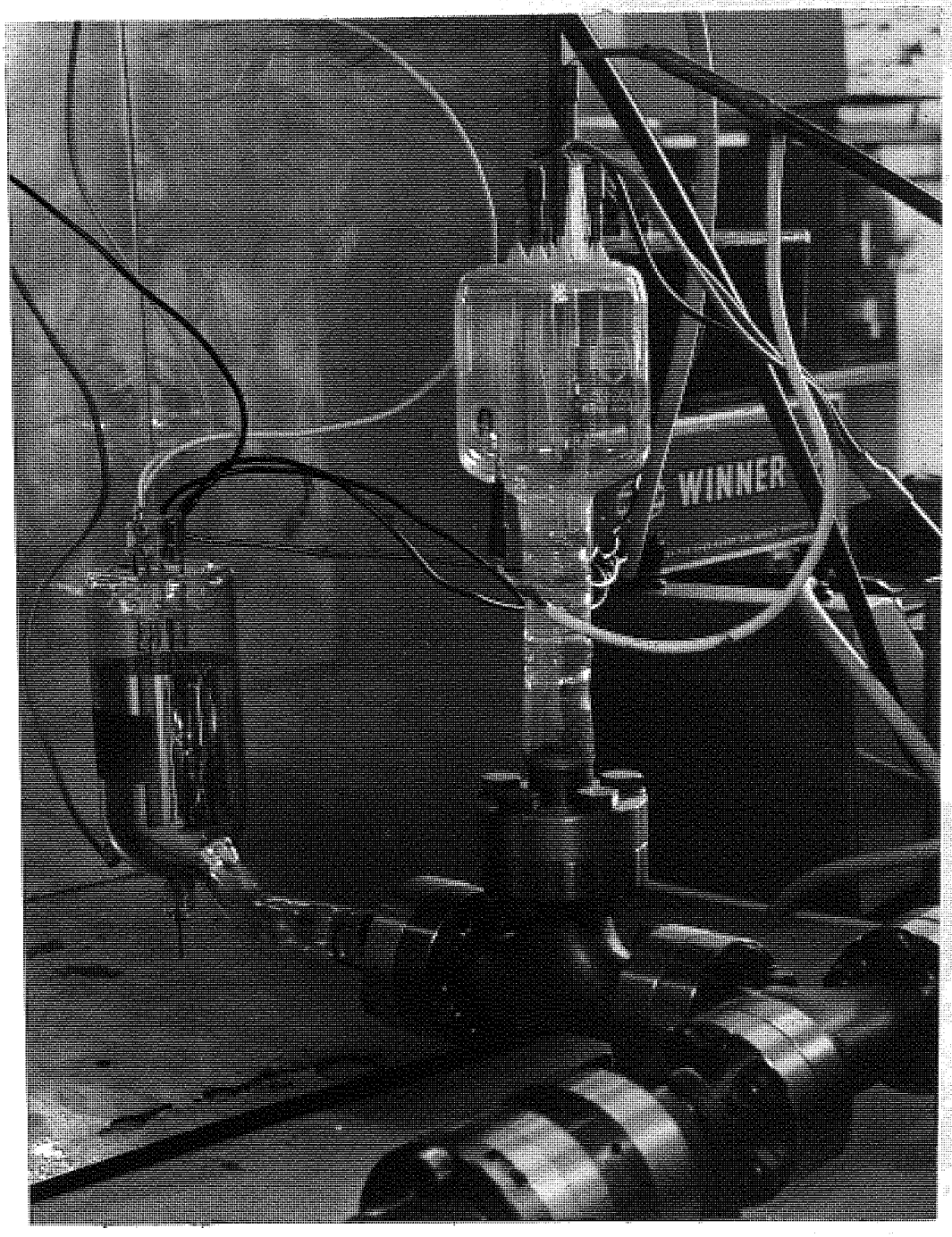

Figure 4

and are reflected at either end of the cylinder by suitable reflector plates or cylinders. However, it is reasonable to suppose that many electrons are collected prematurely following their deflection by the potential disturbance subsequent to their ejection. It can therefore be seen that while the potential disturbance is necessary for ejection purposes it is not wanted once the electrons are in flight.

It has been shown by Mourad Pauly and Herb [38] and by Gammon [39] that the sensitivity of these radial field gauges, named 'orbitrons', are strongly dependent on the bias voltage applied to the filament structure, as shown in Fig. 3. Gammon [39] attributes these ion current instabilities to unfavourable trajectories arising from different filament bias conditions; however Fitch and Thatcher [40] found that a small volume orbitron with modified axial field termination gave stable ion current characteristics. An orbitron of this design is shown in Figure 4. The orbitron as shown exhibited a sensitivity of 5000 torr $^{-1}$, although other workers, notably Meyer and Herb [41] have constructed orbitrons with sensitivities as high as 10^5 torr $^{-1}$.

It is obvious that the presence of a potential disturbance in the radial field, while necessary in order to inject the electrons, is undesirable because it is likely to destroy the trajectories of electrons already in flight. One method of overcoming this problem is to inject the electrons from an externally mounted gun in the manner originally suggested by Gabor [7] for an electrostatic ion pump. This method has been used by Fitch, Norris and Thatcher.[42] Preliminary results show that sensitivities of the order of 10^4 torr^{-1}

can be achieved using this arrangement. The sensitivity is not strongly dependent on the filament or gun modulator potential, but is dependent on the gun anode potential since this determines the electron velocity. Resistance paper field plots reveal less disturbance to the logarithmic field than in the case of the orbitron. However, injection of the electrons into the radial field still presents a problem, since the exact way in which the electron gun behaves is not fully understood. For this reason it is necessary to consider other possible ways in which electrons are capable of performing long ionizing trajectories in electrostatic fields alone.

1.4. An Electrostatic Charged Particle Oscillator

In 1966 McIlraith [43,44] described a principle which also makes use of an electrostatic field alone, in which electrons are constrained in such a way that they oscillate between two equally charged poles. Unlike the orbitron and gun orbitron devices, there is no need for a complicated launching mechanism in the oscillator which may also be operated as a cold cathode device. Electrons in this new device are capable of travelling extremely long paths before eventual collection.

The purpose of this thesis is to study the experimental and theoretical aspects of this device. The principles of the oscillator will be discussed in the following chapter, and subsequent chapters will show that this principle may be applied to several vacuum devices for example as an electrostatic ion pump, thermionic ion gauge, and ion source.

CHAPTER 2

PRINCIPLES OF THE TWIN WIRE ELECTROSTATIC CHARGED PARTICLE OSCILLATOR

2.1 Saucer shaped fields and Earnshaws Theorem

It is well known that a particle starting from rest in a saucer-shaped, or logarithmic, potential field follows an oscillating trajectory passing through the point of lowest potential. However Earnshaw's Theorem - which states that "A charged particle, acted on by an electrostatic field alone, cannot exist in a state of stable equilibrium" - indicates that a perfect saucer shaped field cannot exist in practice because it possesses a point of stable equilibrium. However it has been shown by McIlraith [43] that a pair of equally charged poles produce an approximation to this type of field that is logarithmic everywhere except in the immediate vicinity of the poles. The point midway between the poles is a saddle point. Since there will be a tendency for particles to go to one pole or the other this saddle point is a point of unstable equilibrium. If a particle, with charge opposite in sign to that of the two poles, is released within a certain boundary which depends upon the charge separation and diameter of the poles, it will perform an oscillatory motion which passes through the saddle point. This

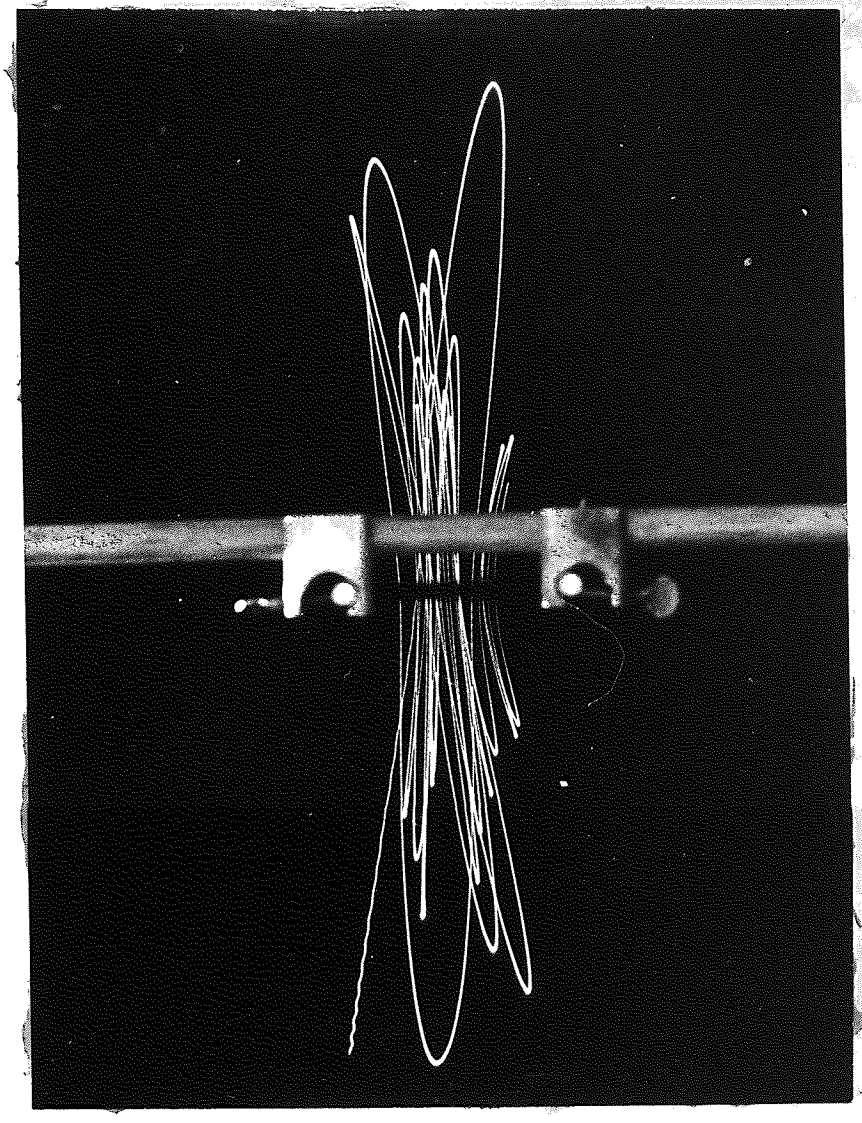

Figure 5

is therefore a class of motion in which particles perform stable oscillations about a point of unstable equilibrium. Oscillatory trajectories of this type have been demonstrated by McIlraith [43] on a rubber model analogue constructed at the National Physical Laboratory. This analogue consists of a thin rubber sheet stretched lightly and evenly over a circular metal framework. Depressions in the rubber sheet were made using copper rods, the depth of the depressions being taken as proportional to the electrode potential. The particle trajectories were simulated using highly polished steel ball bearings. By releasing the steel ball from various positions on the rim of the model McIlraith showed that a family of particle trajectories can be obtained of which Figure 5 is one member. The trajectory was recorded by mounting a camera vertically above the rubber sheet and holding the shutter open.

Because of their simplicity rubber models have been used for qualitative work with a high degree of success in the past. White and Perry [45] discuss some of their limitations, and methods of improving particle trajectory simulation. In the case of the oscillator the rubber model serves to give a good experimental approximation to the type of potential field and particle trajectory attainable with this device.

In order to investigate the potential distribution of the oscillator field a little more quantitatively, experiments were carried out at the University by the author using a carbon

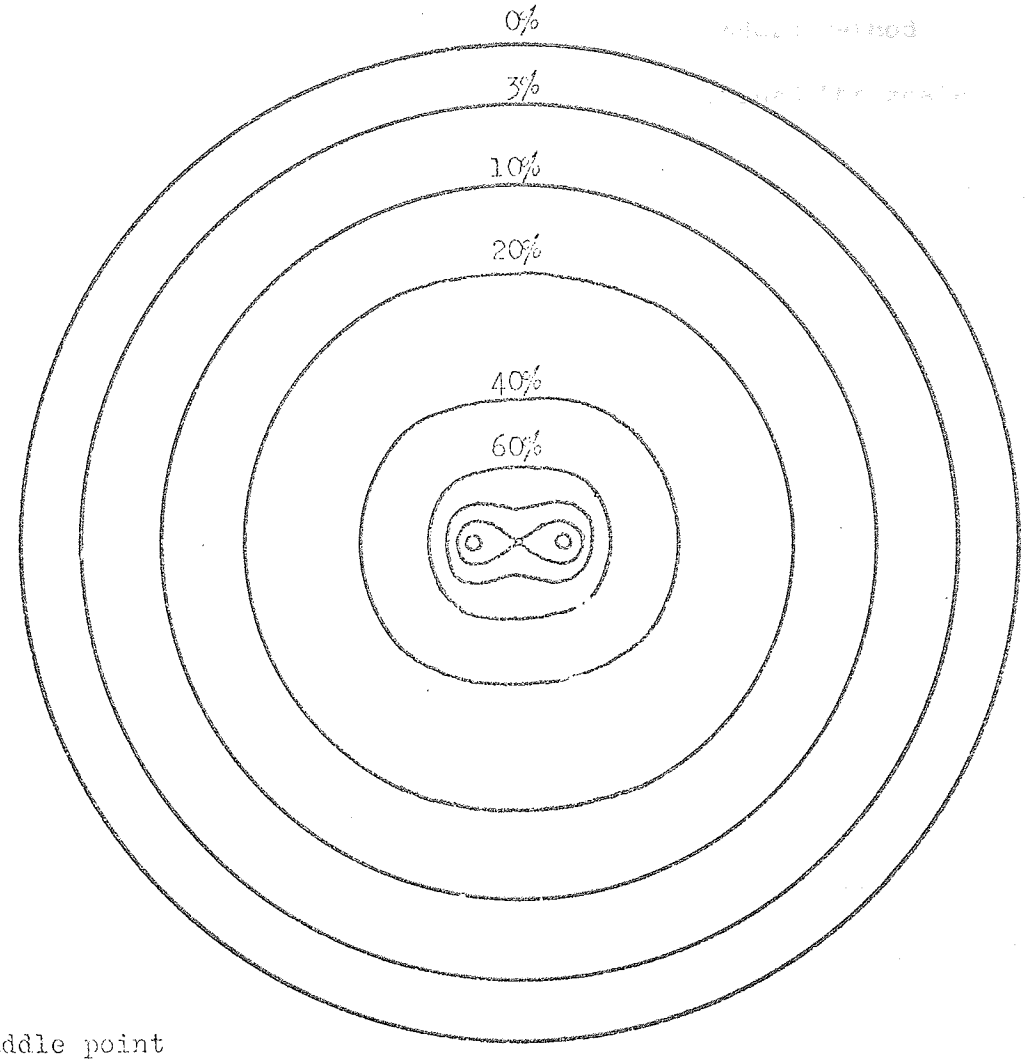

Saddle point
approximately 80%
of anode potential

Figure 6

resistance paper analogue. This is a fairly standard method of investigating potential distributions and, provided the scale of the field plots obtained by it are large, the method is capable of achieving an accuracy of a few per cent.

The electrode arrangements were painted onto the resistance paper using silver paint. A potential difference of a few volts was put across the electrode system and the lines of equipotential plotted using a 'servomex' potentiometer. Figure 6 shows a typical field plot obtained using this technique. It can be seen that by fixing a circular boundary condition the equipotential distribution is approximately logarithmic (or saucer shaped) except in the region of the anodes. The saddle point potential appears to be approximately 80% of the anode potential. The actual saddle point is single valued, the magnitude of which depends upon the anode potential and geometrical arrangement of the electrodes. It will be shown in subsequent calculations how this saddle point potential may be obtained.

It can be seen from Figure 6 that charged particles which travel normally to the lines of equipotential will be accelerated towards the saddle point. Such a particle will follow a trajectory as shown in Figure 5. Both the above experimental methods are limited in the way in which they represent the electrostatic field and particle trajectory. The rubber model is limited in many aspects such as the size of the steel ball used to simulate the charged particle and the imperfect

simulation of the field by a sheet of rubber. The resistance paper analogue gave a good approximation to the equipotential distribution, but does not allow the particle trajectories to be calculated with any ease.

By making use of the calculated field strength at any point within the electrode system a more accurate set of trajectories have been obtained at the N.P.L. by A.H. McIlraith, using digital computer techniques. These trajectories were all calculated on the assumption that the charged particles start with zero kinetic energy. The computer results have shown that a charged particle should be capable of following an extremely long path in a medium free of perturbations, collison processes and other energy loss mechanisms.

2.2. Calculation of the potential distribution and the containment of oscillating particles.

In section 2.1 only a two dimensional model of the oscillator was considered. In this section the motion of charged particles in the axial direction will also be taken into account.

The calculations carried out in this chapter and also in Appendix I and II are based on some unpublished work kindly made available by A.H. McIlraith [46]. In these notes the electrostatic field distribution within the oscillator has been calculated using analytical and numerical methods. The effect of a magnetic field on oscillating electrons is discussed and possible loss mechanisms are put forward by which an oscillating particle could be collected by the anode

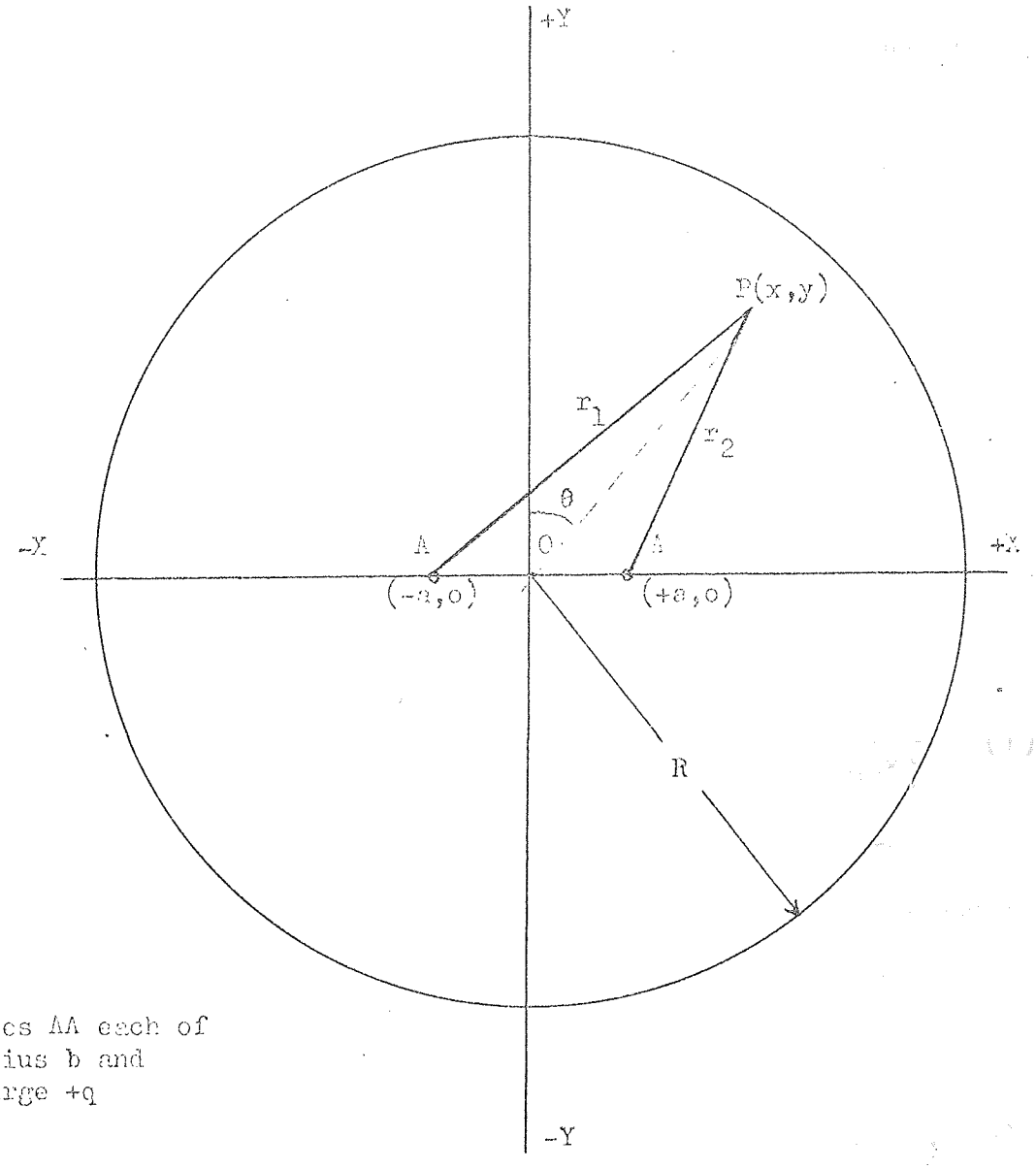

Poles AA each of radius b and charge +q

Figure 7

wires. Finally calculations have been made to demonstrate the possible applications of the oscillator.

Since the calculations mentioned above were originally made using C.G.S. units the author has modified them slightly by recalculating them using M.K.S. units in order to express the results in a more practical form. Suppose the radius of each pole is 'b' metres, and the separation of their centres is '2a' metres. If a charged particle is considered as starting from rest at some point P (xy) as shown in the two dimensional model of Figure 7 and that the poles bear an equal positive charge of +q coulombs per metre then it is shown in Appendix I that the potential at P (x,y) relative to that at the saddle point O (o,o) is V_{xy} when

$$V_{xy} = \frac{q}{4\pi\epsilon\epsilon_o} \ln \frac{a^4}{(y^2+(x-a)^2)(y^2+(x+a)^2)} \qquad (1)$$

ϵ and ϵ_o are the dielectric constant and permitivity of free space. Differentiation of this expression with respect to x and y yields the electrostatic fields in the x and the y directions, respectively E_x and E_y.

$$E_x = \frac{-4qx(x^2+y^2-a^2)}{4\pi\epsilon\epsilon_o(y^2+(x+a)^2)(y^2+(x-a)^2)} \quad \ldots (2)$$

$$E_y = \frac{-4qy(x^2+y^2+a^2)}{4\pi\epsilon\epsilon_o(y^2+(x+a)^2)(y^2+(x-a)^2)} \quad \ldots (3)$$

It can be seen from equation (3) that E_y is such that any negatively charged particle is always accelerated towards the x axis. However equation (2) indicates that $[E_x]$ given by

$$[E_x] = \frac{4qx(x^2+y^2-a^2)}{4\pi\epsilon\epsilon_o(y^2+(x+a)^2)(y^2+(x-a)^2)}$$

is positive and greater than zero only if $x^2+y^2 > a^2$ consequently charged particles bearing a negative sign are accelerated towards the y axis only in the region outside a circle radius 'a' metres centre O(o,o). Inside this circular region, with the exception of the saddle point O, the value of $[E_x]$ is negative indicating a repulsion from the y axis. This indicates the difference in the field configuration from a perfect logarithmic field in which $[E_x]$ and $[E_y]$ would always be positive.

The equation of motion of an electron in this field configuration given by equations (2) and (3) is complicated. In order to evaluate the frequency of an oscillating electron it is simpler to consider motion on the y axis only. It is shown in Appendix I that with an outer collector electrode radius R at zero potential.

$$q = \frac{4\pi\epsilon\epsilon_o V_A}{2\ \mathrm{en}\left(\frac{R^2+a^2}{b(2a-b)}\right)} \quad \ldots\ldots (4)$$

when V_A is the potential applied to the equal poles with respect to the collector. Using equation (4) it is shown that the equation of motion of an electron on the y axis is:-

$$\ddot{y} + \frac{2\, e/_m\, V_A}{\ln\left(\frac{R^2+a^2}{b(2a-b)}\right)} \cdot \frac{y}{y^2+a^2} = 0 \quad \ldots \quad (5)$$

when e/m is the charge to mass ratio of an electron and $\ddot{y}$ is the acceleration of the electron in the positive y direction. Unfortunately a solution of equation (5) is not possible analytically and so it was necessary to integrate it numerically. For this purpose it becomes necessary to assume values for the various parameters. These values were taken from an experimental oscillator, and yielded the information that if an electron starts its trajectory from the outer electrode on the y axis then its frequency of oscillation is about 1.7×10^8 c/s. Independent calculations made by Dr. McIlraith at the N.P.L. and by the author at the University were in very good agreement. Table 1 Appendix I shows how the frequency of oscillation depends upon the starting position, while table 2 Appendix I shows that the particles perform a reasonable approximation to simple harmonic motion only when the electron starts near to the poles, as can be seen in Figure 8. This result can also be obtained by putting $y \ll a$ in equation (5).

The model set up in this way indicates that electrons experience electrostatic fields in the xy plane such that they are constrained in an oscillatory motion between the poles. The model also serves to indicate a typical oscillation frequency. However in a practical three dimensional model electrons will also tend to drift axially parallel to the Z direction which is normal to the (x y) plane, and passes through the point (o,o).

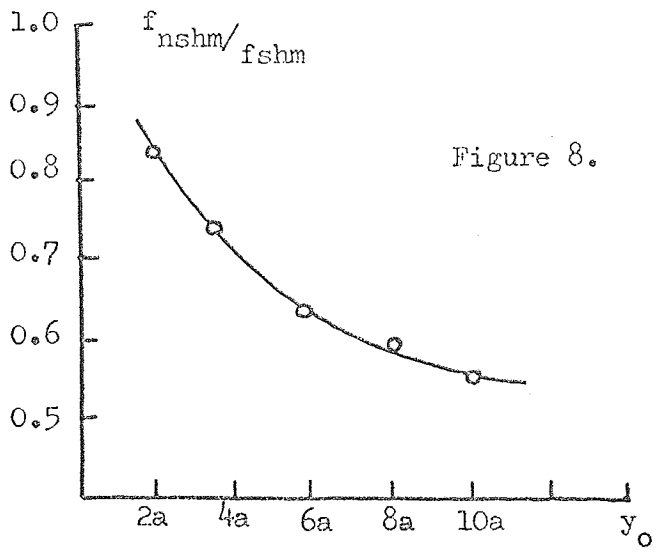

Figure 8.

Hence an electron will oscillate about the z axis in the (yz) plane and will also drift in the z direction under the influence of a force F_z acting away from the plane xy.

It is therefore necessary to consider the motion of electrons in the z direction. In order to do this McIlraith[46] has suggested a model oscillator consisting of a single central electrode of radius 'a', arranged on the axis of a cylinder of length 2L and radius R and having plane end plates. Such an arrangement is shown in Figure 9. The potential on the cylinder is assumed zero and the potential on the central pole assumed to be V_o with respect to the cylinder. The results of table 3 Appendix II show that in order to simplify the analysis the use of a single central pole is justified. It is also shown in Appendix II that the dependence of the field E_z with the distance z from the flat end plates is, as expected, most marked near the outer cylinder. The variation of the field E_z is small except

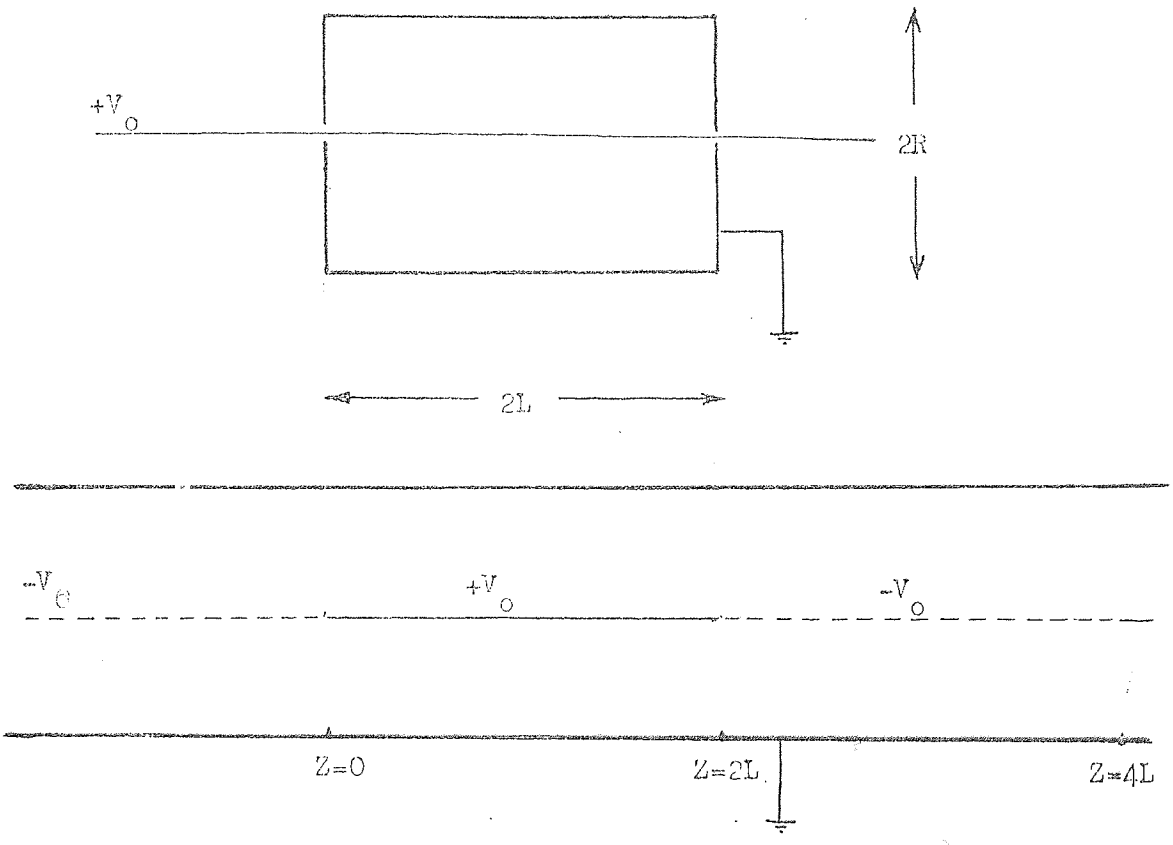
+V0
2R
2L
-Ve
+V0
-V0
Z=0
Z=2L
Z=4L
central electrode
radius 'a'
potential V0
r
R
0

Figure 9

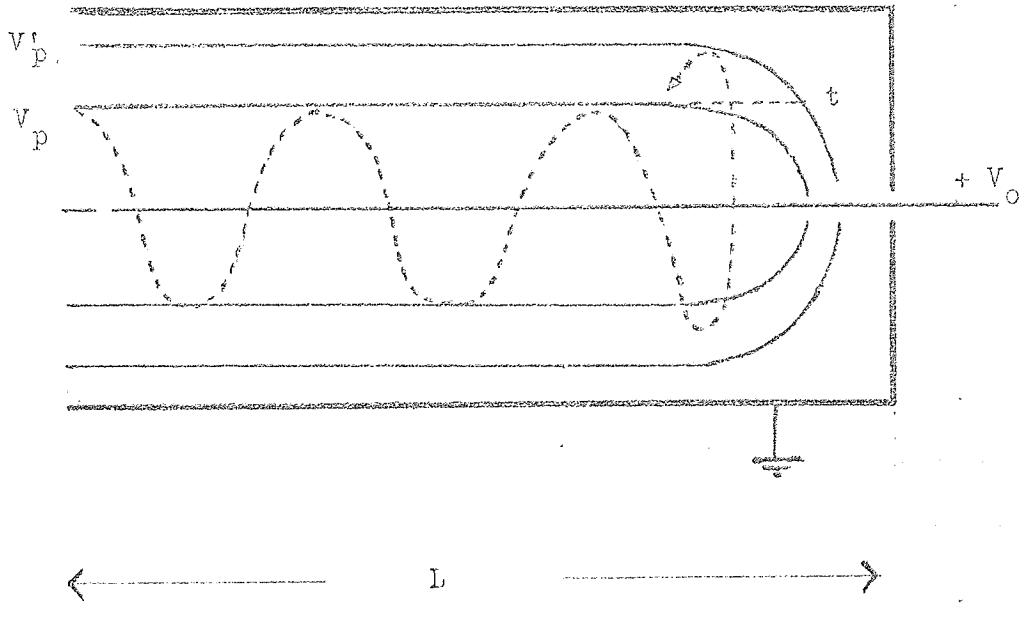

Figure 10

in the immediate proximity of the flat end plates. Hence it seems that the use of flat end plates in order to reflect the electrons axially makes adequate use of the oscillator volume.

This leads to the question of the stability of electrons with components of velocity in the z direction. If the field components E_z in the z direction were independent of z the motions of the electrons parallel to, and perpendicular to the z axis would be independent of one another. However it is shown in Appendix II that E_z is slowly dependent on z for 95% of the oscillator length and very rapidly at either end. It is shown in table 3 that if motion is considered such that the electrons approach no closer than z = 0.786 R to the ends then there is very little dependence of E_z with z.

Suppose an electron approaches the end plates as shown in Figure 10, and that it has an axial velocity v_z and starts on the equipotential V_p at the diametral plane z = L. The total energy of the electron is therefore:-

$$E = eV_p + \tfrac{1}{2} mv_z^2 = eV_p'$$

when

e = electron charge (coulombs)

V_p, V_p' are potentials relative to the saddle point V_o.

For one reflection an electron moves forward a distance δz, with a reduction in velocity v_z as it approaches the end plates given by:

$$\delta(\tfrac{1}{2}mv_z^2) = -eE_z\delta z$$

if E_z is dependent only on z.

If $E_z(t)$ is the value of E_z at the turning point of the transverse oscillation then

$$\delta(\tfrac{1}{2}mv_z^2) = -eE_z(t)\,\delta z$$

But $E_z(t)$ is less than E_z as shown in Figure 10, since the latter is closer to the z axis i.e.

$$E_z(t)\delta z < E_z(\delta z)$$

Consequently the change in potential energy $e\delta V$ where

$$e\delta V = eV_p' - eV_p$$

is greater than $eE_z(t).\,\delta z$. Hence the electron moves to equipotential V_p' i.e. the value of v_z becomes zero before the electron reaches point t. Thus electrons do not experience as large a change in the transverse field at the plane of reflection relative to the transverse field z = L as might at first be expected from Appendix II.

2.3. The influence of magnetic fields on electron trajectories

The presence of a magnetic field could be expected to have considerable influence on the electron trajectories in the oscillator. Stray electrostatic fields may be easily screened and present no serious problem but this is not completely possible with a stray magnetic field. A magnetic field B will give rise to a force F on an electron whose velocity is v such that:-

$$\underline{F} = e(\underline{B} \wedge \underline{v}) \quad \ldots\ldots\ldots\ldots\ldots\ldots \quad (6)$$

The force $\underline{F}$ is always perpendicular to the directions of both $\underline{B}$ and $\underline{v}$. Consequently stray fields in the x and y directions give rise to a set of forces:-

$$\underline{F}_z = e(\underline{B}_y \wedge \underline{v}_x) \quad \ldots\ldots\ldots\ldots (7)$$

$$\underline{F}_x = e(\underline{B}_y \wedge \underline{v}_z) \quad \ldots\ldots\ldots\ldots (8)$$

$$\underline{F}_z = e(\underline{B}_x \wedge \underline{v}_y) \quad \ldots\ldots\ldots\ldots (9)$$

$$\underline{F}_y = e(\underline{B}_x \wedge \underline{v}_z) \quad \ldots\ldots\ldots\ldots (10)$$

Force $\underline{F}_z$ in equation (7) will be small and harmless since in general $\underline{v}_x$ is small. Similarly $\underline{F}_x$ and $\underline{F}_y$ of equations (8) and (10) respectively will also be small. However $\underline{F}_z$ of equation (9) will be large since $\underline{v}_y$ is large in magnitude at the z axis, but $\underline{F}_z$ will be directed in the z direction and provided there is no region of disturbance - say for example due to a filament in the field - this value of $\underline{F}_z$ will also be harmless.

Thus stray fields in the x and y directions are not harmful to the electron trajectories. A magnetic field parallel to the z axis however acts on both $\underline{v}_x$ and $\underline{v}_y$ to produce a rotation of the trajectory about the z axis. This is the Larmor precession. Eventually this precession is halted by the electrostatic forces acting on the electron. Consider an electron starting from rest at some point P on the y axis in the presence of a magnetic field $\underline{B}_z$ and a saucer shaped electrostatic potential field in the plane normal to the z axis. The electron would precess as shown in Figure 11.

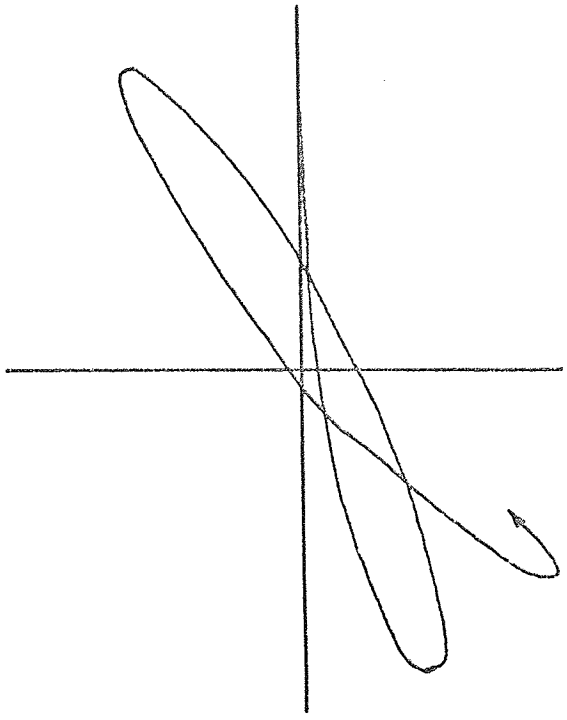

Figure 11.

The frequency of rotation f would be

$$f = \frac{eB_z}{4\pi m}$$

when e/m = electron charge to mass ratio

B_z = axial magnetic field

McIlraith [46] has shown that the angular deviation of an electron released from rest at a point (a,10a) under the influence of an electrostatic field alone is 0.08 radians per cycle. This corresponds to the value of θ in Figure 7 being 0.1 radians. From table 1. Appendix I, for a starting point of (o,10a) and with V_A = 10 kV for an oscillator of 0.027 metres radius, the

frequency of the electron oscillation is 1.74×10^8 cps.

Therefore the rate of precession is:-

$$1.74 \times 10^8 \times 0.08 \quad \text{radians per second}$$

$$= 1.39 \times 10^7 \quad \text{radians per second}$$

From equation (11) the rate of precession due to a magnetic field B_z in the presence of a perfect saucer shaped electrostatic field is:-

$$f = \frac{eB_z}{2m} \quad \text{radians per second}$$

For a field B_z of 10^{-4} webers/metre^2 this is 0.88×10^7 radians per second. Hence the magnetic field necessary to deflect the trajectory of an electron oscillating on the y axis through 0.1 radians is

$$B_z = \frac{1.39}{0.88} \times 10^{-4} \quad \text{webers m}^{-2}$$

$$= 1.57 \times 10^{-4} \quad \text{webers m}^{-2}$$

This is several times the horizontal component of the earths magnetic field. It is therefore expected that a magnetic field several times that of the earths field would cause a deterioration of the performance of a practical oscillator. This will be shown in the following chapter. The expected shape of an electron trajectory subject to the forces described above, after many oscillations, is shown in Figure 12.

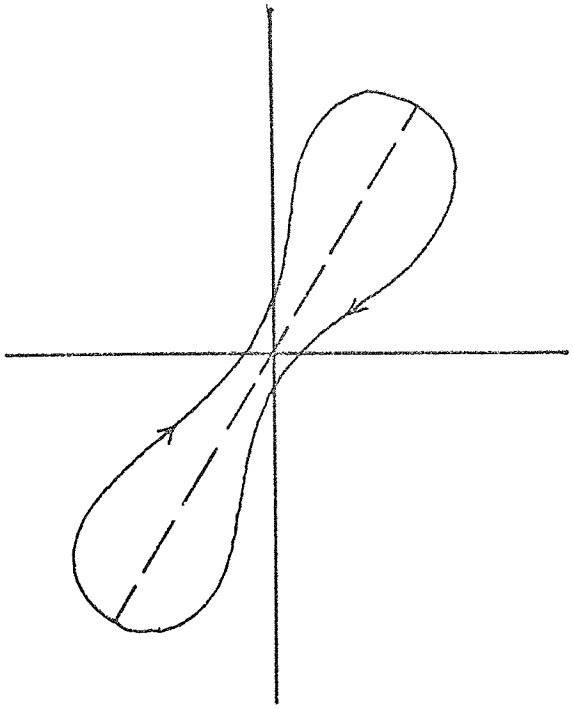

Figure 12.

2.4. Possible applications of the oscillator principle

It has been shown in chapter 1 that at low pressures thermionic vacuum gauges need either high emission currents or long electron paths. Furthermore all ion pumps make use of increased electron trajectories in order to produce ions as efficiently as possible.

Any device which is capable of sustaining electrons in flight so that they travel very long paths before they are eventually collected therefore has application in the field of ultra high vacuum for example as an ion pump or gauge. The only devices which make use of an electrostatic field alone in order

to obtain long electron paths are the radial field ion pumps based on the original idea of Gabor [7]. The potential application of the oscillator principle to an electrostatic ion pump or gauge therefore looks attractive, particularly as the oscillator does not suffer from the electron injection problems associated with the orbitron devices. In order to investigate the manner in which electrons oscillate, using the configuration described in this chapter an experimental oscillator was constructed by McIlraith [43] at the N.P.L. This consisted essentially of a copper cylinder with flat copper gauze end plates at each end of the cylinder and two fine tungsten wires arranged symmetrically about the cylinder axis, held parallel under tension. By applying a suitable potential difference between the central anode wires and the cylinder a glow discharge was maintained to pressures as low as 10^{-5} torr, thus showing that electrons are capable of following very long paths in the oscillator. The following chapters will discuss the variation of some of the parameters of a practical oscillator and show how the oscillator princple may be applied to an electrostatic ion source, gauge and pump.

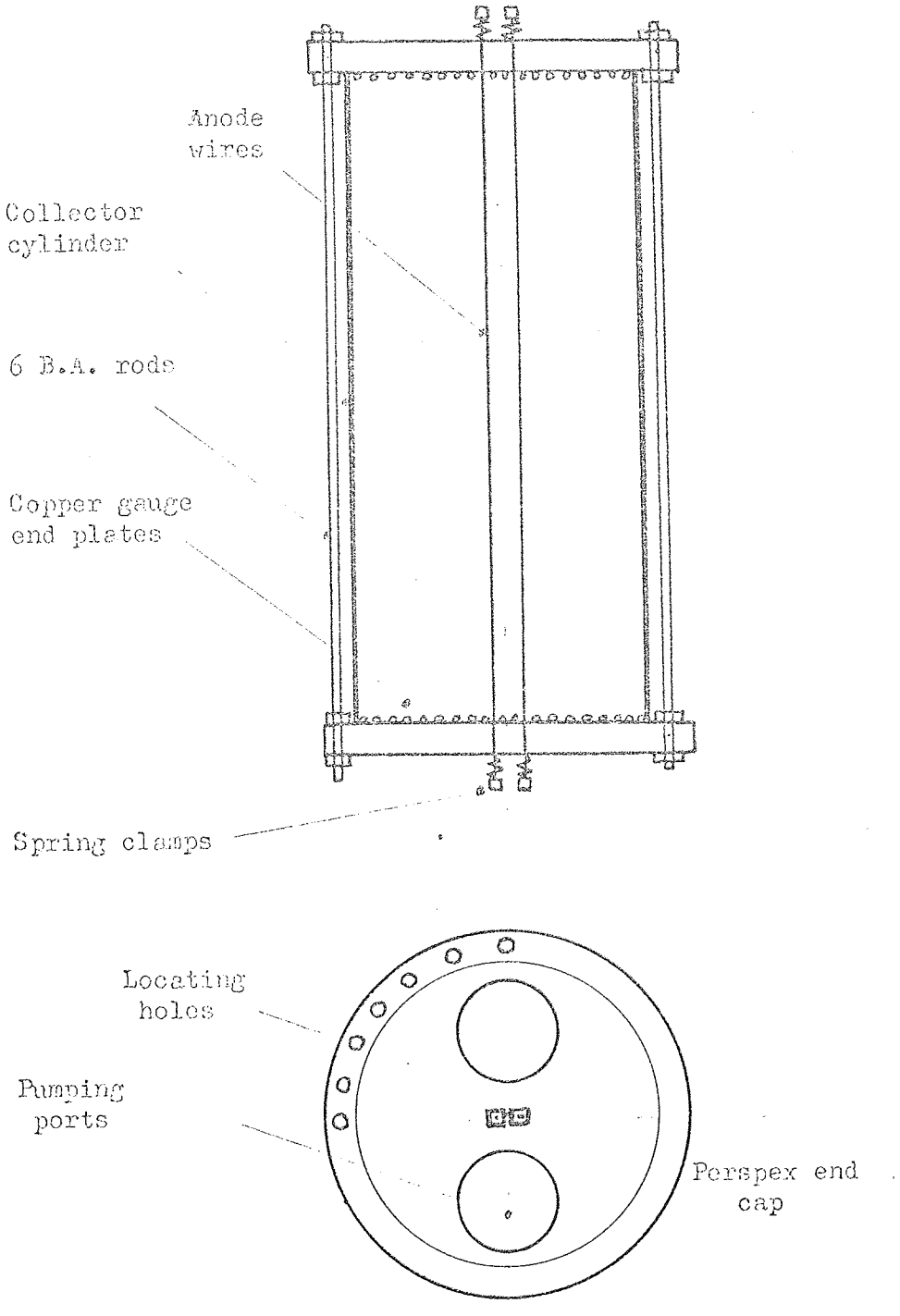
Anode wires
Collector cylinder
6 B.A. rods
Copper gauge end plates
Spring clamps
Locating holes
Pumping ports
Perspex end cap

Figure 13

CHAPTER 3

EXPERIMENTAL INVESTIGATION OF THE PROPERTIES OF THE OSCILLATOR AS A COLD CATHODE DEVICE

3.1 The experimental oscillator

An experimental oscillator was constructed at the University based on the original McIlraith design described in the previous chapter, but constructed in such a way that the physical parameters could be varied. This design is shown in Figure 13. The cylinder or collector was of stainless steel 5.7 cms internal diameter 0.16 cms thick and 20 cms long.

The two anode wires of 0.025 cm diameter tungsten, mounted parallel to the cylinder axis had a centre to centre separation of 0.5 cms, and were located by passing each wire through perspex end plates recessed to fit onto the ends of the cylinder. The wires were held under even tension by compressed spring clamps. Circular pieces of copper gauze with a mesh of 0.2 cms were mounted in the recess as shown in Figure 13. These acted as axial reflector plates as discussed in section 2.2. The mesh was cut to enable the anode wires to pass through it without making contact. Holes were drilled in the perspex end plates to enable the twin anode wires to be moved in directions parallel and perpendicular to their original plane. Holes

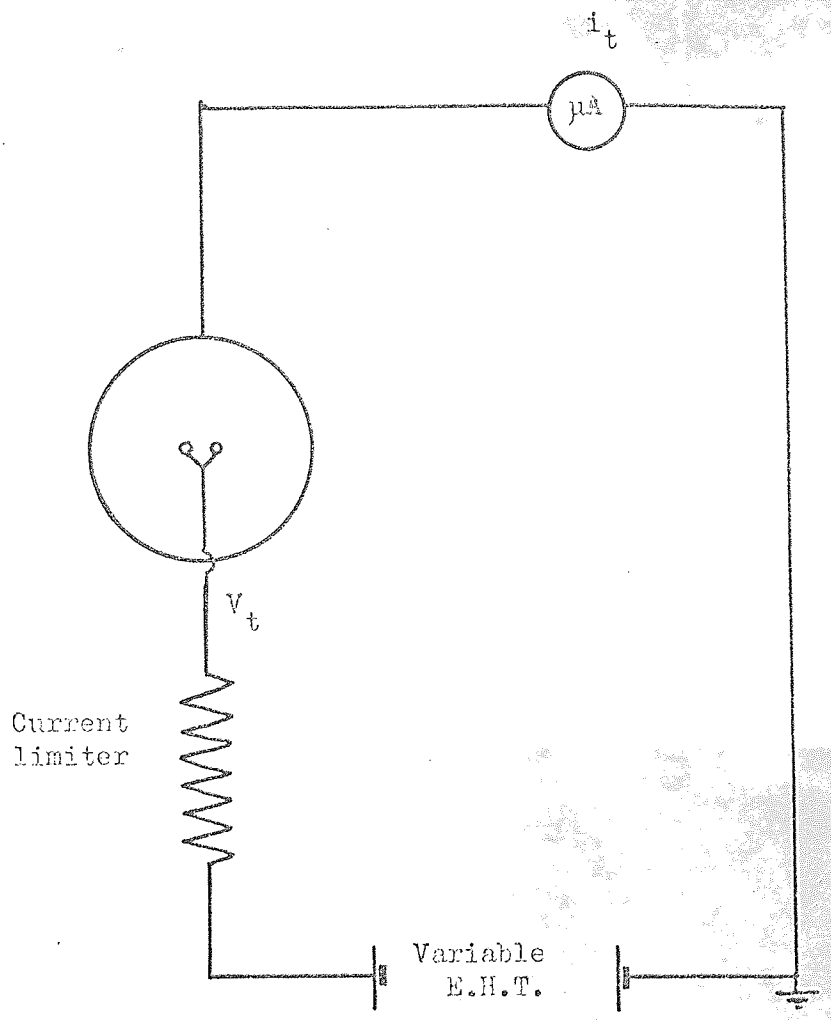

Figure 14

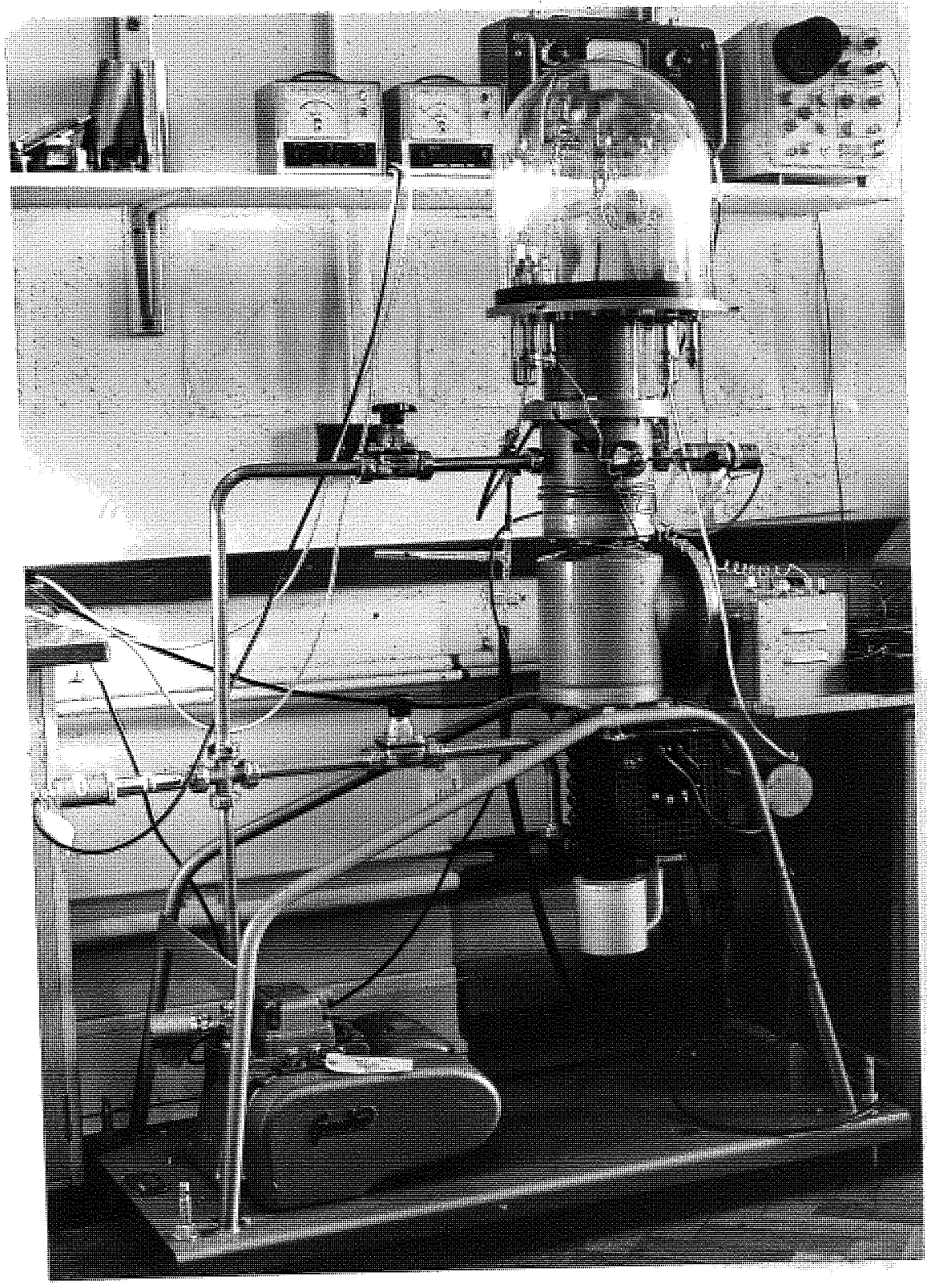

Figure 15

were also drilled at 15^{o} intervals on the rim of the perspex end plates so that it was possible to twist the anode wires about one another.

3.2. The electrical circuit

The circuit used for the experimental investigation is shown in Figure 14. The potential of the anodes with respect to the cylindrical collector was controlled by means of an H.T. power unit capable of a peak output of 50 mA at 12 kV. Initially a 1.33 M Ω current limiter was placed between the output of the H.T. set and the anode wires. The voltage drop across the limiter has been taken into account in all subsequent measurements. The tube current i_t was measured using a Unipivot microammeter capable of measuring 0.2 μA to 120 mA.

3.3. The high vacuum system

The high vacuum system consisted of a Genevac PL 77/3 high vacuum unit, comprising a rotary pump of 1.88 litres/sec. displacement, backing a 3 inch air cooled oil diffusion pump with a baffled speed of 85 litres/sec. The diffusion pump was surmounted by a cold trap and baffle-isolation valve. The chamber consists of a 12 inch diameter glass bell jar mounted on a 14 inch baseplate, drilled to take 2 H.T. and 4 L.T. electrical feed throughs. The vacuum system is shown in Figure 15.

The pressure in the system was measured by a Pirani gauge mounted in the backing line and a Penning gauge mounted just above the baffle valve. The pressure in the chamber was measured using a B.A. gauge and the values obtained were compared with those

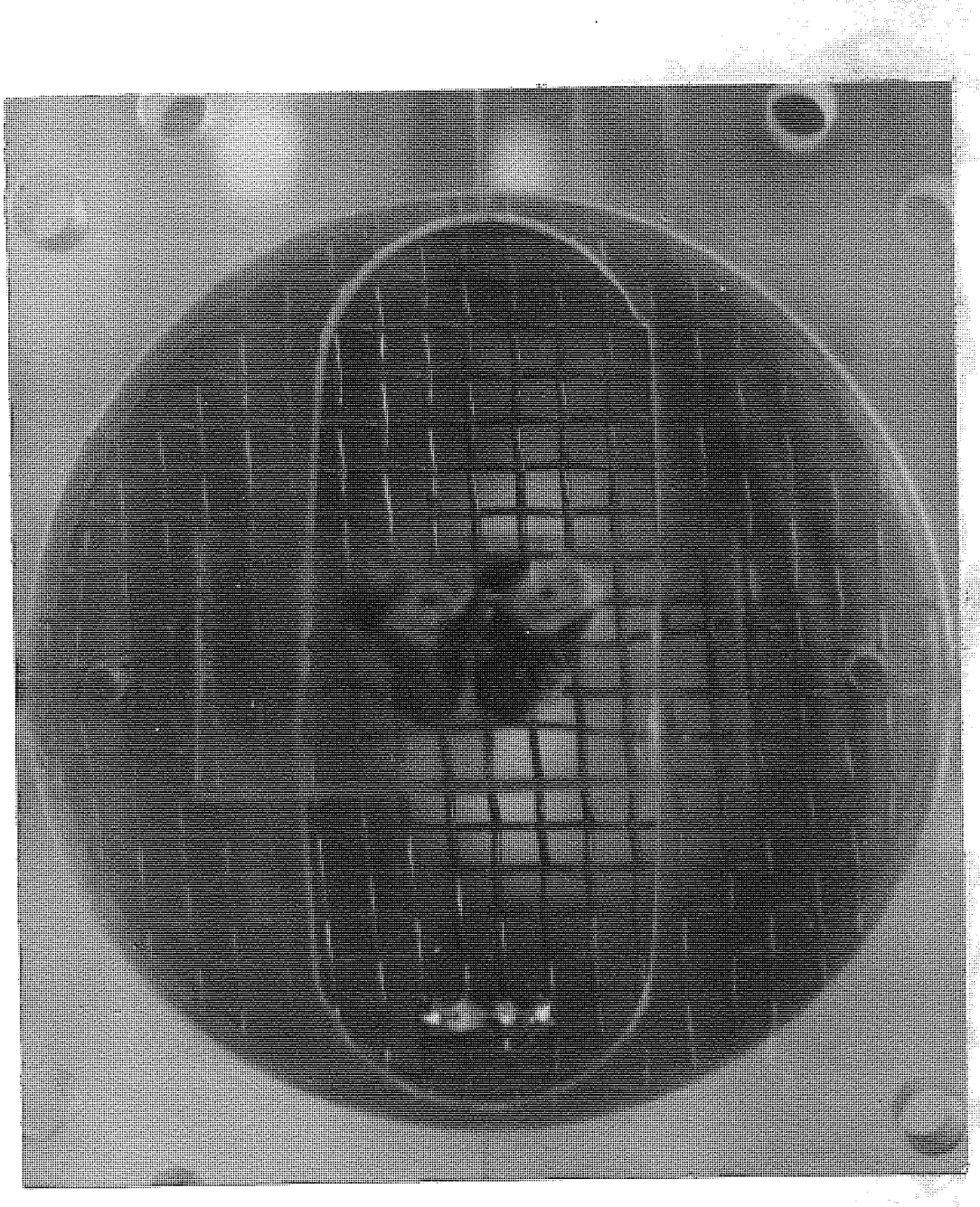

Figure 16

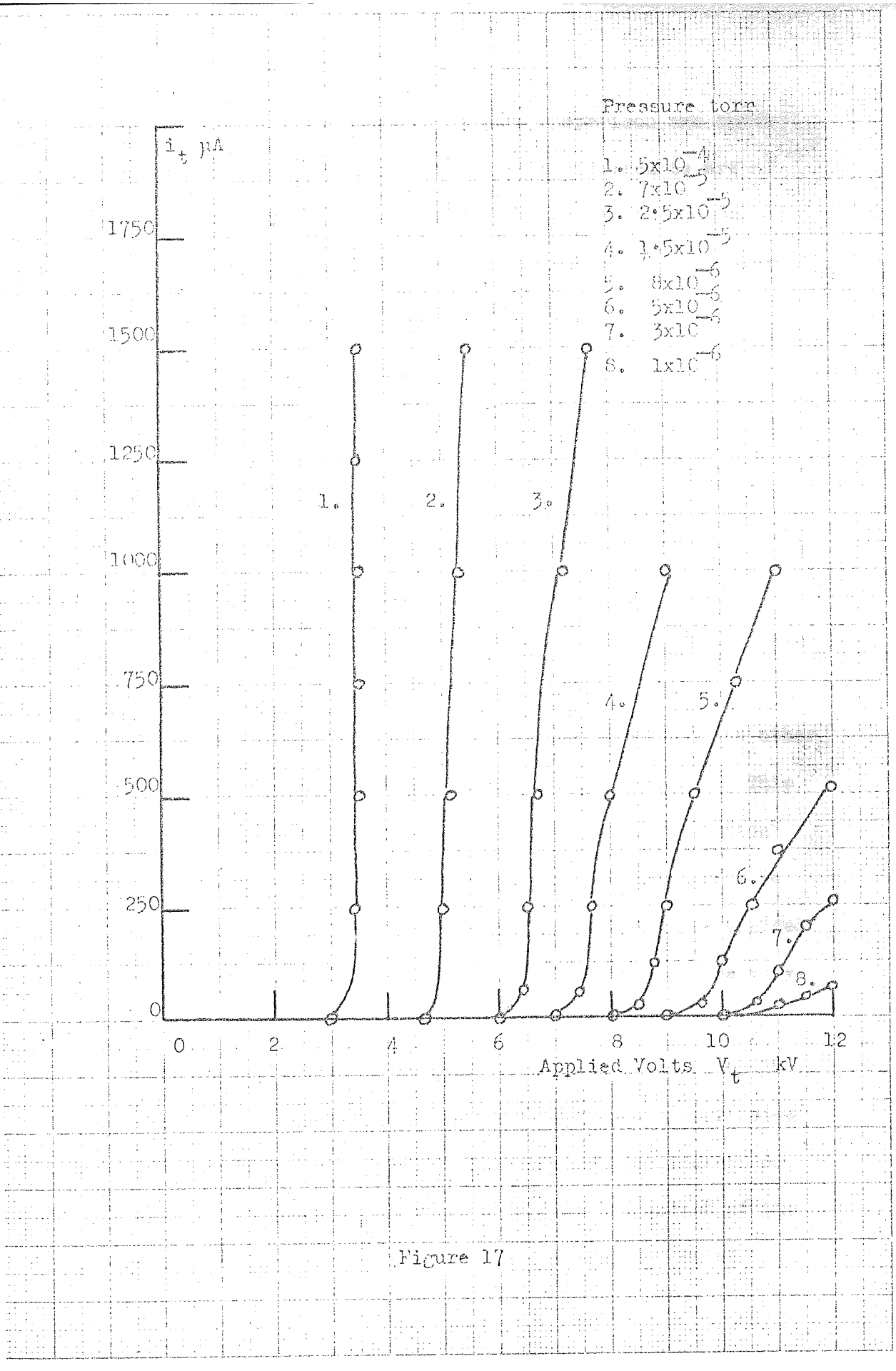
Pressure torr
1. 5x10⁻⁴
2. 7x10⁻⁵
3. 2·5x10⁻⁵
4. 1·5x10⁻⁵
5. 8x10⁻⁶
6. 5x10⁻⁶
7. 3x10⁻⁶
8. 1x10⁻⁶
i_t μA
1750
1500
1250
1000
750
500
250
0
0
2
4
6
8
10
12
Applied Volts V_t kV

Figure 17

of the Penning gauge. The results of this comparison are shown in Appendix III. All pressures subsequently referred to are those of the equivalent B.A. gauge air pressure in the vacuum chamber. Pressure in the system was controlled by a leak valve also mounted just above the baffle valve. The system was used in the pressure range 2×10^{-3} torr to $< 10^{-6}$ torr.

3.4. Investigation of the cold cathode discharge

3.4.1. The voltage-current characteristics

In order to investigate the variation of the discharge current i_t with the applied voltage V_t the oscillator was constructed as described in section 3.1. With a pressure of approximately 10^{-3} torr in the vacuum chamber, the applied voltage was increased until a glow discharge was observed. The discharge has a figure of eight shape with two lobes, one above and the other below the plane of the anode wires, as shown in Figure 16. This is to be expected from the discussion of chapter 2. Variation of the discharge current i_t with applied voltage V_t gave rise to the set of characteristics shown in Figure 17. These are typical Voltage-Current characteristics for a glow discharge and are very similar to those obtained for example by Guseva [48], in a uniform electrostatic field. However it will be noticed from Figure 17 that the applied voltage at which the glow discharge is initiated is dependent on the gas pressure, whereas initial considerations indicate that this striking potential should be indpendent of the gas pressure. McIlraith [47] - who obtained a similar set of

voltage current curves indpendently - has suggested a possible explanation for this. In order to clarify the situation it is necessary to make use of three parameters.

First, suppose the distance an electron is able to travel in the oscillator in the absence of all particles is l_g. Second, suppose the cross-section for a useful collison, i.e. one which results in the production of a secondary electron in such a position that it too goes into a stable trajectory, is σ_i. Finally, suppose the cross-section for scattering an electron out of a useful oscillating trajectory, so that it is collected by the anode wires, is σ_s. The distance l_i which an electron must travel in order to produce a useful collision is:-

$$l_i \sigma_i = \frac{1}{NP}$$

when P is the operating pressure and N the number of molecules per cc. at unit pressure; thus

$$l_i = \frac{1}{NP\sigma_i}$$

Similarly the distance l_s which an electron will travel before encountering a scattering collison is:-

$$l_s = \frac{1}{NP\sigma_s}$$

If l_i is greater than l_s or l_g a self sustained discharge cannot occur, since the electron would be collected before it could have

a useful collision. The threshold for a self-sustained discharge occurs when each electron has just one useful collision. The condition for this to happen is that l_i should be just less than the smaller of l_g or l_s.

(a) Suppose l_g is infinite. A self-sustained discharge would occur when $l_i \leqslant l_s$ i.e. the condition for a self-sustained discharge is:-

$$\frac{l_i}{l_s} \leqslant 1$$

but $$\frac{l_i}{l_s} = \frac{\sigma_s}{\sigma_i} \qquad \text{so} \quad \frac{\sigma_s}{\sigma_i} \leqslant 1$$

is the condition for a self-sustained discharge in the case of l_g being infinite. This expression is independent of pressure.

(b) Suppose l_g is finite, and that $l_i < l_g < l_s$. In this case the condition for self-sustained discharge is:-

$$l_i \leqslant l_g$$

$$\text{i.e.} \quad l_i = \frac{1}{NP\sigma_i} \leqslant lg$$

The threshold occurs when:-

$$\sigma_i = \frac{1}{NPl_g}$$

Since σ_i is dependent on the energy of the electron, it is also dependent on the threshold voltage. Hence the threshold voltage increases as the pressure falls. This variation of

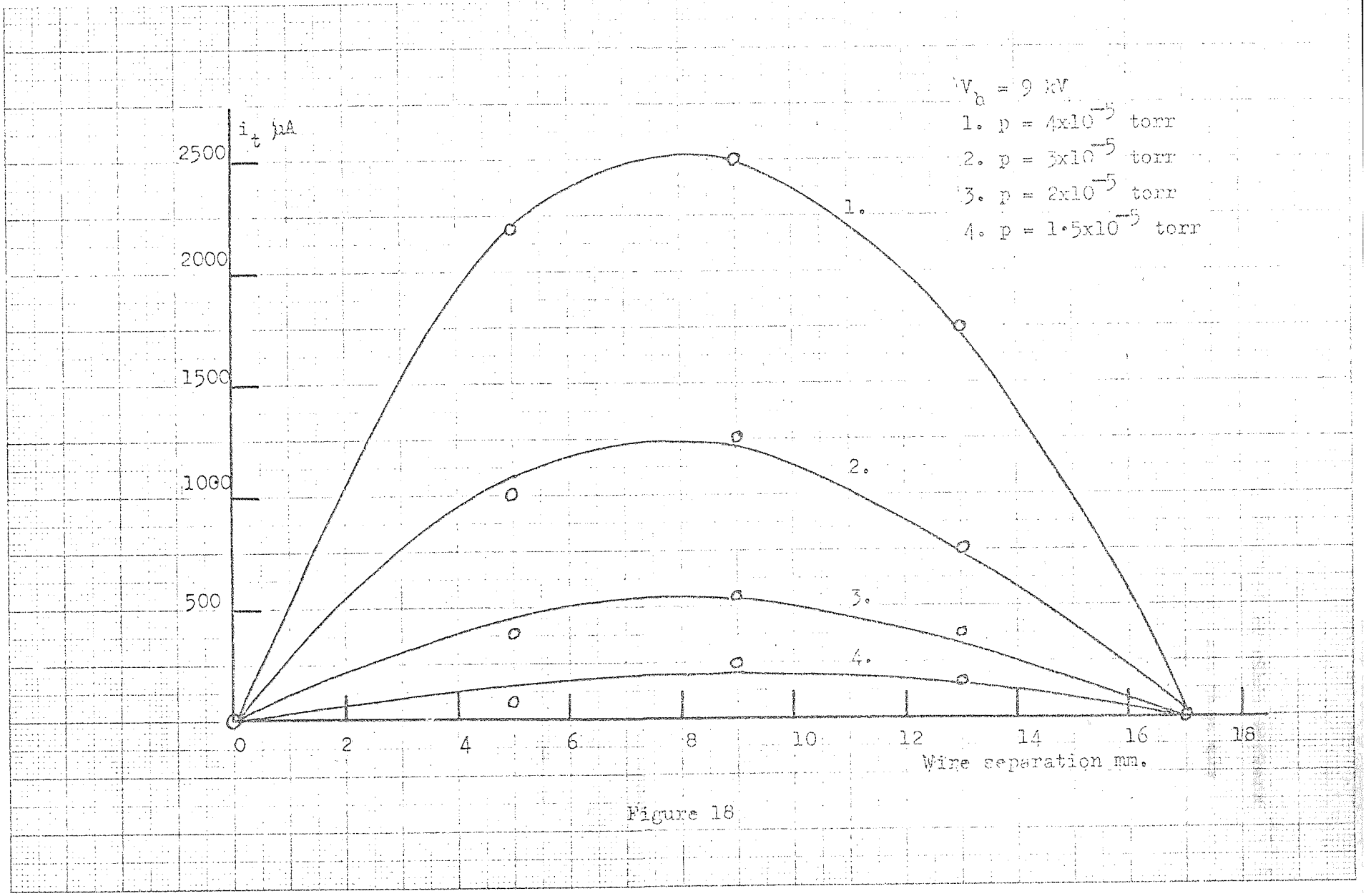
V_b = 9 kV
1. p = 4x10^{-5} torr
2. p = 3x10^{-5} torr
3. p = 2x10^{-5} torr
4. p = 1·5x10^{-5} torr
i_t μA
2500
2000
1500
1000
500
1.
2.
3.
4.
0
2
4
6
8
10
12
14
16
18
Wire separation mm.

Figure 18

threshold voltage with pressure has been observed by other workers in a variety of other discharge devices notable amongst them the works of McClure [49], and Guseva [48]. Indeed Guseva [48] points out the strong dependence of threshold voltage upon the electron trajectories in a discharge. On these grounds it would seem reasonable to suppose that while the electrons certainly travel extremely long paths, as indicated by the ability of the oscillator to hold a discharge at 10^{-6} torr, the electron path is finite in length.

3.4.2. The effect of separation and twist of the anode wires.

Investigation of the variation of the discharge current with the separation of the anode wires yielded the set of curves shown in Figure 18. For this experiment the diameter of the anode wires was increased to 0.05 cms. For each curve the applied voltage and gas pressure were kept constant. Since separation of the anode wires will alter both the shape of the electrostatic field and the magnitude of the saddle point voltage, it seems likely that for any given gas pressure and applied voltage, there will be one separation of the anode wires which correspond to a maximum path length of the electron trajectory. Such an explanation would account for the distinct maxima obtained in Figure 18. Furthermore results from the computer programme at the N.P.L., discussed in section 2.1, also predict an optimum trajectory for different anode separations. However, it has not so far proved possible to predict analytically the optimum

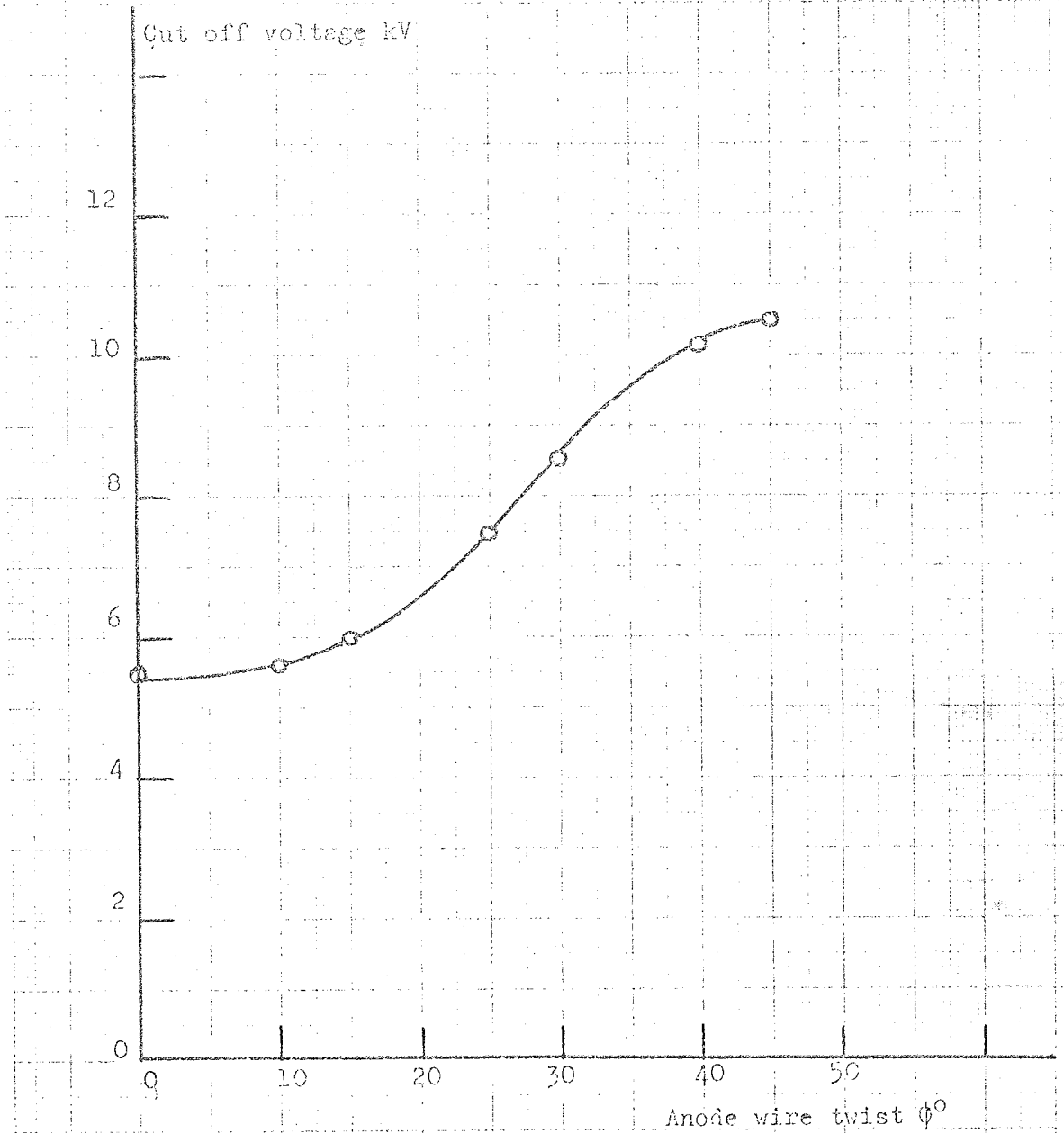
Cut off voltage KV
12
10
8
6
4
2
0
0
10
20
30
40
50
Anode wire twist ϕ°

Figure 19

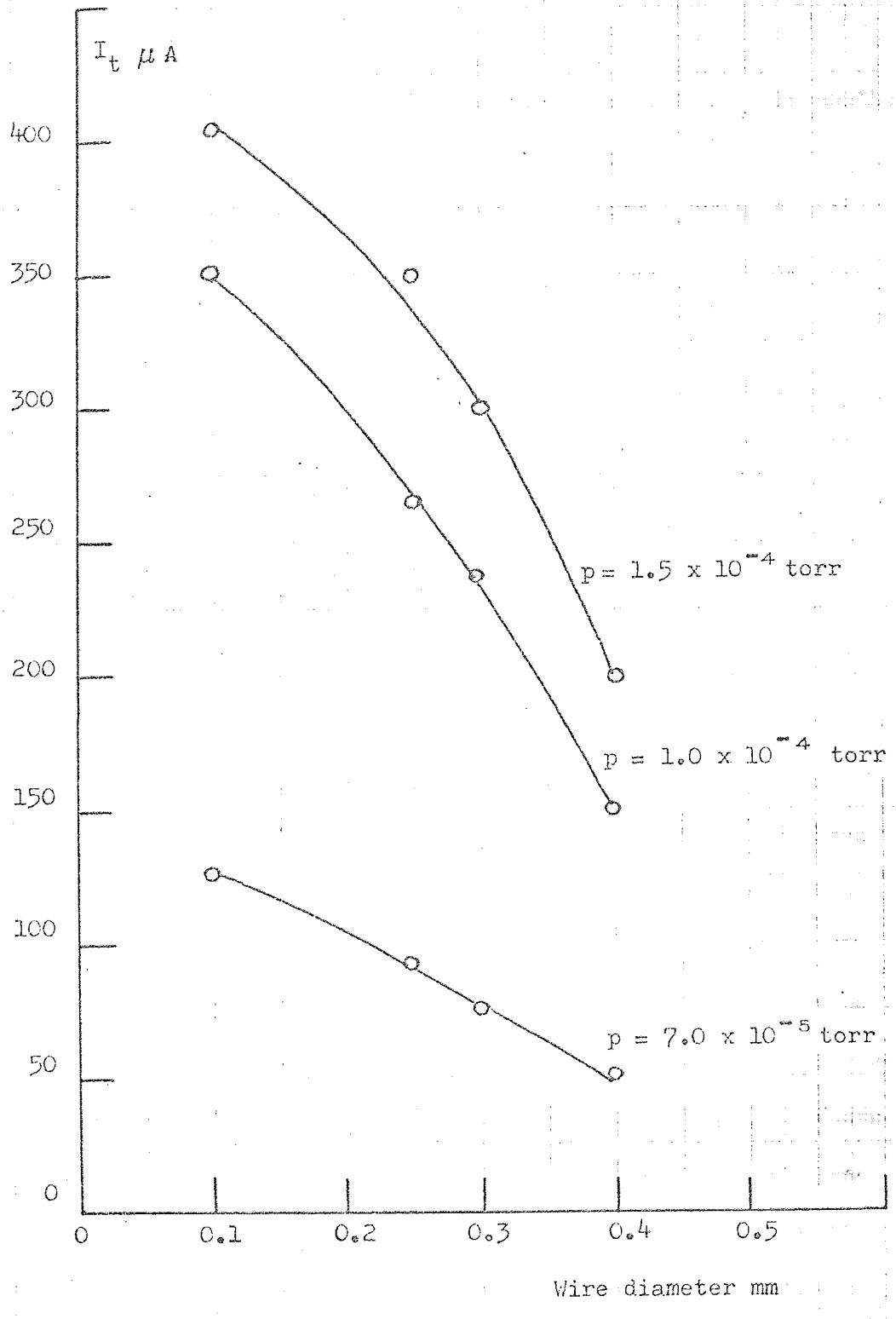
I_t μA
400
350
300
250
200
150
100
50
0
0
0.1
0.2
0.3
0.4
0.5
Wire diameter mm
p = 1.5 x 10⁻⁴ torr
p = 1.0 x 10⁻⁴ torr
p = 7.0 x 10⁻⁵ torr

Figure 20.

geometrical arrangement which gives rise to a maximum electron trajectory.

The effect of twisting the anode wires about one another was expected to cause a decrease in the electron path as a result of the axial drift of the electrons carrying them into an unstable trajectory. The effect of twisting the wires in practice caused greater difficulty in striking the discharge with increased twist which is consistent with the above supposition. However, the effect of twisting the wires is not marked until the angle of twist is approximately 15°, as shown in Figure 19. Consequently the tolerances in constructing a practical oscillator with regard to anode twist are nor particularly exacting - say $\pm 10^{\circ}$.

3.4.3. The effect of variation of the diameter of anode wires and their displacement from the axis of symmetry.

The effect of varying the diameter of the anode wires was expected to produce the same effect as the separation of the anodes, since both the saddle point potential and the shape of the field will be affected. Variation of tube current i_t with anode diameter is shown in Figure 20. The tube current decreases with increased wire diameter for the separation of 0.5 cms shown in the figure. The variation is more gradual than in the case of separation of the anodes because the change of the shape of the field is less marked. It follows that in constructing an oscillator attention should be paid to both the diameter and separation of the anode wires.

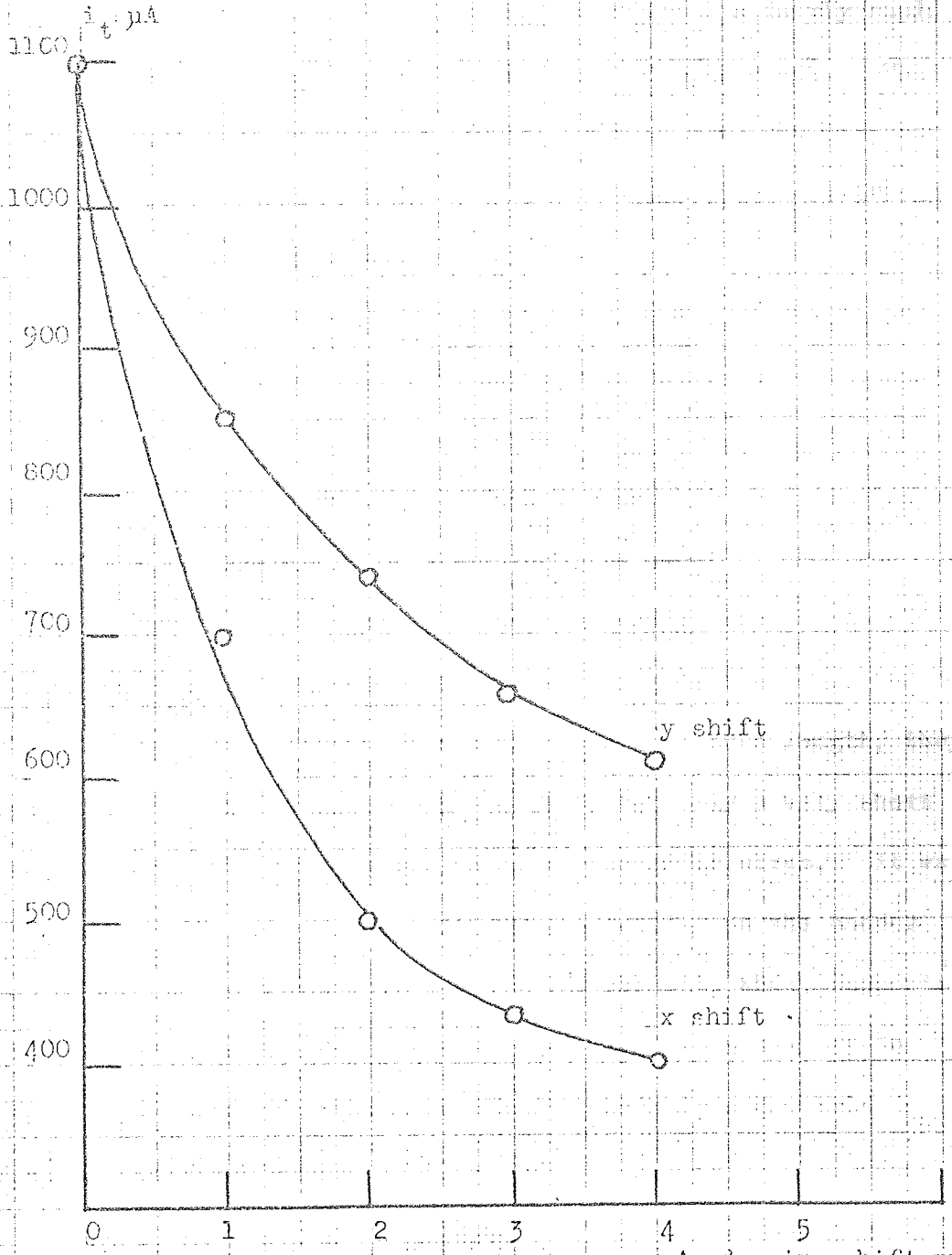
i_t μA
1100
1000
900
800
700
600
500
400
y shift
x shift
0
1
2
3
4
5
Anode wire shift mm.

Figure 21

Conversely the displacement of the parallel wires in the x and y directions as shown in Figure 21. produced a fairly rapid deterioration of performance with increased displacement. This is to be expected since such a displacement affects not only the motion of the electrons in the xy plane but also their reflection at the end plates of the oscillator.

During these experiments it was found that a kink or bend in the anode wires had a disastrous affect on the discharge. Even a small kink prevents a discharge being struck at all even for very high voltages. The explanation for this is very similar to that of 3.4.2. when anode twist was considered and is indeed simply an extension of that argument. A small bend is capable of causing a displacement of the saddle point at the region of the bend. Since electrons drift axially along the tube length, they encounter this disturbance to the field after only a very short time, and are subsequently deflected to the anode wires. It was noticeable that any dust particles which settled on the anodes during the course of experiment became white hot, which supports the above argument. Consequently great care is necessary in construction that the anodes are free of kinks and are held under uniform tension.

3.4.4. The end plates

The purpose of the end plates has been described in chapter 2. Although the axial drift of electrons is expected to be considerably slower than the rate of oscillation between the anodes the end plates still perform a very necessary function

of containing the electrons and preventing them from drifting out of the tube. The copper gauze end plates were removed compltely and it was found that the glow discharge could not be struck at all because of the axial drift. With the end plates isolated from the cylinder and anodes, positive and negative potentials of up to 10% of the tube voltage V_t were applied to them. No change in the discharge current i_t was observed over this range at a given pressure which demonstrates the relative insensitivity of the oscillator in this form to the field termination in the axial direction. More detailed investigations of axial reflection were made using a thermionic oscillator, and these are discussed in chapter 4.

3.4.5. Effects of a magnetic field

Since the oscillator relies entirely on electrostati· fields in order to constrain the electrons, the presence of a magnetic field is neither required nor, as shown in chapter 2, desired. However, it would seem desirable to know within an order of magnitude the strength of the stray magnetic field which could limit the performance of the oscillator. It was early established that the presence of a large permanent magnet near the oscillator was capable of either (a) tilting the figure of eight glow discharge in the manner suggested in Figure 12 or (b) causing the extinction of the discharge altogether. Later work by G. Rushton in the Physics Department of this University established that a non-uniform stray magnetic field with a strength of only ten times that of the horizontal component of the earths field is capable

of reducing the sensitivity of the oscillator, employing a thermionic source of electrons, by more than ten per cent. This result is in good agreement with the predictions of chapter 2. It follows that care is needed with regard to the location of magnets and the presence of stray magnetic fields near the oscillator.

3.5. Conclusions

The series of experiments discussed in section 3.4. were devised in order to investigate the relative importance of various parameters likely to affect the efficiency of the oscillator i.e. the containment of electrons so that they follow long paths. The results obtained, as expected, gave rise to a set of physical limitations existing in an experimental oscillator.

It has been established that the most symmetrical arrangement of the oscillator with the twin wires equally disposed about the cylinder axis is most satisfactory, and that three factors are likely to seriously affect the performance. These are the presence of kinks in the anode wires, the absence of end plates and the presence of stray magnetic fields.

The presence of bends or kinks in the anode wires is regarded as the most serious of these limitations. To what extent a non perfect circular cross-section wire limits the electron path is not known, although using commercial tungsten wires and taking care not to kink them gave reproducible results. In all subsequent oscillators as in the initial design, attention was paid to holding both anode wires at even tension. Lack of tension in

one anode or the other gave rise to more pronounced heating of the slack wire and also considerable vibration, believed to be caused by the vibration of the rotary pump.

The absence of end plates, while seriously limiting the performance of an oscillator does not present a threat to the possible application of the device since it is simple enough to fit an oscillator with plane end plates. It may well prove that the use of hemispherical end plates, as suggested by McIlraith [46] and Fitch and Thatcher [40] would improve the axial reflection of the electron and consequently increase the total electron path. Hemispherical end plates however are not so simple to manufacture as plane end plates. Furthermore it is likely that the effect of hemispherical end plates will be less significant in the oscillator than in the orbitron. The presence of stray magnetic fields could be a serious limitation if an oscillator is to be used in the immediate vicinity of a fairly strong magnet. However in its present form only stray fields several times greater than the horizontal component of the earths field are likely to affect the oscillator. The possible use of mu-metal screening could extend the magnitude of stray field tolerable to the oscillator still further.

The oscillator in the form described in this chapter is inadequate as a cold cathode ion gauge since a discharge can only be maintained to pressures as low as 10^{-6} torr. The use of a collector with a higher secondary electron emission such as copper could extend this perhaps by an order of magnitude.

However at pressures in the region of 10^{-4} torr it is apparent from Figure 17 that it is possible to obtain fairly large numbers of ions. It follows that the oscillator also has potential as a low pressure electrostatic ion source, with possible applications in the field of ion etching and ion thinning. It was anticipated that this particular application would lead to further understanding of the properties of the oscillator, and consequently the oscillator was constructed as an ion source as described in the following chapter.

CHAPTER 4.

THE OSCILLATOR AS AN ION SOURCE

4.1. Introduction

The work described in the preceding chapter has shown that the oscillator is capable of maintaining a self sustained discharge down to pressures of at least 10^{-6} torr. It follows that if the positive ions formed in the discharge could be extracted the oscillator could be used as an ion source which is free from magnetic fields and operates at much lower pressures than most other sources. It was noticed during the investigations described in chapter 3 that two regions inside the oscillator cylinder had the appearance of being highly polished. These regions were immediately above and below the plane of the anode wires as shown in Figure 22.

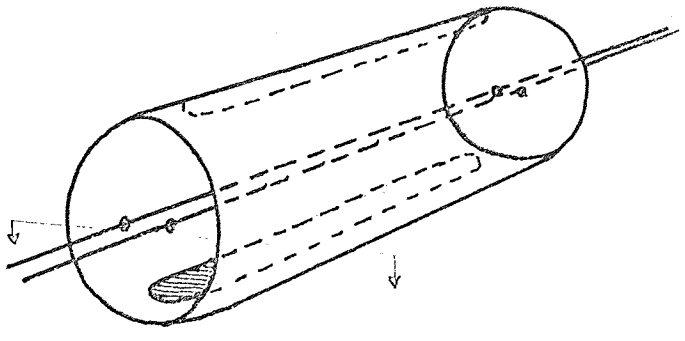

Figure 22.

These polished regions were due to the bombardment of the cylinder walls by positive ions formed in the discharge. Such an effect was observed for example by Penning [31] and investigated by Penning and Moubis [50] in the well known Penning gauge.

In the oscillator the total area of the sputtered regions was approximately 36 cm^2. By ignoring the effect of secondary electron production at the cylinder walls it was possible to estimate the ion current density at the walls within an order of magnitude. With a chamber pressure of 5×10^{-4} torr and applied voltage of 8 Kv across the tube the beam density was about 140 μ A cm^{-2}. It has been shown by Wehner [51] that ion beams extracted from a glow discharge of less than 100 μ A cm^{-2} can be used to cause ion etching. It was suggested by McIlraith that the oscillator should be investigated as an ion source for use in conjunction with ion etching.

4.2. Construction of the Oscillator as an Ion Source

The dimensions of the oscillator are essentially the same as those described previously. The anode wires were 0.03 cm tungsten, spaced 0.5 cm apart. A small rectangular slot 2.5 x 0.5 cm was milled in the cylinder wall at a position midway along and on the 'y' axis of the cylinder. The ion collector originally consisted of a small rectangular nickel plate 0.65 x 0.25 cm situated 4 cm directly above the slot. This was later replaced by a Faraday cage in order to reduce the secondary emission from the collector. The Faraday cage was constructed as shown in Figure 23.

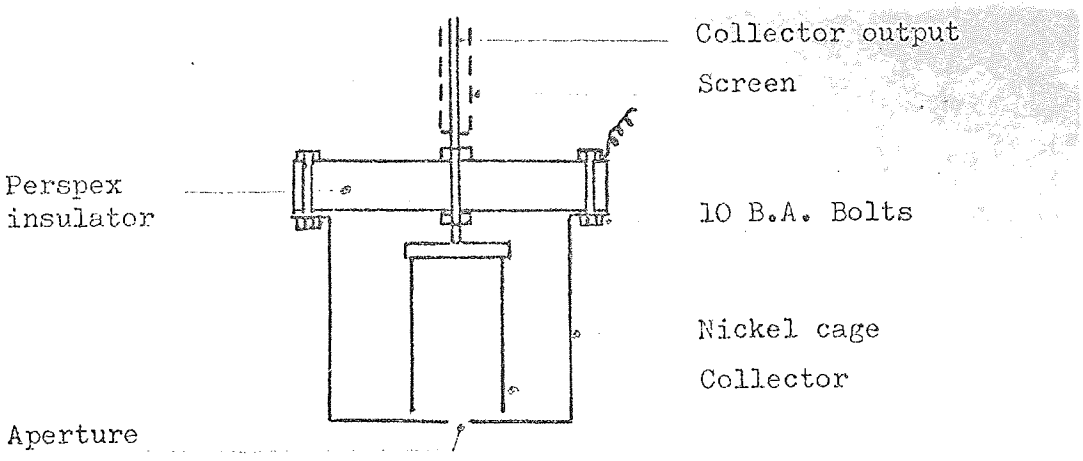

Figure 23

The collector assembly was mounted on a perspex slide in such a way that it could be moved in the x, y and z directions as shown in Figure 24. The oscillator was mounted in the high vacuum system described in chapter 3.

4.3. The Electrical Circuit

The circuit used for the twin wire ion source - hereafter called the ion source - is shown in Figure 25. The circuit is essentially the same as used before. The bias to the collector and Faraday cage V_c and V_f respectively were supplied initially by dry batteries. The lead to the collector cup contained within the Faraday cage was screened using co-axial cable, and the lead to the cage itself was coated with a plastic insulation layer.

4.4. Ion Beam Density Distribution

With a gas pressure of 5×10^{-4} torr in the chamber a glow discharge was struck with the applied voltage at 8 Kv and a tube

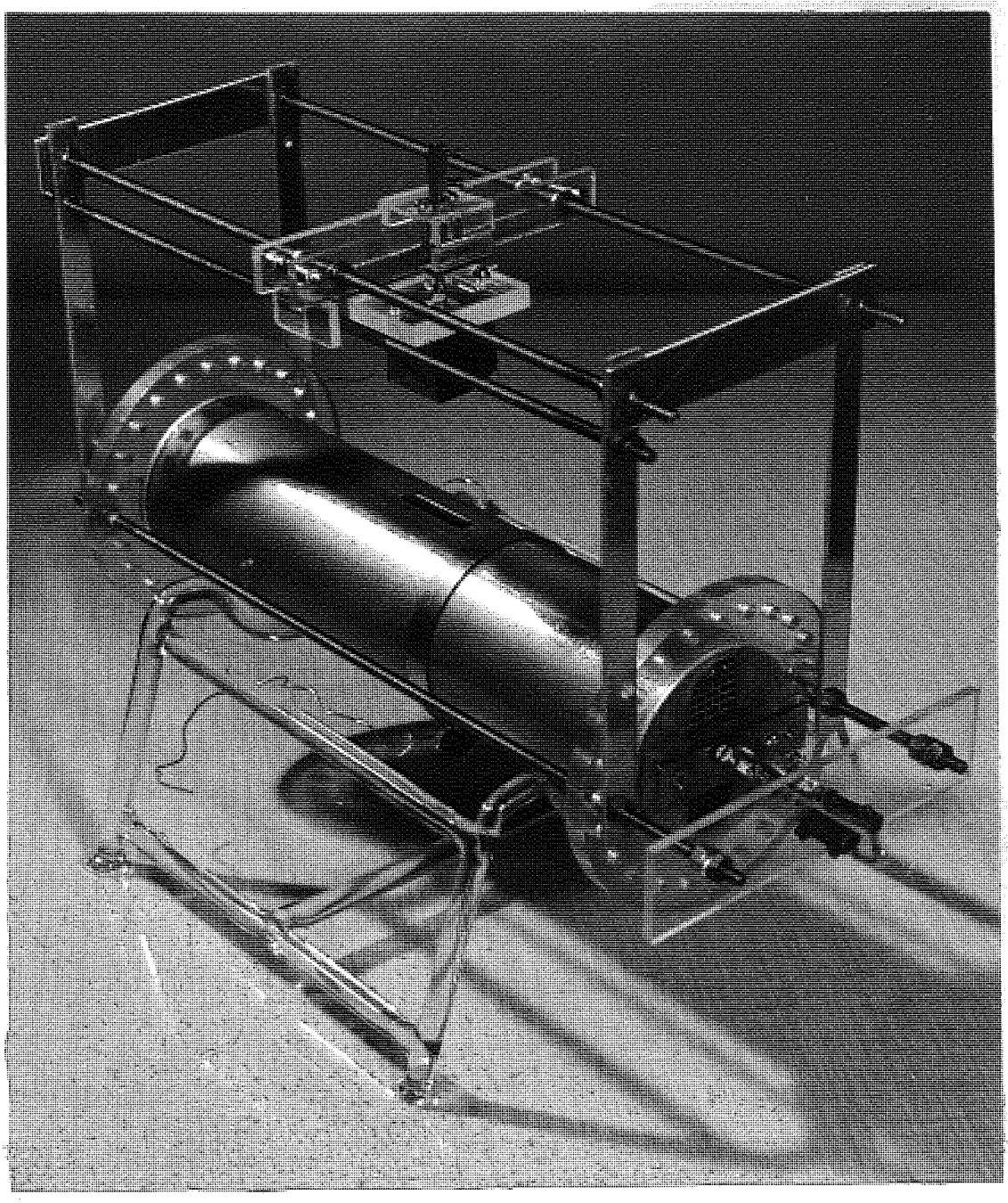

Figure 24

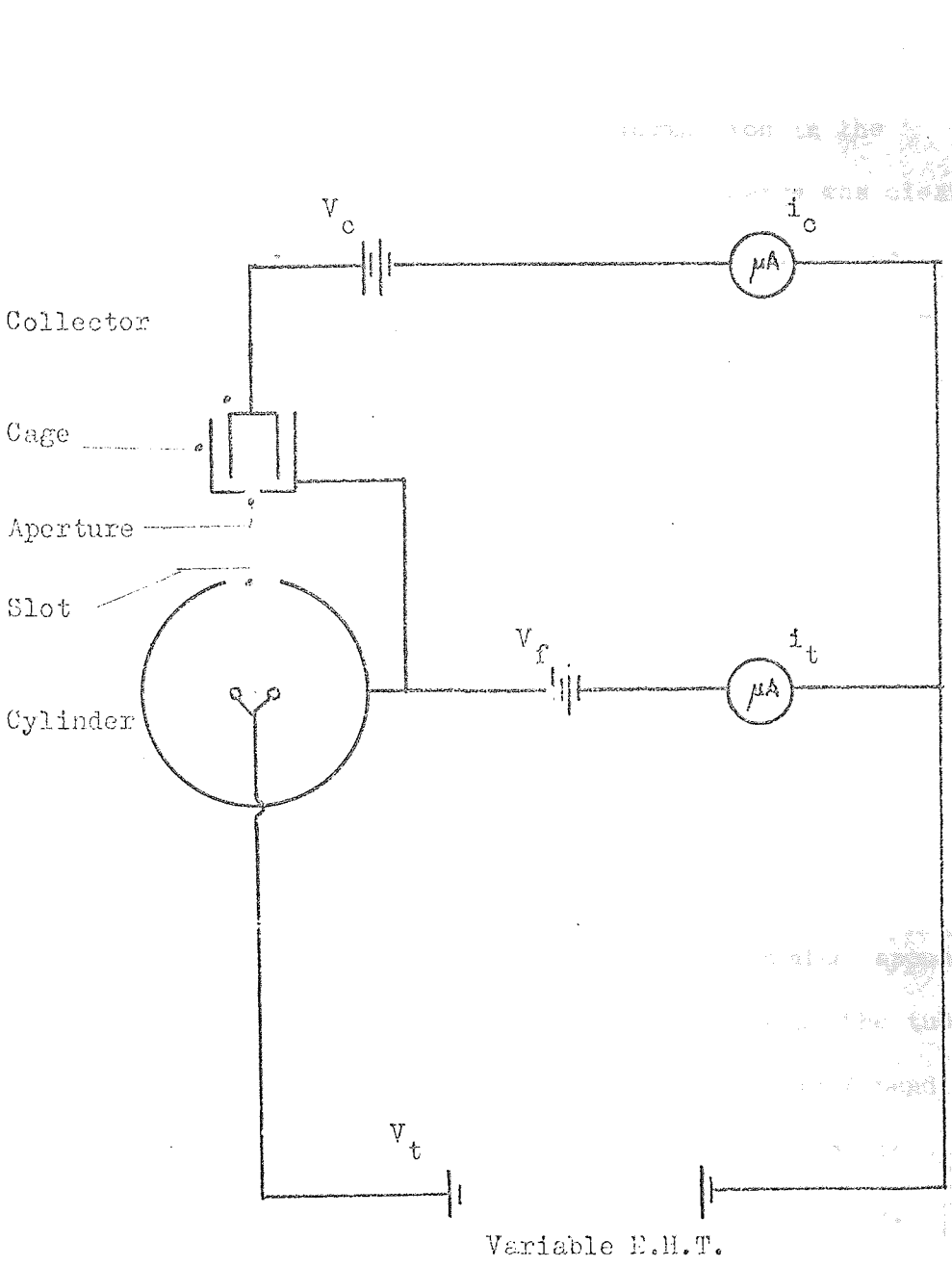
V_c
i_c
μA
Collector
Cage
Aperture
Slot
Cylinder
V_f
i_t
μA
V_t
Variable E.H.T.

Figure 25

current of 5mA. With the intensity of illumination in the laboratory sufficiently reduced a collimated discharge was clearly visible emerging from the slot as shown in Figure 26. When viewed from the end on position - i.e. the xy plane - the beam appeared to diverge at an angle estimated at 5 to 10^{o}. In the yz direction the beam appeared parallel sided and no divergence was apparent. The shape of the emergent beam supports the previous measurements and theoretical predictions in the following way. Since positive ions produced within the cylinder tend to travel along field lines they tend to travel radially except in the immediate vicinity of the anode wires. Consequently there will be a tendency for ions to diverge in the xy plane. Consequently any excitations or recombinations occuring in this plane are expected to give rise to a discharge which also appears divergent. Similarly in the yz plane at the centre of the tube there are no field lines in the z direction as shown in Appendix II. Thus all ions are accelerated parallel to the y axis and the resultant discharge appears well collimated in the yz plane.

Observation of the visible discharge thus served to give an approximate representation of the ion beam density (ρ_c) distribution. In order to measure the beam density the Faraday cage was initially positioned vertically above the centre of the slot, that is on the y axis at a distance of 7 cms from the plane of the anode wires. The Faraday cage represented an effective collecting area of 0.075 cm which corresponds to the area of the aperture in the cage. Values of ρ_c have been expressed as

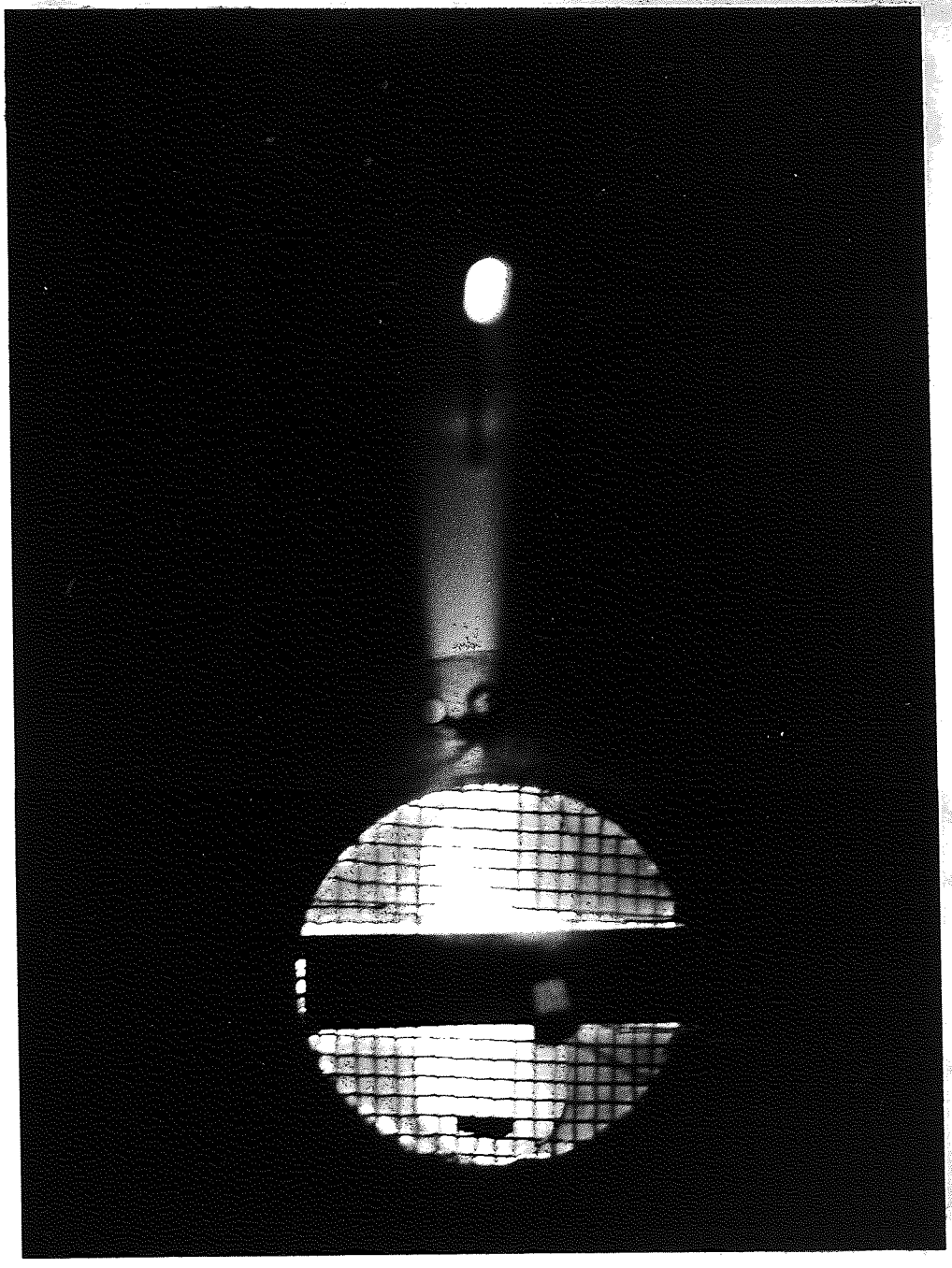

Figure 26

μ A cm^{-2}. The cage aperture was chosen so that the measurements recorded corresponded reasonably well to a point aperture but at the same time allowed sufficiently large currents to be recorded with a reasonable degree of accuracy on the microammeter. In order to check on the effectiveness of the cage the value of V_c was put at 0 volts - at which it remained for the rest of the beam density measurements - and the cage was held at 12 volts negative with respect to the collector. Thus any secondary electrons produced in the collector were repelled by the cage and returned to the collector. With a tube current i_t of 5 mA the beam density collected was 47μ A cm^{-2}. With the cylinder, cage, and collector all the same potential the density was recorded as 50μ A cm^{-2} i.e. not appreciably different from the case when a very small bias was applied as above. However when the cage was disconnected from the circuit as shown in Figure 25, and held at a positive potential of 12 volts with respect to both the cylinder and the collector, with i_t at 5mA the beam density reaching the collector was only 10μ A cm^{-2} which indicated as expected that a small positive bias on the cage alone screened the collector from incoming ions. Consequently the circuit was reconnected as shown and V_f made 0 volts for the remainder of the beam density measurements. In general measurements made with a bias applied to the cage or collector were more difficult to interpret. This will be illustrated in more detail later in this chapter. With no bias applied to either electrode however the values of ρ_c are in good agreement with those indicated by the sputtering of the cylinder

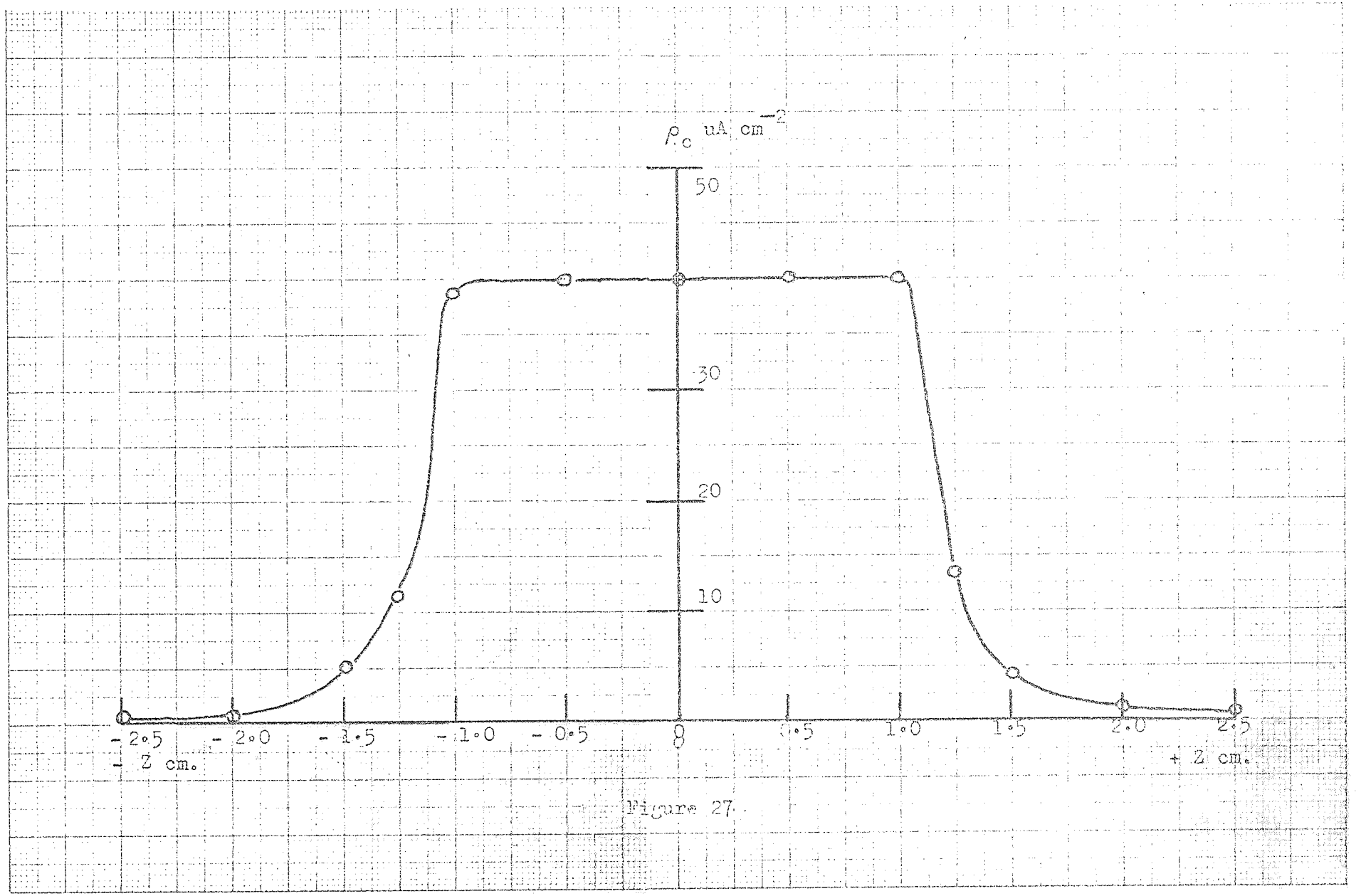

Figure 27.

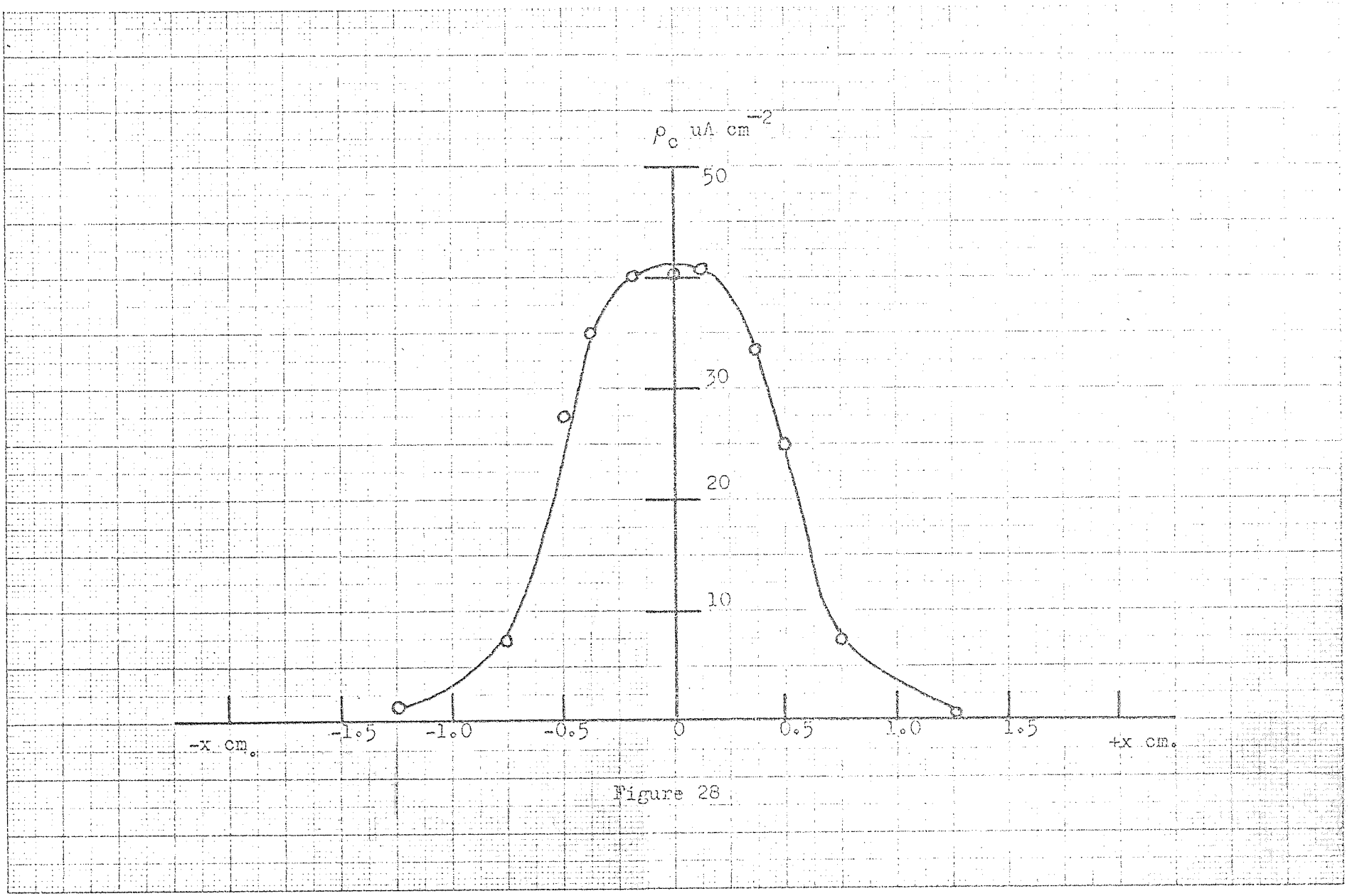

Figure 28

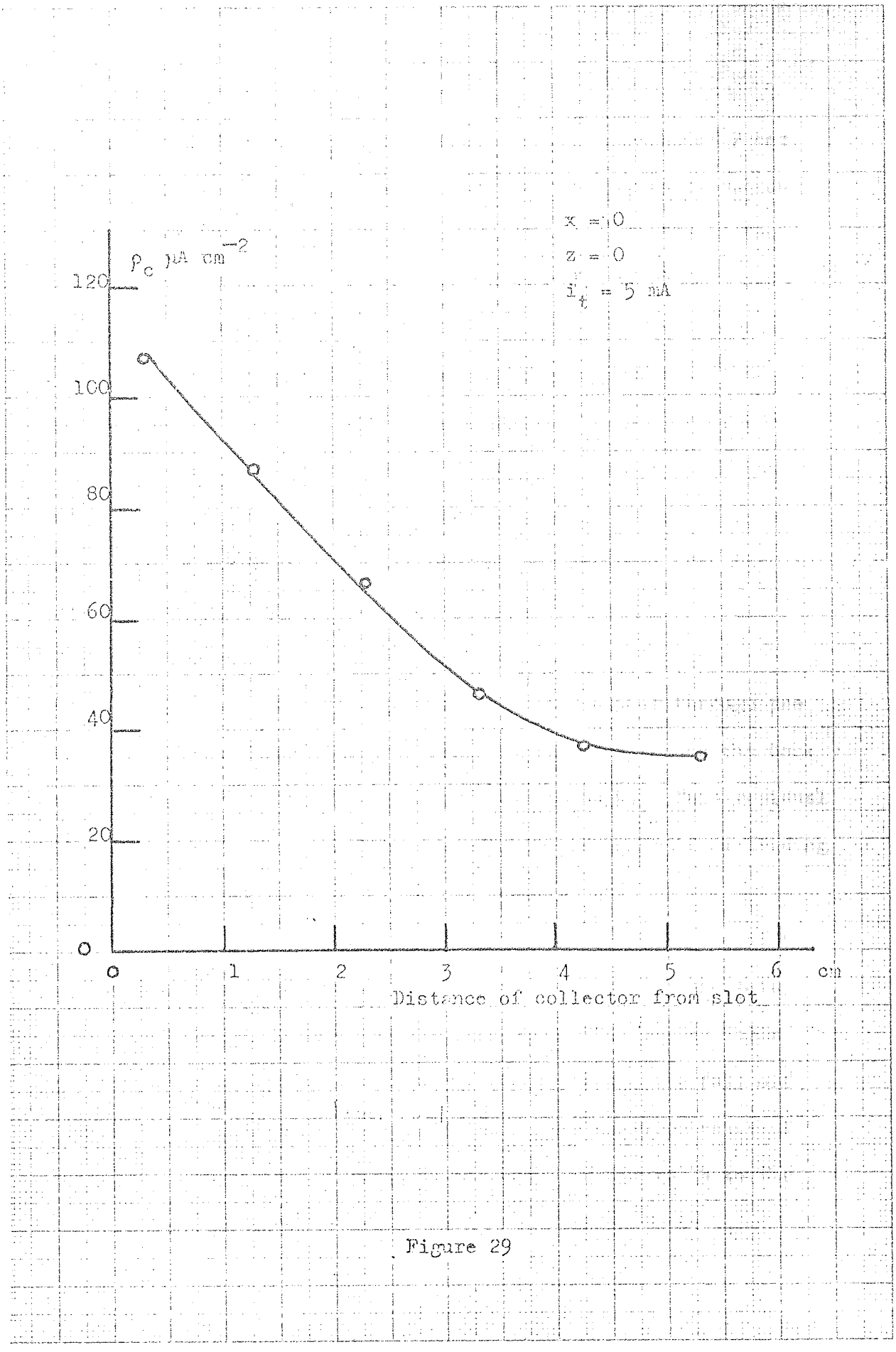
x = 0
z = 0
i_t = 5 mA
ρ_c μA cm^{-2}
120
100
80
60
40
20
0
0
1
2
3
4
5
6
cm
Distance of collector from slot

Figure 29

as explained in section 4.1.

With the cage aperture maintained at a height of 7 cms from the plane of the anode wires the beam density distribution was measured in directions both along and perpendicular to the slot as shown in Figure 27 and 28. The shape of these curves are in good agreement with both visual observations and earlier measurements made with a small plate collector. The tail on the curves as indicated are probably due to the finite size of the cage aperture although the distributions indicate that the beam is not so well collimated in the xy plane as in the yz plane - a result to be expected from the previous discussion. The ion density does not fall to zero outside the region of the tail. This is probably due to the backscattering of low energy ions from the bell jar which are subsequently collected either through the aperture of the Faraday cage or small exposed regions on the back of the collector or on the collector feed through. This residual low energy ion current will be shown to be the cause of misleading interpretation of later experimental results.

The Faraday cage was mounted vertically above the slot on the y axis and the density distribution measured along this axis, as shown in Figure 29. As expected the intensity falls off with increased distance from the slot although the fall off does not appear to follow a simple law. The measured value of ρ_c obtained from extrapolation of the curve in Figure 29 to the slot is in good agreement with the density estimated in section 4.1.

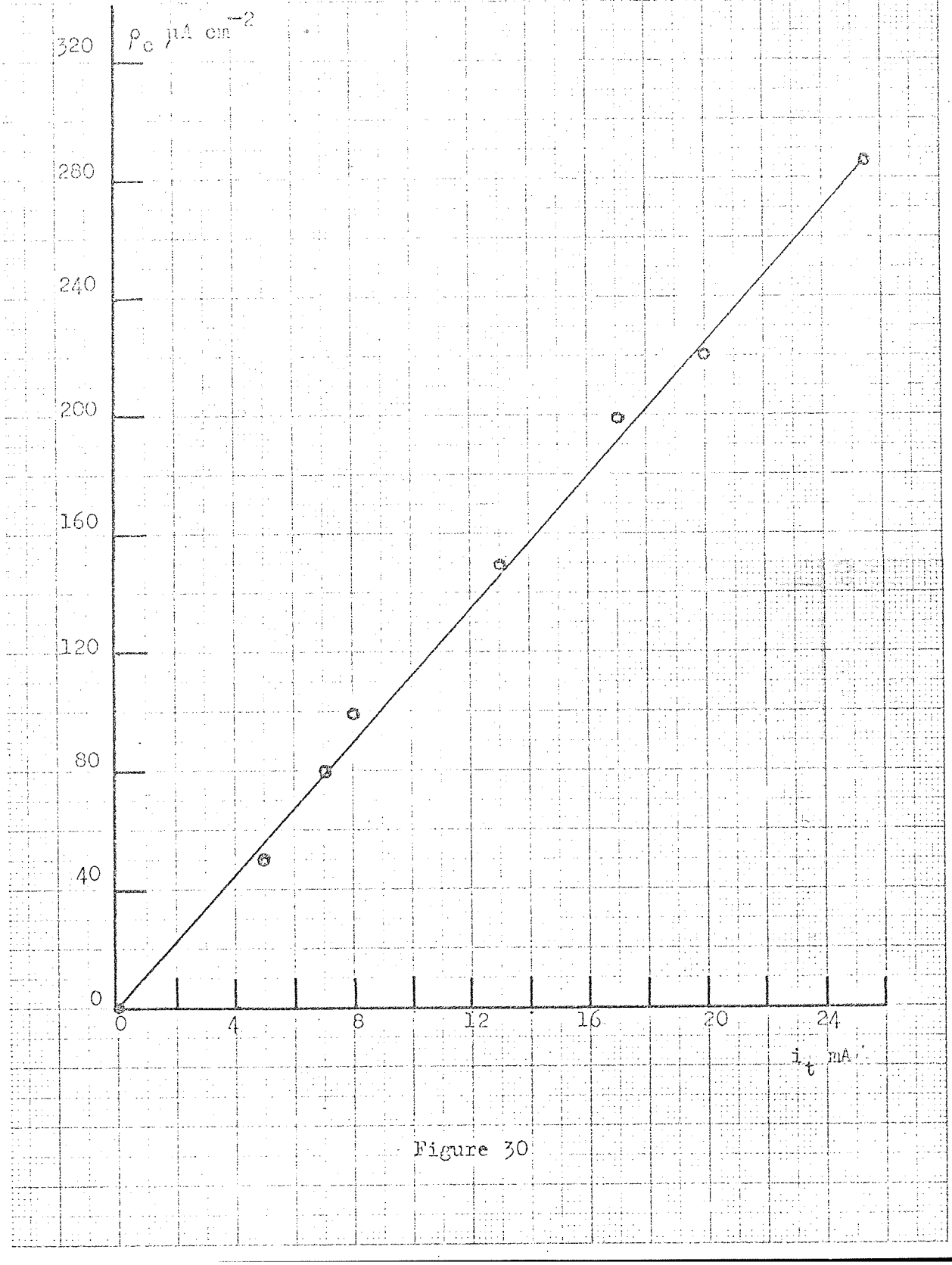

Figure 30

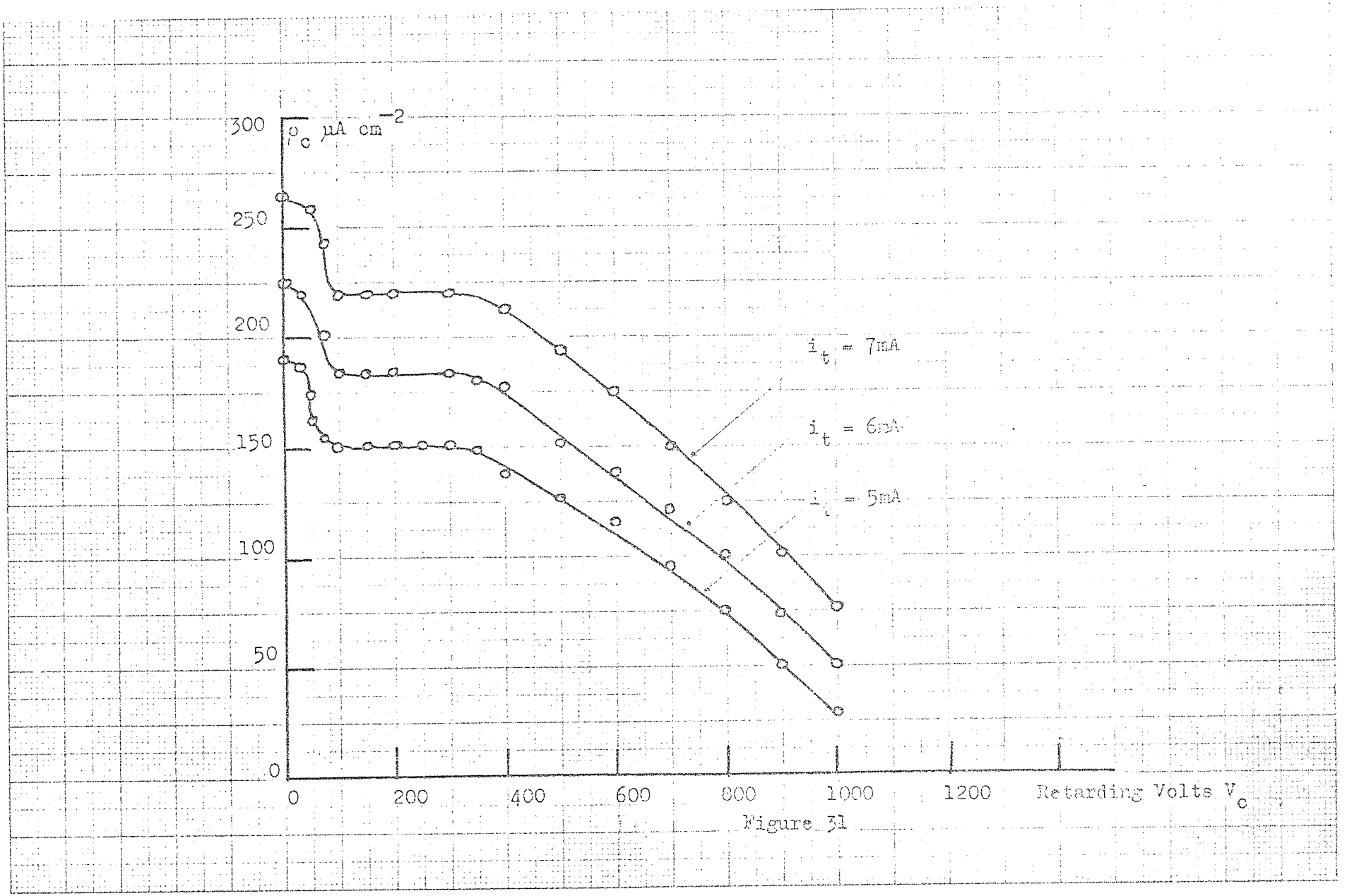
300
250
200
150
100
50
0
i_c μA cm^{-2}
i_t = 7mA
i_t = 6mA
i_t = 5mA
0
200
400
600
800
1000
1200
Retarding Volts V_c

Figure 31

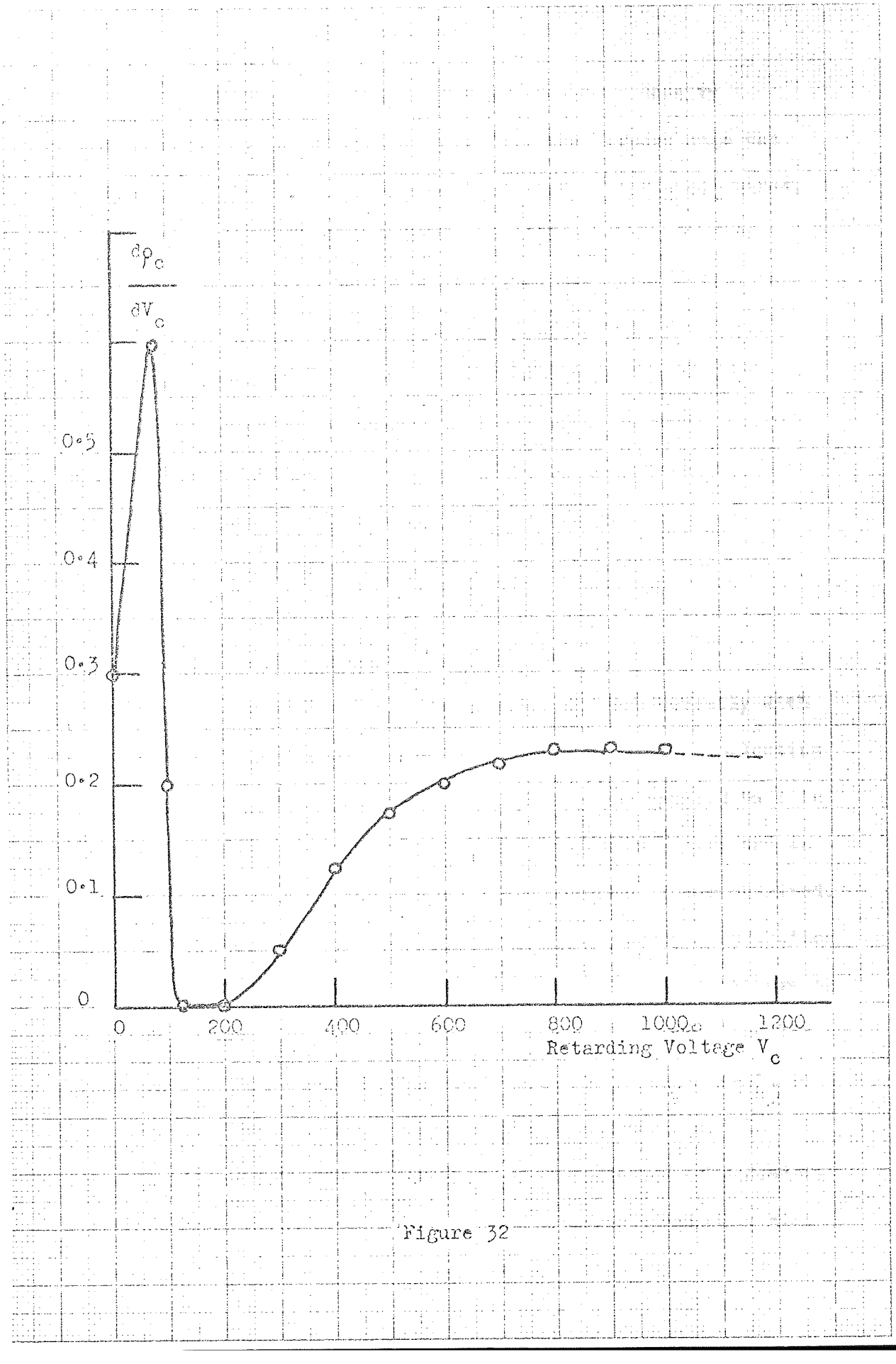
$\frac{d\rho_c}{dV_c}$
0·5
0·4
0·3
0·2
0·1
0
0
200
400
600
800
1000
1200
Retarding Voltage V_c

Figure 32

In order to investigate the maximum beam density possible with the ion source in this form the Faraday cage was mounted on the y axis 4.2 cms from the plane of the anode wires, and the current reaching the collector, i_c, was increased by increasing the potential difference across the tube. With the pressure maintained at 5×10^{-4} torr as before beam densities as high as $300 \mu A\ cm^{-2}$ were recorded as shown in Figure 30, although the anode wires reached such a high temperature due to electron bombardment in the process of obtaining these high beam densities that the perspex end plates were damaged.

4.5. Ion energy distribution

Initial attempts at measuring the energy distribution of the positive ions contained in the beam were made by using the flat plate collector described in section 4.2., and subsequently with a copper cylinder, closed at one end with an effective collecting area of $0.78\ cm^2$. A retarding potential V_c was applied to this collector, and with the chamber pressure at 5×10^{-4} torr and an applied voltage of 5 kV the curve shown in Figure 31 was obtained. Differentiation of this curve leads to the ion energy distribution shown in Figure 32. At first the distribution shown in Figure 32 proved difficult to interpret until it was realised that the low energy peak was probably due to the background of back scattered ions observed in the earlier beam density measurements. In order to eliminate as far as possible the production of secondary electrons from the collector - which was causing spuriously high ion current density readings - as well as screening the collector

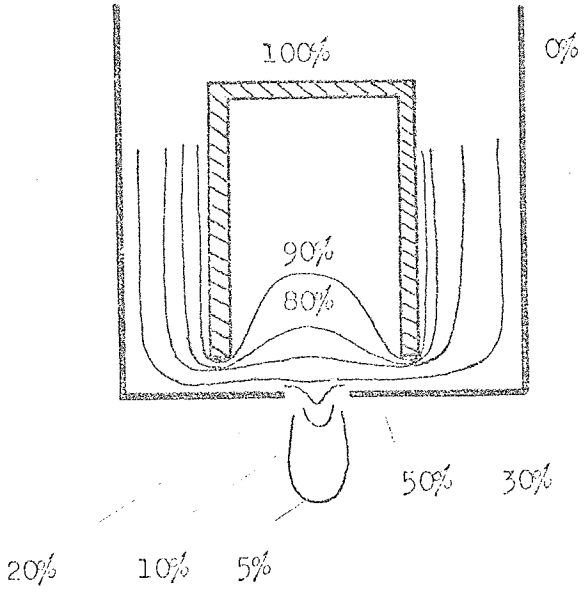

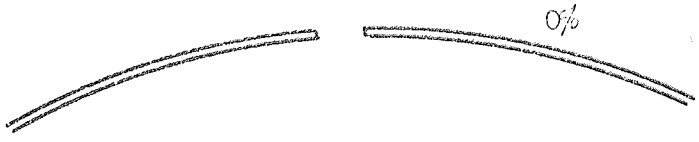

Figure 33

from much of the back scattered ions an attempt was made to use the Faraday cage for measuring the ion energy distribution. However the results obtained from the use of the Faraday cage still showed a marked low energy peak with considerably reduced beam densities, making interpretations of the results extremely difficult. It is likely that the use of a collector in the form described above, and to which a small bias is applied invariably distorts the electrostatic field in the vicinity of the collector causing deflection of the ion beam. Hence it is difficult to measure the ion energies using such a technique. Figure 33 shows a field plot of a Faraday cage, with a biased collector illustrating the relatively large amount of field disturbance in the vicinity of the aperture, supporting this viewpoint.

Some of the difficulties associated with the measurement of electron energy distributions in various discharges have been discussed by Barnes [52] and these indicate that the measurement of electron or ion energies can be rather complicated. It was therefore felt necessary that in the first instance an alternative technique should be used in order to obtain at least a qualitative idea of the energy spectrum.

Prior to the experimental work discussed so far in this section it had been noted that the oscillator had been cleaned by ion bombardment as explained in section 4.1, and also that the base of the Faraday cage had been polished by the

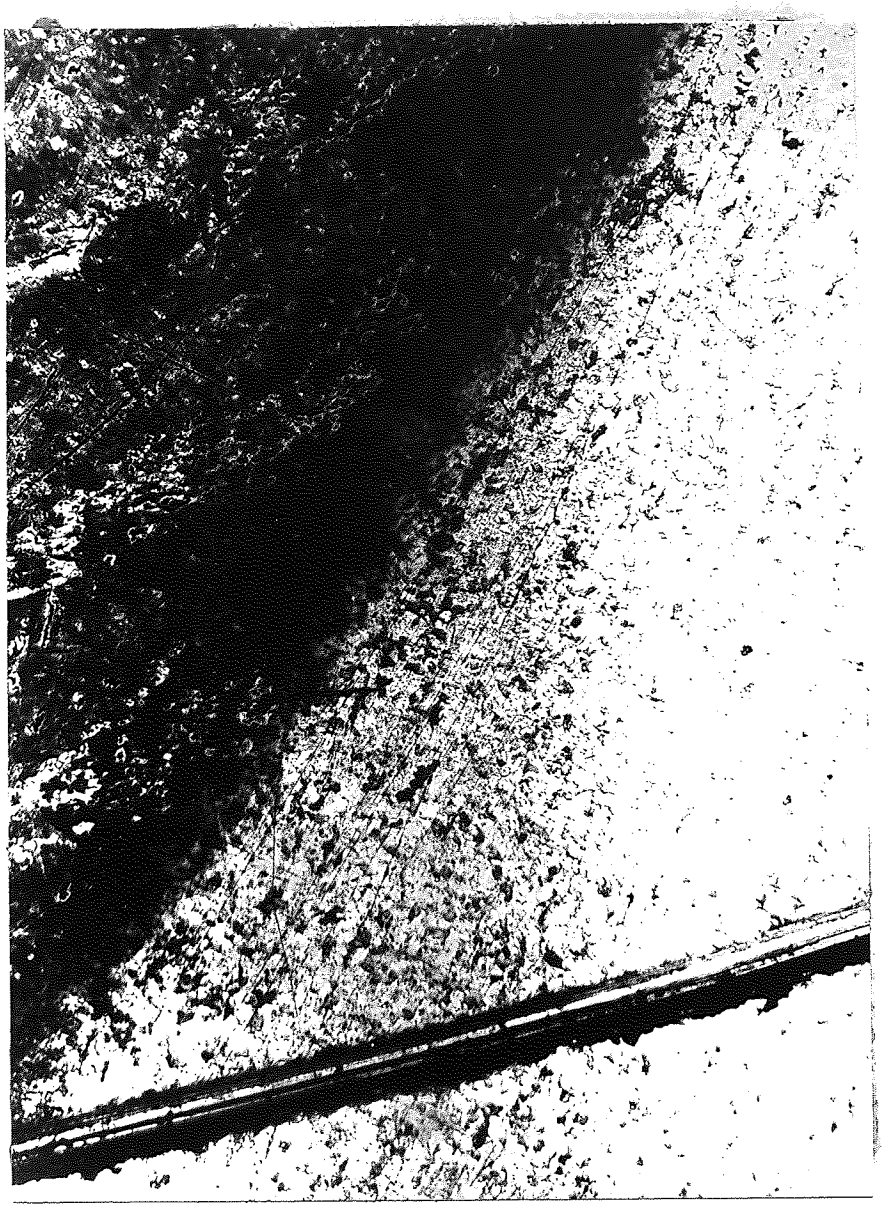

Figure 34

emergent ion beam. Figure 34 is an optical micrograph showing both the polished or etched region and the contaminated, unpolished, region. It is well known that the sputtering rate of many materials depends on the number of incident particles in unit time and also on their mean energy. It therefore appeared that measurement of the sputtering rate of a known material placed in the ion beam would yield an estimate of the average beam energy.

4.6. Ion etching technique

Sputtering rate measurements were made using the weight loss technique of Laegreid and Wehner [53] in which the sample under investigation is bombarded by ions for a period ranging from several minutes to several hours, depending upon the nature of the target material. The target loses weight according to the equation.

$$\text{yield } Y = \frac{10^5 \times (\text{Wt. loss in grams})}{\text{A.W.} \times I^+ \times T} \quad \ldots \quad (12)$$

when Y = yield in atoms per ion

A.W. = atomic weight of the target material

I^+ = ion current received by the target

T = time of bombardment in seconds.

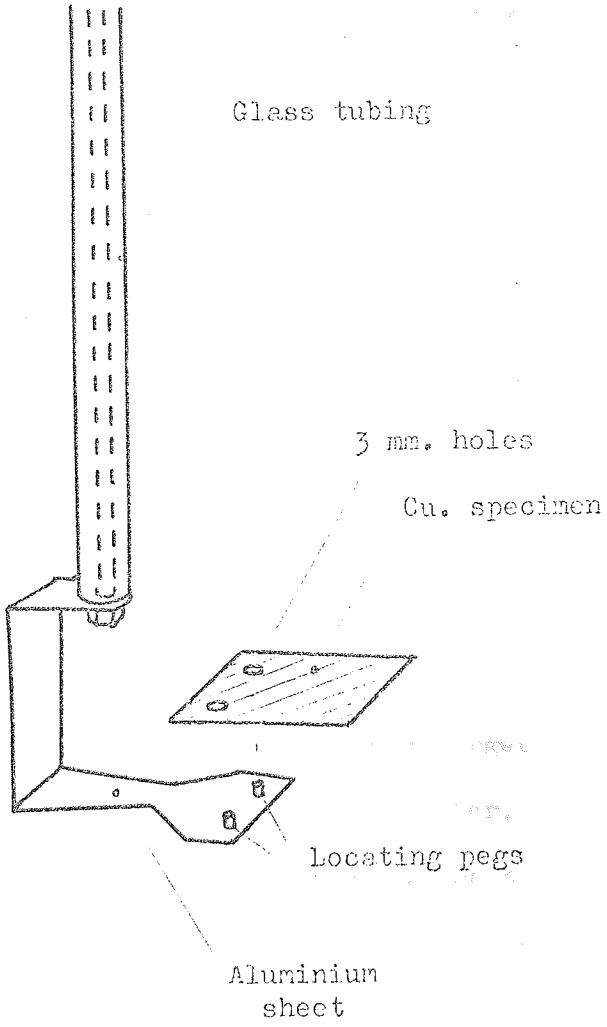
Glass tubing
3 mm. holes
Cu. specimen
Locating pegs
Aluminium sheet

Figure 35

Copper was chosen as the target material firstly because it has a very high yield rate compared with other metals and secondly because there is a considerable amount of data available concerning the etching of copper particularly with argon ions. The copper targets were made from thin OFHC copper sheet cut 2 cm square with two 0.3 cm holes drilled 1 cm apart on one edge. These targets were then cleaned in concentrated sulphuric acid, washed in distilled water and then stored in an evacuated dessicator. The targets - or samples - were carefully weighed prior to mounting them on the target holder shown in Figure 35. Since weighing was carried out to 5 places of decimals and also because the loss of weight of the samples was small considerable care was taken in handling the target material, using nylon gloves and tweezers. It was also important to avoid touching the face of the target because of the risk of contamination, as will be shown later. The sample was mounted 2 cms above the slot in the cylinder so that its plane was normal to the emergent ion beam, and so that it was centred on the y axis.

The assembly described above was placed in the high vacuum chamber described previously and facilities were arranged so that argon could be bled into the chamber via the leak valve.

The electrical circuit used was essentially the same as that of Figure 25, except that the Faraday cage was replaced by the target and that V_c and V_f were both made zero volts.

4.7 Experimental Results.

With the above arrangement the chamber was pumped down

to 10^{-5} torr and then flushed with argon via the leak valve, with the diffusion pump baffle valve closed. The chamber was then evacuated a second time and with a steady leak of argon into the system an equilibrium pressure in the chamber of 5×10^{-4} torr for argon was recorded. Because of the variation of ion gauge sensitivity with gas composition it was decided that all pressures would be quoted in terms or argon pressure throughout the sputtering experiments.

In order to measure the current collected by the specimen in the ensuing experiments reference was made to the earlier beam density experiments of section 4.4. With the target in the position described in section 4.6, the ion density on the y axis 2 cms above the slot was $65 \mu A\ cm^{-2}$ (after correction had been made for the residual background of low energy ions) with a tube current i_t of 5 mA. Consequently with this tube current chosen for the following experiments equation (12) becomes:-

$$Y = \frac{2.44 \times 10^{7} \times W}{T \times \delta A} \quad \text{atoms per ion} \qquad (13)$$

when W = weight loss of the sample in grams

δA = sputtered area of the target in cm^2.

The first sample placed in the chamber was bombarded for 6 minutes with argon ions, the chamber pressure being 5×10^{-4} torr obtained as described previously. The anode voltage V_t was 7.5 kV. After bombardment the chamber was let up to air and the specimen inspected. The region of ion bombardment was clearly

defined but was also heavily contaminated. Contamination of the sample could have been due to a number of possible causes; for example grease on the tungsten anode wires could have been deposited on the target, or the vacuum chamber had not been flushed with argon adequately, no cold trap had been used and the sample had been exposed to the air too rapidly after bombardment with the result that the hot sample became oxidised. Alternatively the H.T. on the anodes had been increased too slowly so that initially the ion beam density was rather low. Laegreid Wehner and Meckel [54], Laegreid and Wehner [53], Wehner [51], Hagstrum and D'Amico [55] and others, have shown that in order to avoid contamination it is necessary to observe two main points. Firstly that the gas pressure is below 10^{-2} torr and secondly that the beam density ρ_c should be as high as possible. The limitations on the beam density depend on the type of vacuum system, the target material and any other potential source of contaminating material contained within the system.

In order to overcome the problem of contamination the following processes were adhered to. The anode wires were cleaned with fine emery paper each time the ion source was dismantled. The vacuum chamber was flushed at least three times before sputtering commenced, liquid nitrogen was used in the cold trap and the sample was not exposed to the atmosphere for ½ hour after sputtering had ceased. The H.T. was increased rapidly until the required tube current i_t was obtained. It was found that whenever one or more of these precautions were

Sputtering of Copper

Data from Yield rates.

Figure 36

Anode Volts	Approximate Yield.	Average Ion Energy.
(Kv.)	(Atoms/Ion)	(Kv.)
8.0	6.0	>5.0
7.0	5.0	4.0
6.0	4.5	2.0
5.0	2.0	1.0
4.0	0.7	0.6

Figure 37

Etch Width data.

Anode Volts	Average Ion Energy.
(Kv.)	(Kv.)
8.0	6.4
7.0	4.2
6.0	1.9
5.0	0.9
4.0	0.7

neglected contamination occured.

A series of copper samples were etched, the region of the etch being clearly visible, and appearing cleaner than the original unetched surface. The samples were etched for periods varying between ½ and 1 hour. The weight losses of the samples were in the region of 1 milligram or about ¼ % of the original sample weight. The variation of the yield calculated using equation (13), with applied volts is shown in Figure 36. Although it was thought that the values obtained for the yield may be high because of initial cleaning of the impurities of the copper surface, the results are in good agreement with those of other workers e.g. Almen and Bruce [56] and Keywell [57]. Using the data collected by Keywell [57] the corresponding average ion energies are displayed on Figure 37. From these figures it can be seen that the average ion energy in the oscillator varied from 0.20 to 0.83 of the applied volts. At first these values seemed rather high although Wear [58] had shown that ion energies in Penning sputter ion pumps vary from 0.5 to 0.8 of the applied pump potential.

It was noticed that on each of the copper samples the width of the etched region corresponding to the xx scan of the Faraday cage was strongly dependent on the anode potential. For example the width of the etched region with the applied volts at 8 kV was 9 mm, whereas with the applied volts at 4kV it was 19 mm. The slot in the oscillator cylinder acted as a cylindrical electrostatic lens with a focal length which was dependent on the cylinder radius and the ion energy. By measuring the width of

the etch and determining the focal length of the slot it has been possible to calculate the starting point of the ions in the oscillator corresponding to the given anode potential. The results are shown in Figure 37 and the calculations in Appendix IV. It can be seen that the ion energies calculated from sputtering data, and from measurement of the width of the etched region are in reasonable agreement. At higher anode potentials the etch width method indicated lower ion energies than the results from the sputtering data which supports the argument that the sputtering yields from the copper samples are high.

In order to investigate the process of sputtering further and at the same time obtain more accurate measurements of the yield, it was necessary to obtain samples upon which more accurate measurements could be made. With a typical weight loss of 1 milligram and an etched area of 1.5 cm^2 it was calculated that a step should be visible on the sample with a depth of about 1 micron. The original copper samples had such an uneven surface from a microscopic viewpoint that the step was not easily distinguished. Furthermore Holland [59], Wehner [51] and others have shown that the sputtering yield varies considerably with the angle of incidence that the bombarding ion makes with the surface of the metal. Consequently, the yield from a rough surface is difficult to interpret. Thus it became necessary to use a specimen with a flat smooth surface.

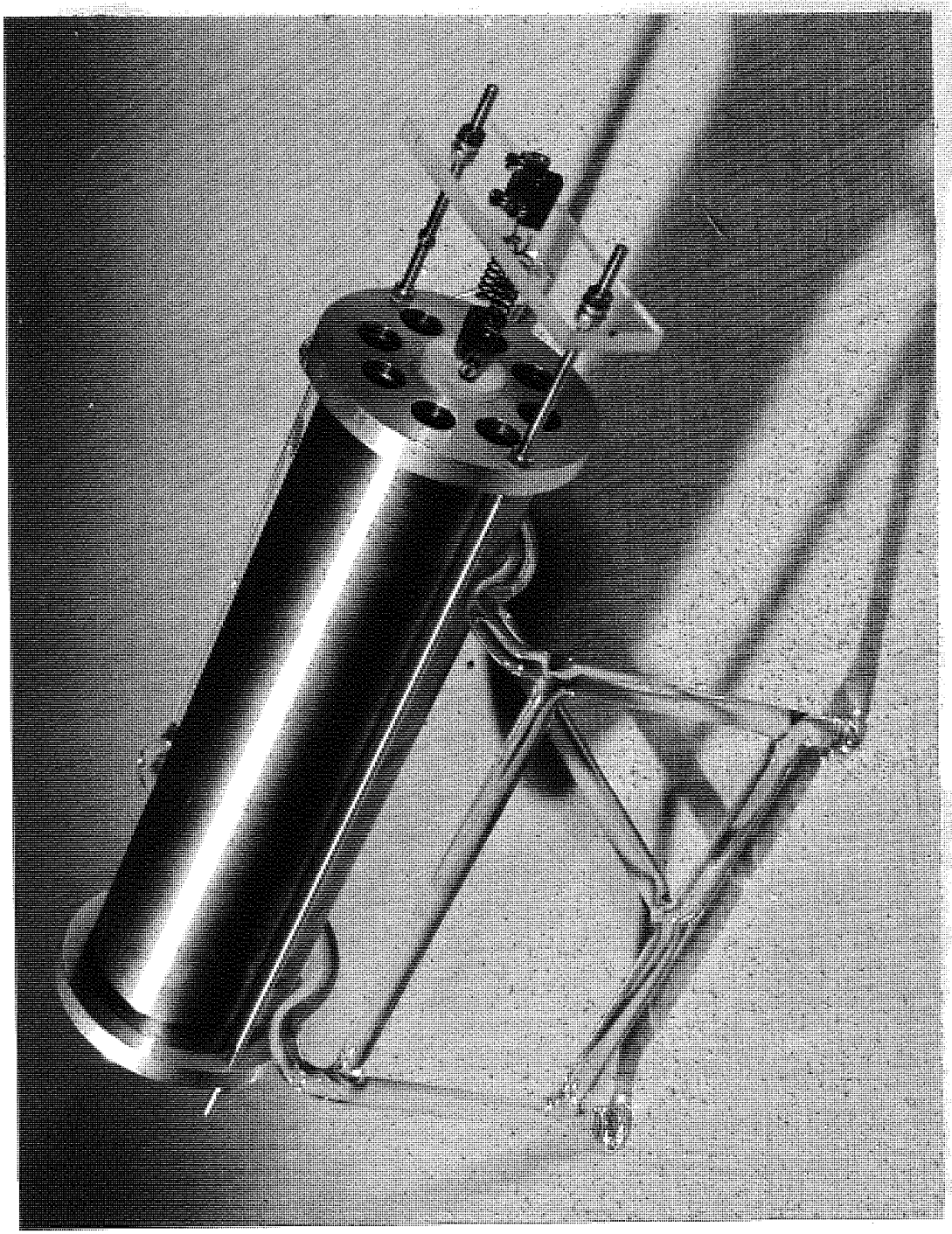

Figure 38

4.8. Etching of highly polished specimens

Because of the high anode temperatures obtained during these experiments - over 2000°c - it became necessary to re-design the end plates of the oscillator. A new set of end plates were constructed from duralumin as shown in Figure 38, and modified spring loading of the anode wires was used which enabled the oscillator to be used with higher discharge currents without the problems of arcing across the end plates previously experienced.

Flat surfaces of copper were produced by evaporating a thin film of OFHC copper onto glass microscope slides. These were mounted onto the target holder by means of small clips. The fragile nature of the slides coupled with the care taken in handling made this process rather difficult. Using the technique described previously these samples were etched using applied voltages between 6.5 and 9 kV. Since the copper films were only a few thousand Angstrom Units thick the ion beam stripped these completely off the glass, in about 6 minutes. The yield values calculated using this arrangement ranged from about 2.5 atoms/ion for V_t = 7 kV to 4 atoms/ion for V_t = 9 kV. However, these results cannot be taken as representative of the bulk material for two reasons. Firstly, the properties of thin films vary considerably from the properties of the bulk materials, and secondly, the total removal of the film means that for part of the sputtering time the ions were bombarding nothing but the glass substrate. As a result of these

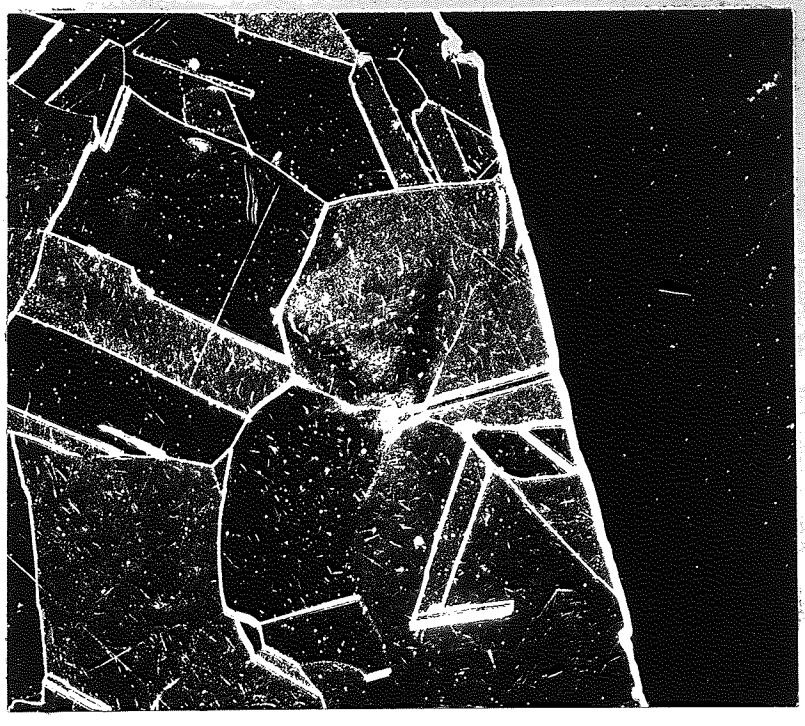

(a)

(b)

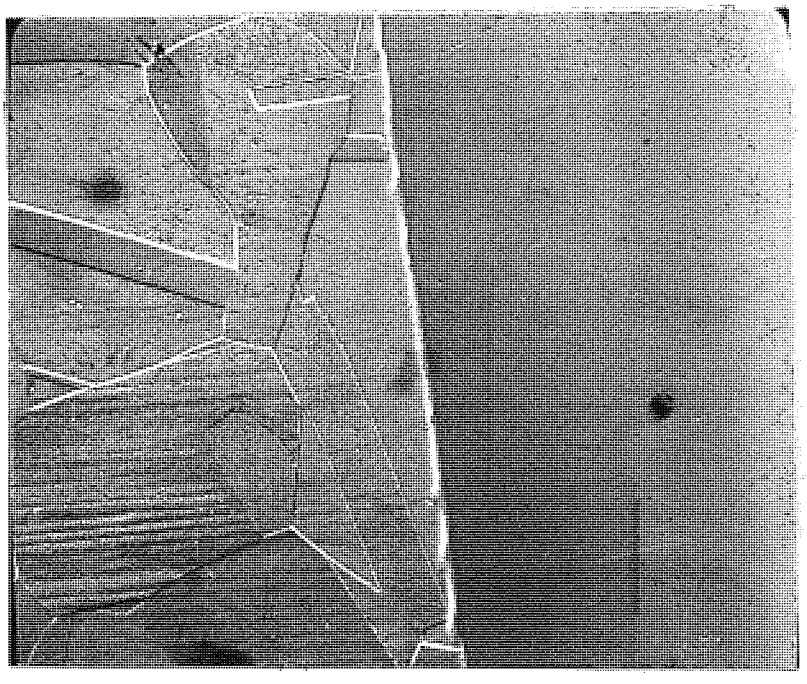

Figure 39

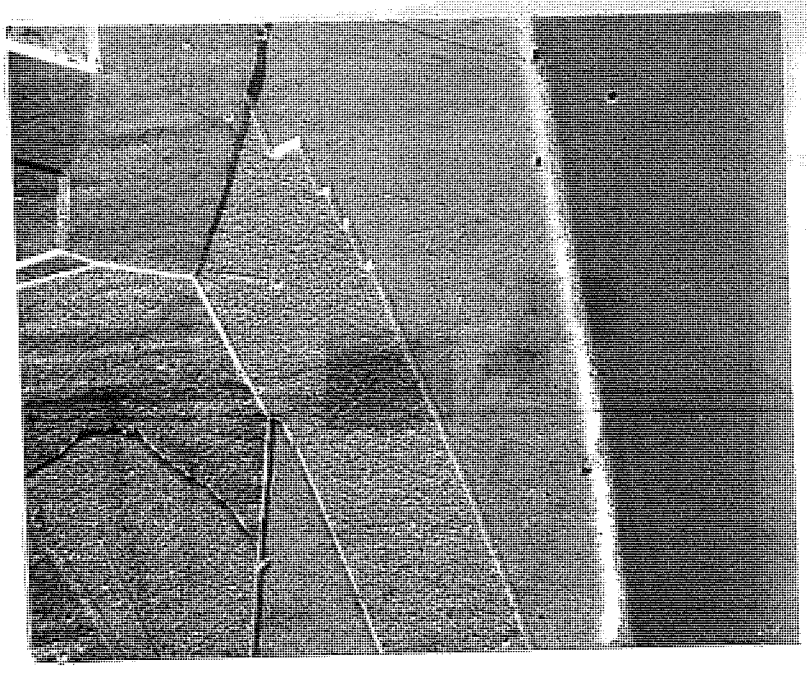

(c)

(d)

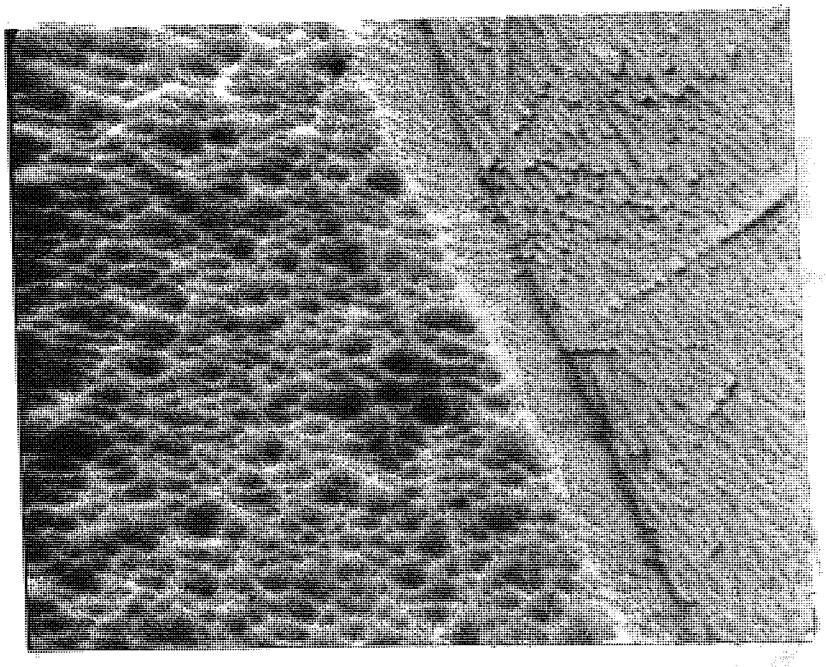

Figure 39

experiments arrangements were made through Dr. A.H. McIlraith and the Division of Inorganic and Metallic Structures at the N.P.L. for the preparation of some highly polished copper specimens. The preparation entailed the successive polishing of copper with progressively finer grain sized diamond grit, until the peak to trough ratio of the final surface was no greater than a few hundred Angstrom units.

The sample was etched on the modified ion source apparatus using exactly the same technique as described previously. The anode voltage was 8 kV with respect to the cylinder and the anode wires reached a temperature of 2880°c. The modified anode tensioning made the control of the discharge current very simple without the tendency to fluctuate that had been observed previously.

Figure 39(a) is an optical dark field micrograph viewed normal to the surface of the sample, magnified 240x. The shadow edge can be clearly seen with the original unetched surface to the right and the etched surface to the left. The ion etching has revealed the polycrystalline nature of the copper surface.

Figure 39(b) is a scanning electron micrograph of magnification 260 x viewed normal to the surface, which also reveals the shadow edge and the polycrystalline nature of the etched surface. The original surface to the right appears very smooth. Figure 39(c) is the same view magnified further - total magnification 640 x - which reveals considerable difference between the individual crystals. The dark rectangle in the

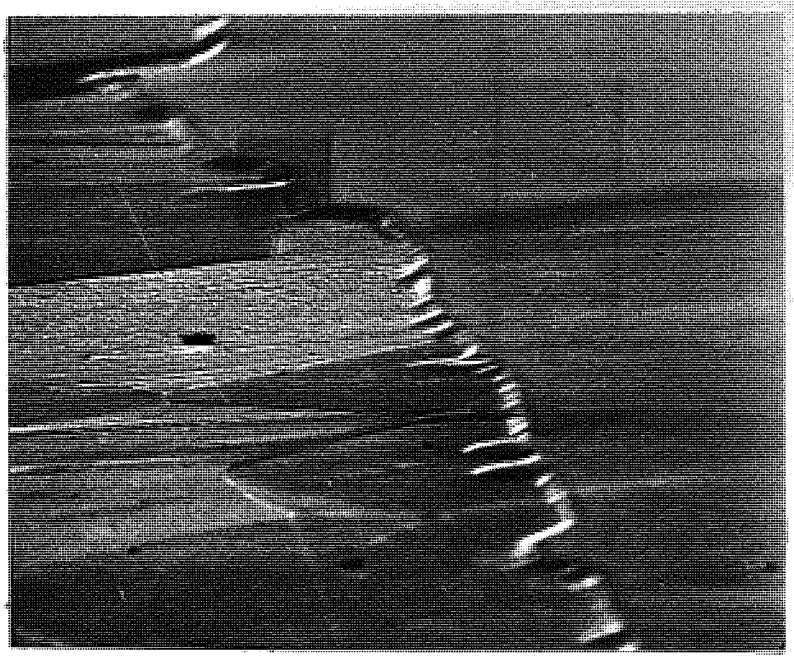

(e)

(f)

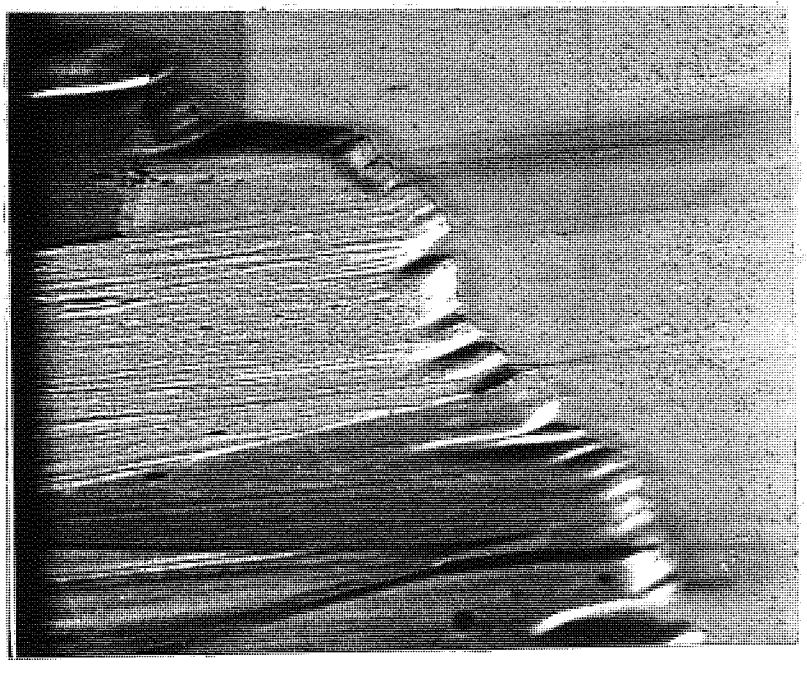

Figure 39

centre is the area shown in the scanning electron micrograph 39(d) and reveals a twin grain boundary at a magnification of 6300 x. The difference between the individual crystals is even more noticeable in this photograph.

Figures 39(e) and 39(f) are also scanning electron micrographs viewed at an angle of 15° to the surface. The magnifications are 600 x and 1200 x respectively. From these figures the 'step' etched into the surface is clearly visible and has an estimated depth of about 1 micron. It is interesting to note the flatness of the etched as well as the un-etched regions.

The etching of these highly polished specimens provided conclusive evidence firstly that ions from the ion source were capable of etching and secondly that they were of sufficiently high energy and present in sufficient quantity to produce a fairly high sputtering rate of about a milligram per hour. The yield of the above sample was calculated at about 5 atoms per ion, and for a second sample at about 6 atoms per ion. These yields give ion energies in fairly good agreement with the energies previously obtained by other methods.

It was interesting to note that the copper sputtered from the polished samples was deposited on the oscillator cylinder around the edge of the slot immediately below the sample.

4.9. Conclusions

4.9.1. Conclusions from the density distribution

The ion beam which was allowed to escape from the slot in the oscillator cylinder appeared to be well collimated with an angular divergence of about 5^{o} in one direction and parallel in the other. As expected the beam density was highest in the centre of the slot and decreased with increasing distance from the cylinder. Beam densities up to 300 μA cm^{-2} were obtained at pressures of only 5×10^{-4} torr, which compares favourably with the Penning ion sources described by Wehner [51] in which typical beam densities were about 100 μA cm^{-2} at similar pressures.

It is envisaged that future work on the measurement of ion beam densities would focus some attenion on the problem of eliminating the low energy background of back scattered ions, perhaps by using a Faraday cage with a very narrow acceptance angle and improved screening of the electrical leads.

4.9.2 Conclusions from the measurements of ion energy

These are necessarily less precise because of the general difficulty found in measuring the energy distribution. An estimate of the energy distribution can be made from the curve of Figure 32., although this curve is incomplete because of imprecise ion density measurements.

The methods of measuring sputtering yield and etch width give results related to the average ion energy only.

However, these results are in good agreement, and the average ion energy has been measured as 0.2 to 0.8 of the applied volts - a fairly broad distribution, but in good agreement with the literature published [58] on Penning discharges.

Because of the high ion energies which can be obtained from the oscillator, together with the high beam densities at low operating pressures the oscillator has considerable potential as an ion source, although in its present form not as a monoenergetic ion source. It is expected that future work will investigate the energy distribution further, with perhaps some attention paid to obtaining a narrow energy band. The ways in which the energy spectrum is investigated could include, for example, the use of a large collector cylinder concentric to the existing oscillator cylinder with a greater diameter to which a retarding potential is applied. Alternatively, a Langmuir probe could be used to study the discharge possibly even inside the oscillator cylinder. The use of concentric cylindrical grids within the oscillator cylinder is a further possible method of measuring the ion energies. However, it will be shown in the following chapter that this may not be desirable because of the perturbation effect of the grid on the electrostatic field at the walls of the oscillator.

4.9.3. Advantages of the oscillator as an ion source.

In its present form the oscillator has several advantages over existing commercial ion sources. The oscillator

ion source operates at very low pressures when compared with high density sources. A discharge can be maintained to pressures as low as 10^{-6} torr. The ion beam can be extracted therefore at pressures several orders lower than most commercial ion sources which operate with high current densities. Only Penning ion sources operate at comparable pressures and beam densities. A practical form of a Penning ion source has for example been described by Holland [59].

The oscillator ion source however has several advantages over the Penning source. Firstly, it is entirely electrostatic and therefore does not require a bulky and expensive magnet - including the limitations frequently imposed by a magnetic field. Secondly, the emergent beam is extremely well collimated without the necessity of using separate ion lenses. Finally, the oscillator is extremely simple and robust in construction even in its present form. The oscillator as an ion source therefore looks particularly attractive.

4.9.4. Applications of the oscillator as an ion source.

The oscillator in its present form has the same possible applications that any other high current high voltage source has, although the oscillator source has several advantages over the commercial sources as described in section 4.9.3. Particular applications include ion etching, ion polishing and ion thinning which have all been investigated and described in this chapter.

These processes require ion beams of several KeV and of density ranging between 30 μA cm^{-2} and 300 μA cm^{-2}. Recently, interest has arisen in ion polishing and thinning not only of metallic samples but also of ceramics. Although this application has not been investigated there appears no obvious reason why the oscillator ion source should not be useful in this field.

The oscillator also has potential as an ion source for application in the field of mass spectrometry, and with a thermionic source of electrons if the discharge cannot be maintained below 10^{-6} torr. Such an arrangement could for example be used in conjunction with a quadrupole mass spectrometer; its potential application to a 120° or 180° mass spectrometer might be limited by the presence of strong magnetic fields.

4.9.5. Possible improvements and limitations of the ion source

There are several ways in which the efficiency of the ion source in its present form might be improved, for example arrangements could be made in which a specimen which required etching could be rotated and fitted, so that the incident ion beam could etch individual faces at a glancing angle. Almen and Bruce [56] for example have shown that the sputtering efficiency can be raised by a factor of 3 for a rotation of 60° to the normal.

In order that several specimens could be etched simultaneously it is possible that a series of slots could be cut along the length of the oscillator tube. Higher beam

densities could be achieved by focussing the emergent beam although this would defeat the object of simplicity.

The oscillator is limited as a cold cathode ion source in its present form because of its inability to hold a self-sustained discharge below pressures of 10^{-6} torr. As suggested in the preceding section, it is envisaged that the use of a thermionic source of electrons could extend the application of the oscillator still further. The oscillator with a thermionic source of electrons could also be used as a sensitive total pressure measuring gauge. Consequently, the following chapter describes the oscillator with a hot filament and shows how such an arrangement has been applied to the measurement of total gas pressures.

CHAPTER 5

THE OSCILLATOR AS A THERMIONIC ION GAUGE

5.1. Introduction

In chapter 3 and 4 it has been shown that electrons are capable of following very long paths in the cold cathode oscillator. Such a device may be used as a high sensitivity ionization gauge. Some of the advantages of high sensitivity gauges have already been discussed, but at present the only type of ion gauge which has a high sensitivity and does not require a magnetic field is the orbitron. It is likely that the oscillator may be free of some of the restrictions of the orbitron.

Since it was not possible to hold a self-sustained discharge below pressures of 10^{-6} torr in the oscillator it was necessary to provide a thermionic source of electrons in order to maintain electron oscillations.

5.2. Construction of a thermionic oscillator.

The construction of the oscillator with a small filament was essentially similar to the construction of the ion source described in section 4.2, of the preceding chapter. The only difference was that a hole of 3 mm. diameter was drilled in the steel collector cylinder in place of the slot milled previously. A small 'V' shaped tungsten hairpin filament was

constructed as shown in Figure 40 below.

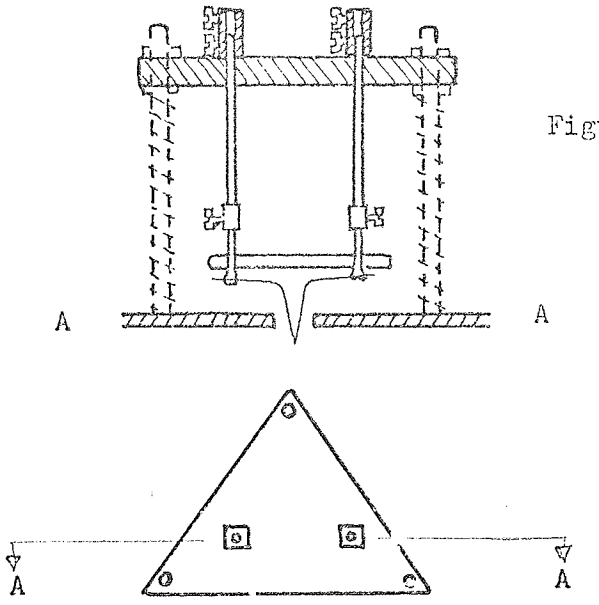

Figure 40.

With the above arrangement a limited amount of vertical movement of the filament within the hole was possible. The tip of the filament was arranged so that it only just protruded into the cylinder. The filament was made from 0.15 mm tungsten wire spot welded to an E.M.6 electron microscope filament base. The assembly described was fully demountable.

5.3. The electrical circuit

The circuit used is shown in Figure 41. The filament supply incorporated a variac transformer and a 6.3 volt step down isolating transformer. The filament current i_f was measured by an A.C. ammeter reading 0 - 10 amps, and a positive filament bias potential V_B was applied with respect to earth by dry batteries. The positive ion current, i_p, collected by the cylinder was measured using a D.C. amplifier, and the electron emission current, i_e, leaving the filament, recorded by a

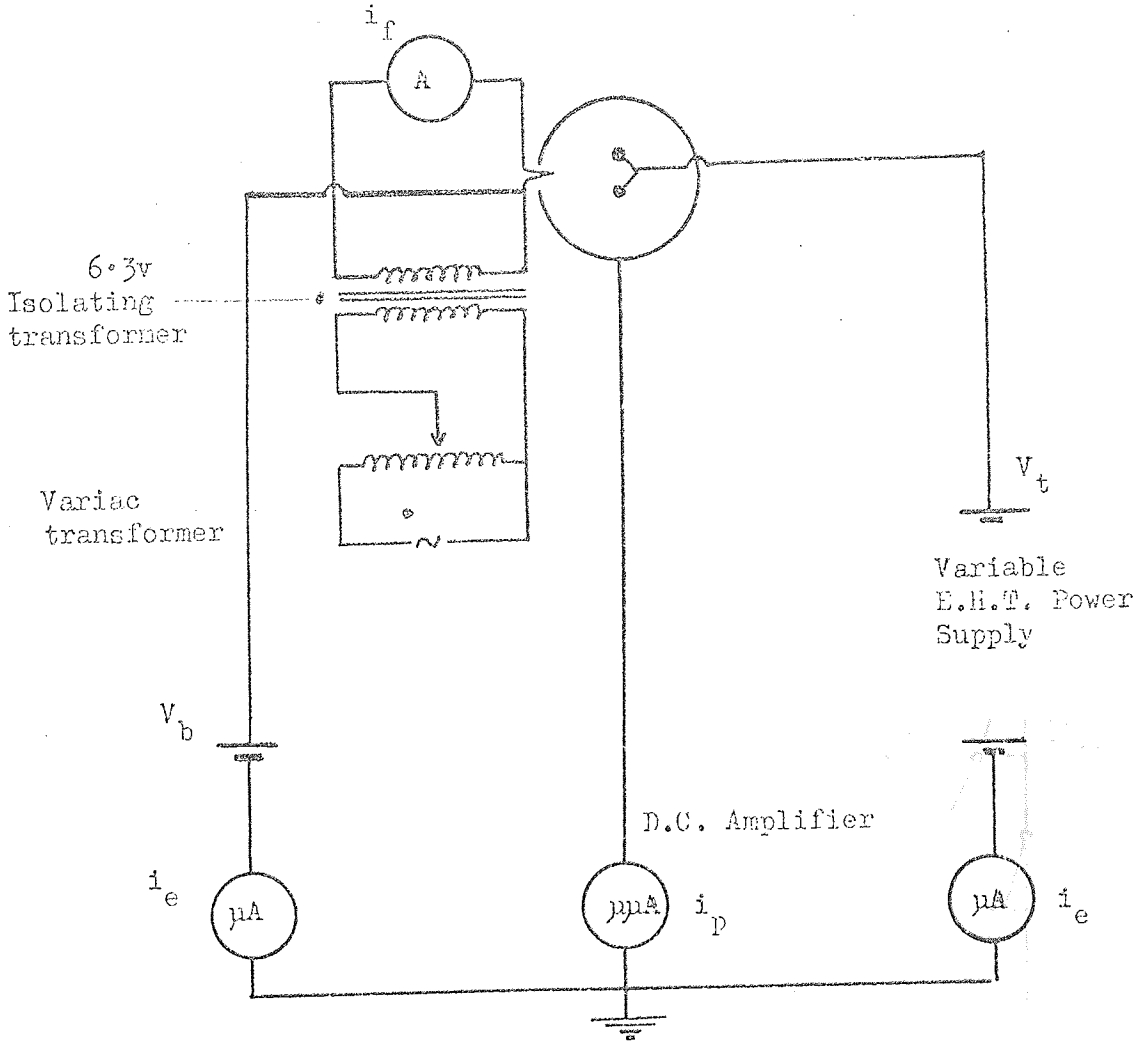
i_f
A
6·3v
Isolating
transformer
Variac
transformer
V_t
Variable
E.H.T. Power
Supply
V_b
D.C. Amplifier
i_e
μA
μμA
i_p
μA
i_e

Figure 41

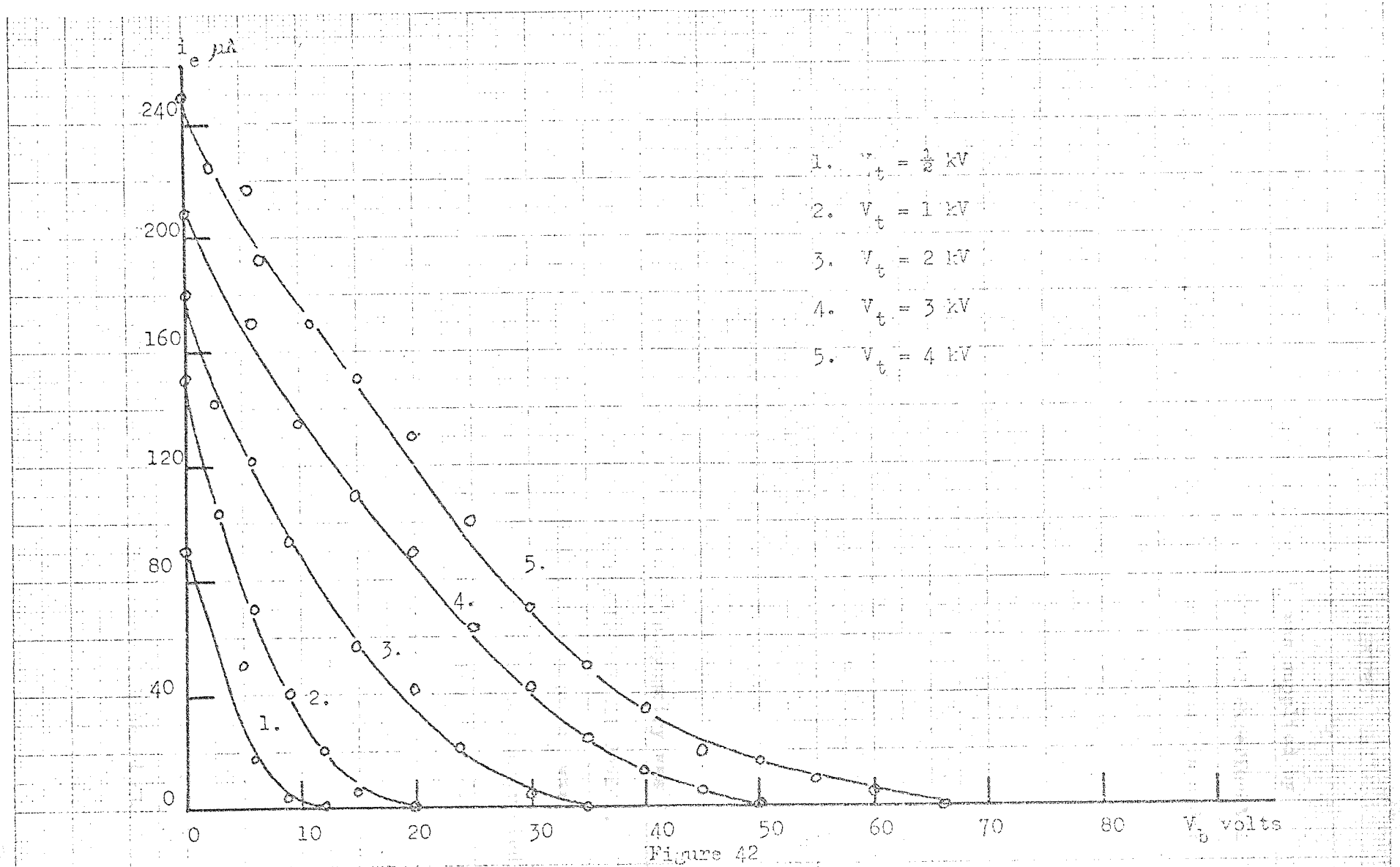
i_e μA
240
200
160
120
80
40
0
0
10
20
30
40
50
60
70
80
V_b volts
1. $V_t = \frac{1}{2}$ kV
2. $V_t = 1$ kV
3. $V_t = 2$ kV
4. $V_t = 3$ kV
5. $V_t = 4$ kV

Figure 42

'Unipivot' microammeter. The anode voltage V_t was supplied by the E.H.T. power pack described previously. In later experimental work the 6.3. volt isolating transformer was centre tapped in order to ensure that the bias V_B was applied to the filament tip. A 'Unipivot' microammeter was placed in the anode circuit in order to measure the electron current collected by the anode wires.

5.4. Experimental investigation of the thermionic oscillator

Before investigating the oscillator as a total pressure measuring device several experiments were conducted in the high vacuum system described earlier, in order to study some of the properties of the thermionic oscillator. Particular attention was paid to variations in electrode geometry. From chapter 3 it was clear that the most symmetrical arrangement of the anode wires about the cylinder axis was the best, and so this symmetry was maintained throughout the experiments with the thermionic device. The filament current was controlled so that the emission i_e was 1 μA for most of the experiments. With the oscillator constructed as described above, the sensitivity of the device was defined in the usual way

$$S = \frac{1}{p} \frac{i_p}{i_e} \text{ torr}^{-1}$$

when 'p' refers to the total gas pressure in the system. The first experiment investigated the variation of the emission current with bias voltage V_B. The triode characteristics of the oscillator are shown in Figure 42. These were obtained at a chamber pressure of 1×10^{-6} torr (air) with a constant filament

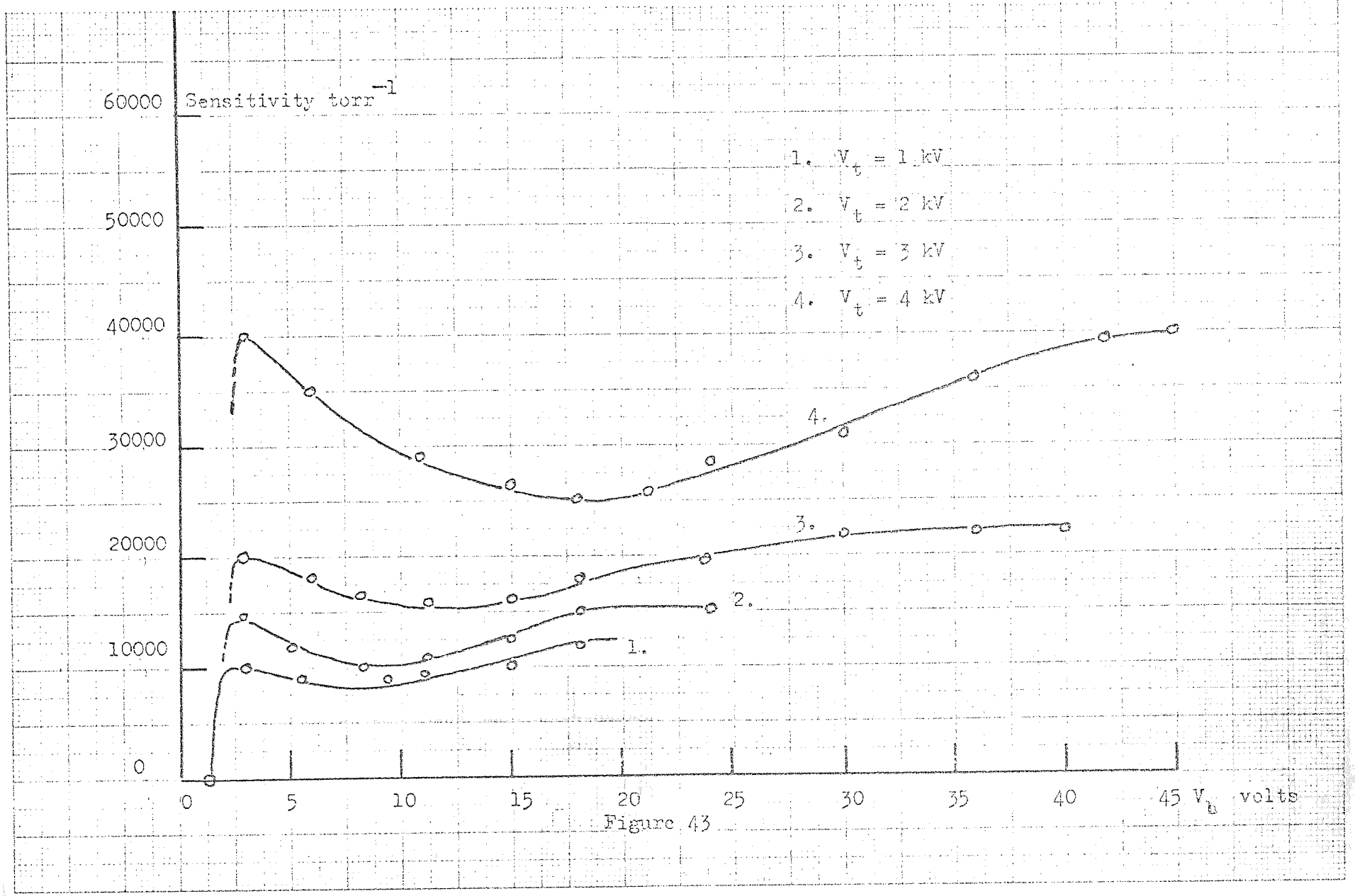
60000
Sensitivity torr^{-1}
50000
40000
30000
20000
10000
0
1. V_t = 1 kV
2. V_t = 2 kV
3. V_t = 3 kV
4. V_t = 4 kV
4.
3.
2.
1.
0
5
10
15
20
25
30
35
40
45 V_t volts

Figure 43

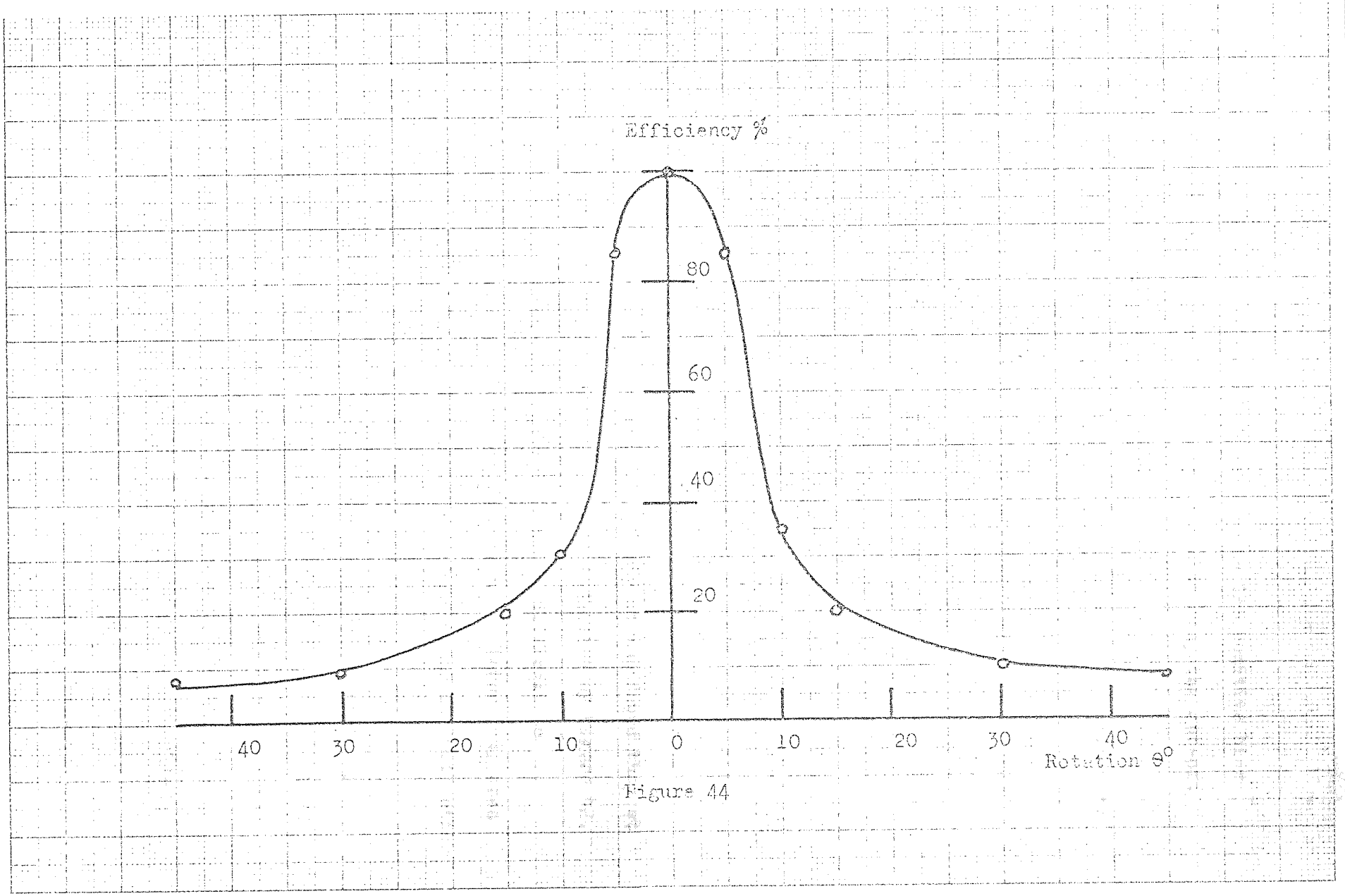

Figure 44

current of 2.4 amps. As expected, increasing the positive bias V_B reduced the emission until a cut-off was obtained, the cut-off being dependent upon the anode voltage.

Variation of the ion current i_p and hence the sensitivity S with the bias V_B is shown in Figure 43. The high sensitivities obtained, together with the absence of irregularities in the bias characteristic - see for example Gammon [39] - with the orbitron - indicated the potential of the thermionic oscillator as an ion gauge. With a bias potential of less than about 1.5 volts it was found that the electrons were collected directly by the collector cylinder. This was expected since the filament was only one or two millimetres from the cylinder and the thermal energies of the electrons alone were sufficient for some electrons to overcome the potential barrier between the filament and collector. Similarly it was found that at high bias voltages a cut-off was obtained as indicated by Figure 42. The dip in the bias curves of Figure 43 remains difficult to explain. More recent work which will be discussed later indicates the possibility that this may be due to different modes of oscillation in the oscillator.

The position of the filament was altered in such a way that the tip was rotated about the cylinder axis. Figure 44 shows that the most efficient use of the injected electrons was obtained with the filament on the 'y' axis i.e. perpendicular to the plane of the anode wires. A deviation of $\pm 5^{o}$ from this axis resulted in 20% loss of sensitivity. At first it was considered that a small rotation from axial symmetry might have been preferable

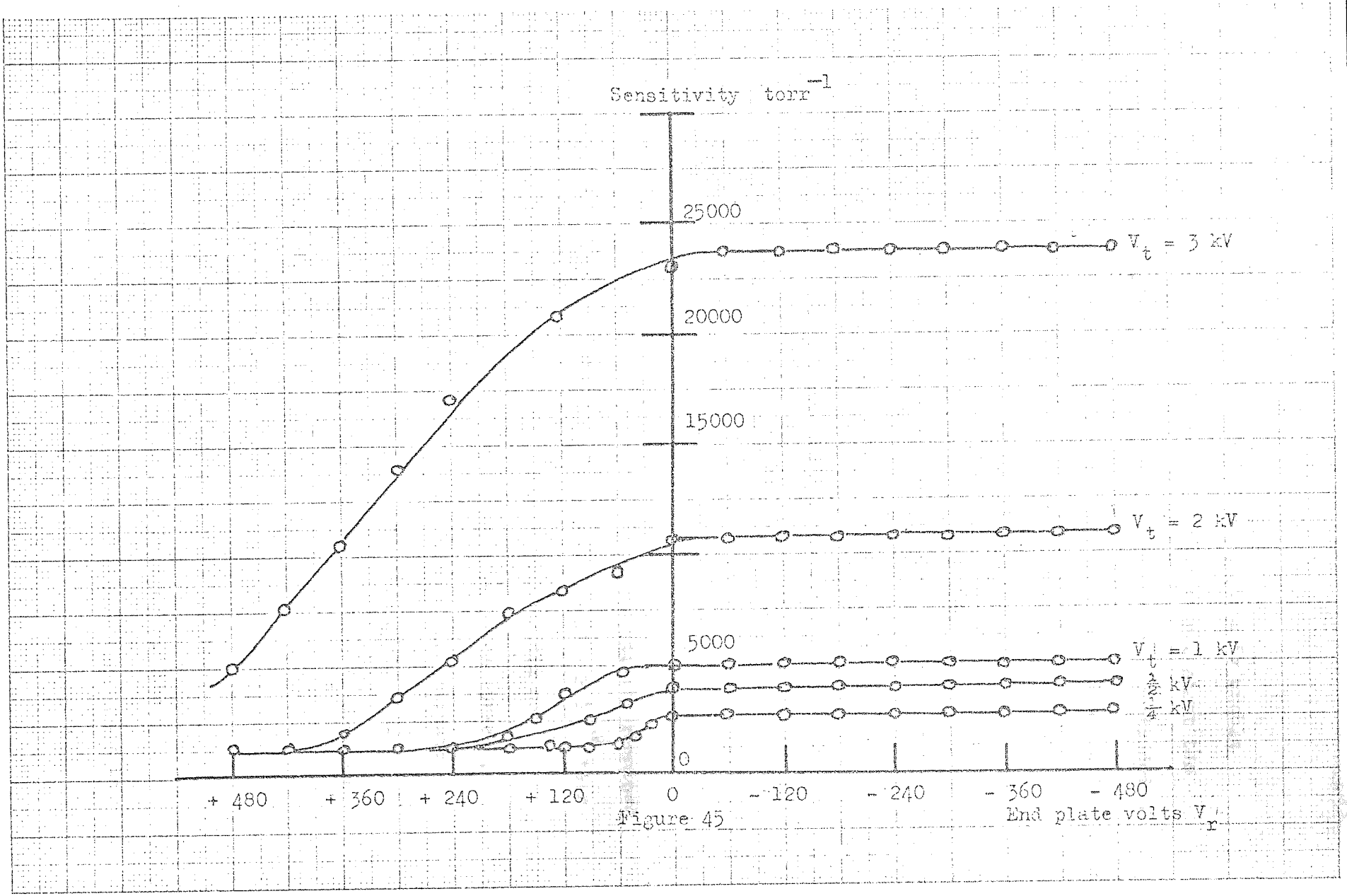
Sensitivity torr^{-1}
25000
20000
15000
5000
0
V_t = 3 kV
V_t = 2 kV
V_t = 1 kV
$\frac{1}{2}$ kV
$\frac{1}{4}$ kV
+ 480
+ 360
+ 240
+ 120
0
- 120
- 240
- 360
- 480
End plate volts V_r

Figure 45

since an electron starting from an off axis position is unable to return to the small region of potential disturbance about the filament tip. In this experimental oscillator the tip protruded only a small distance into the cylinder and hence any disturbance in the region of the filament would be small. The experiments have shown that deviation of the filament from the y axis in practice reduced the sensitivity. This is probably because the electrons are forced to pass closer to the anode wires the greater the rotation of the filament, and hence are collected sooner.

In order to investigate further the effects caused by having large numbers of electrons in flight at the same time the filament was returned to its original 'y' axis position and the variation of sensitivity with increased emission current noted. For emission currents between 0.5 and 7 μA the sensitivity remained about 13,200 $\pm$ 400 $torr^{-1}$, at a chamber pressure of 5×10^{-6} torr and an anode voltage of 2 kV. Thus the oscillator did not appear space charge limited over this range of emission current, pressure and voltage. Another method was used to investigate the effect of increased charge density. The end plates were insulated from the collector cylinder and a potential V_R applied to them with respect to the cylinder. The application of a negative potential V_R tended to repel the electrons so that they became bunched axially about the centre of the oscillator. Negative potentials up to -480 volts were applied but the sensitivity remained unaffected as shown in Figure 45. Thus it appears that the consequent increase in the charge density had

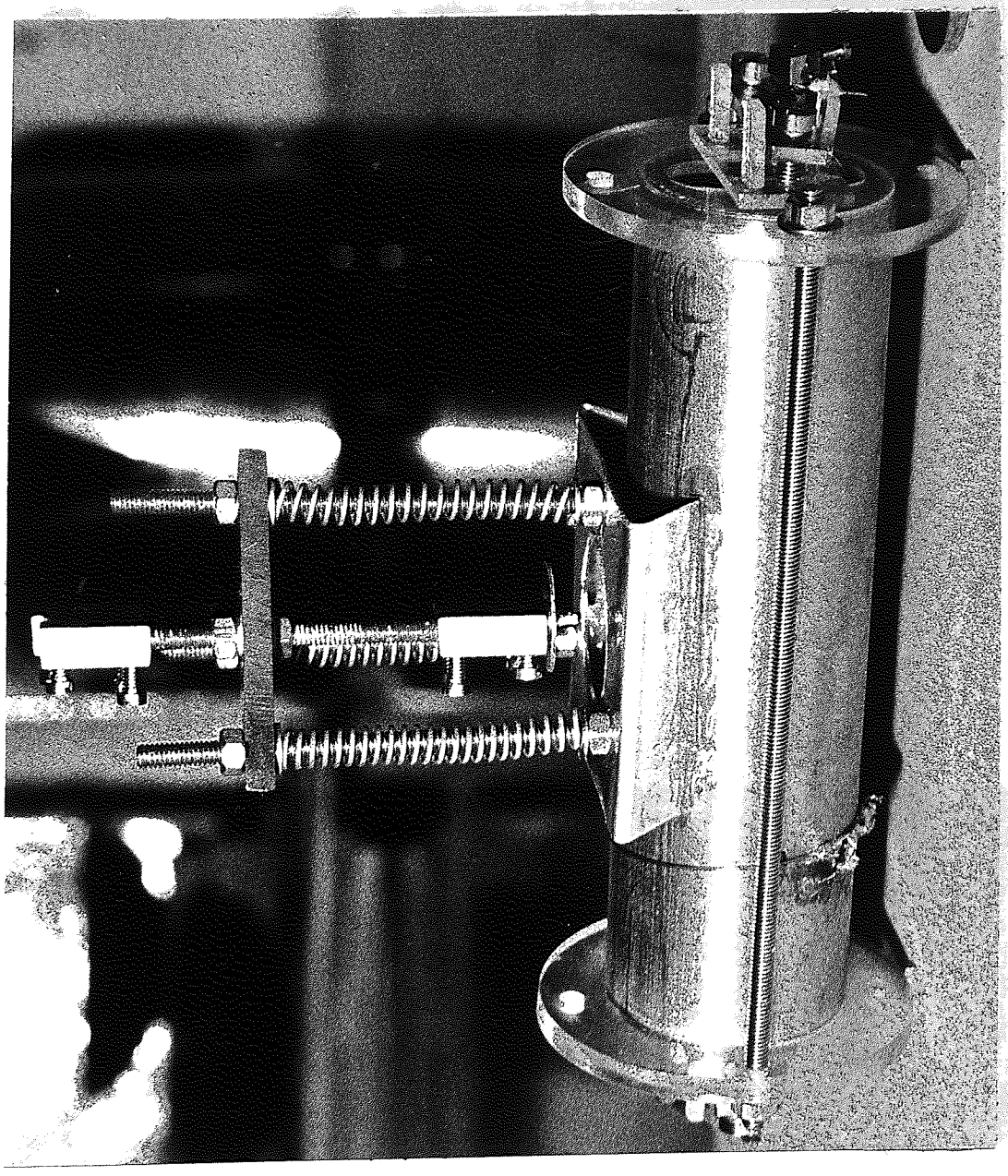

Figure 46

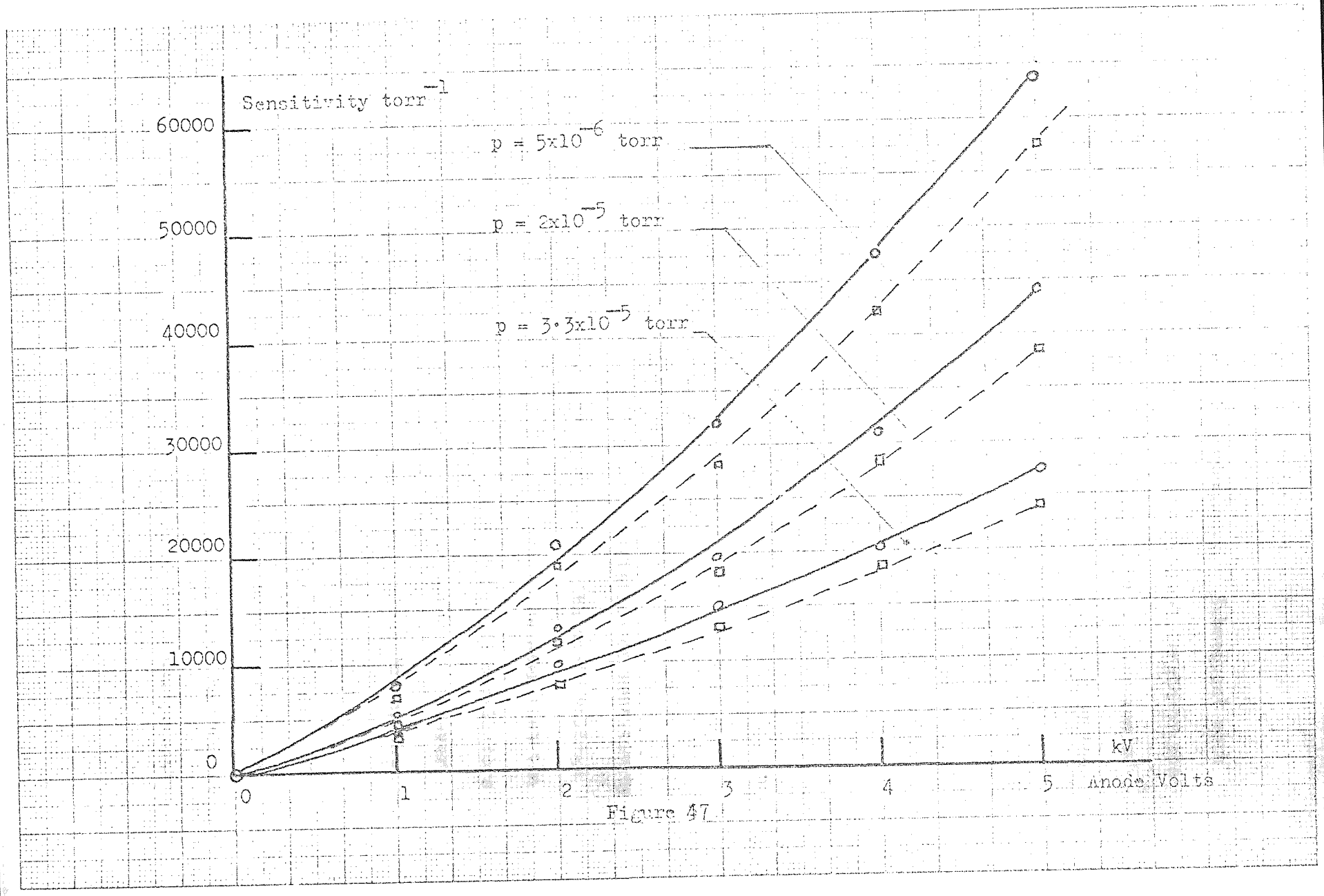
Sensitivity torr^{-1}
60000
50000
40000
30000
20000
10000
0
p = 5x10^{-6} torr
p = 2x10^{-5} torr
p = 3·3x10^{-5} torr
0
1
2
3
4
5
kV
Anode Volts

Figure 47

no effect within the limits of the experiment. Subsequent work carried out in the laboratory in which the physical length of the oscillator was reduced confirm this result. The application of a positive potential caused the electrons to be collected by the end plates and thus the sensitivity fell off with increasing positive end plate potential.

The above experiments indicated that the volume of the oscillator could be reduced without affecting the sensitivity. Consequently a thermionic device was constructed as shown in Figure 46 in which all the dimensions were exactly half those of the oscillator described above, and experiments were conducted in order to investigate the effects of scaling. The variation of sensitivity with bias voltage V_B gave very similar curves to those shown in Figure 43. Figure 47 shows the variation of sensitivity of the small and large thermionic oscillators with anode voltage V_t and for different chamber pressures; it can be seen that the difference in sensitivity between the large and small oscillators is very small for a given pressure and anode voltage. However it should be noted that for all points on the curves shown, the field strength in the small oscillator was greater than that in the large oscillator very approximately by a factor of two. The difference in the sensitivity at different pressures was due to the collector current being of the same order of magnitude as the primary current with the result that the sensitivity was pressure dependent as for example shown by Leck [18].

It was concluded from these experiments that the

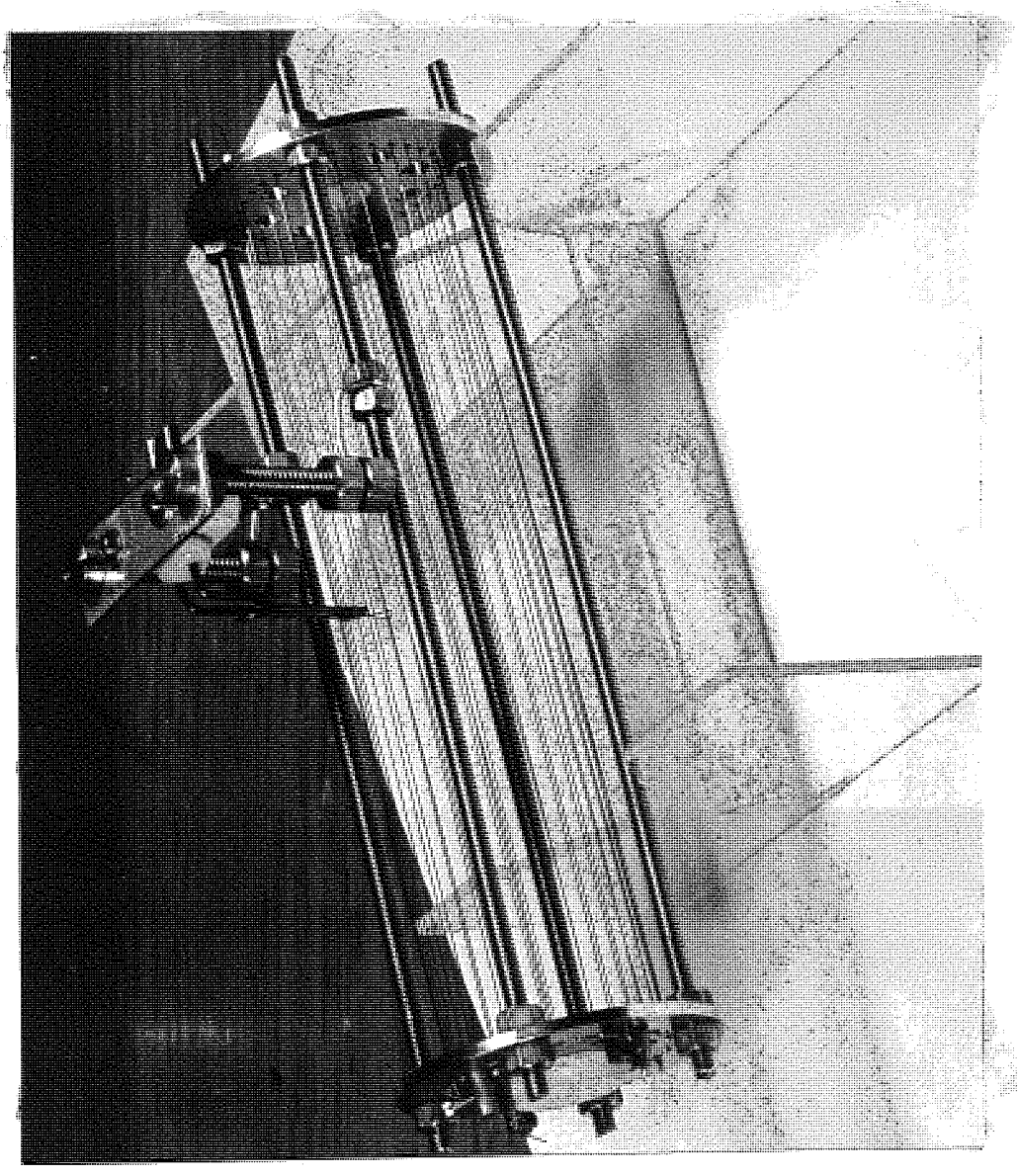

Figure 48

oscillator could be constructed as an ion gauge with dimensions similar to those of the small oscillator described above.

5.5. Design and construction of a U.H.V. gauge

The oscillator shown in Figure 46 was inadequate as a thermionic ion gauge, in several ways. Firstly the collector cylinder would collect nearly all of the soft X-ray photons produced by the energetic electrons striking the anode wires - i.e. the oscillator in this form was expected to have a large residual current due to X-rays. Secondly, the choice of materials of the original oscillators, for example perspex end plate supports, would give rise to outgassing problems under U.H.V. conditions. Consequently the oscillator was redesigned as a nude thermionic U.H.V. gauge as shown in Figure 48. The end plates of the oscillator as shown were made from stainless steel disks 3.75 cm diameter and 0.16 cm thick. A hole was drilled centrally in each disk, with a diameter of 0.76 cm into which were located insulating bushes each containing two 0.015 cm holes drilled symmetrically 0.25 cm apart. The end plates were held 10 cms apart by means of four 6 B A stainless steel rods, located symmetrically at a radius of 1.6 cm from the centre of the end plate disks. The solid collector cylinder was replaced by a cage of tungsten wires the diameter of the cage being 2.54 cms. The cage was formed by threading 0.015 cm diameter tungsten wire through a series of 16 0.025 cm holes drilled symmetrically at a radius of 1.27 cm in the end plates. A further series of holes 3 mm diameter were drilled at a radius of 0.96 cm in order to reduce the area

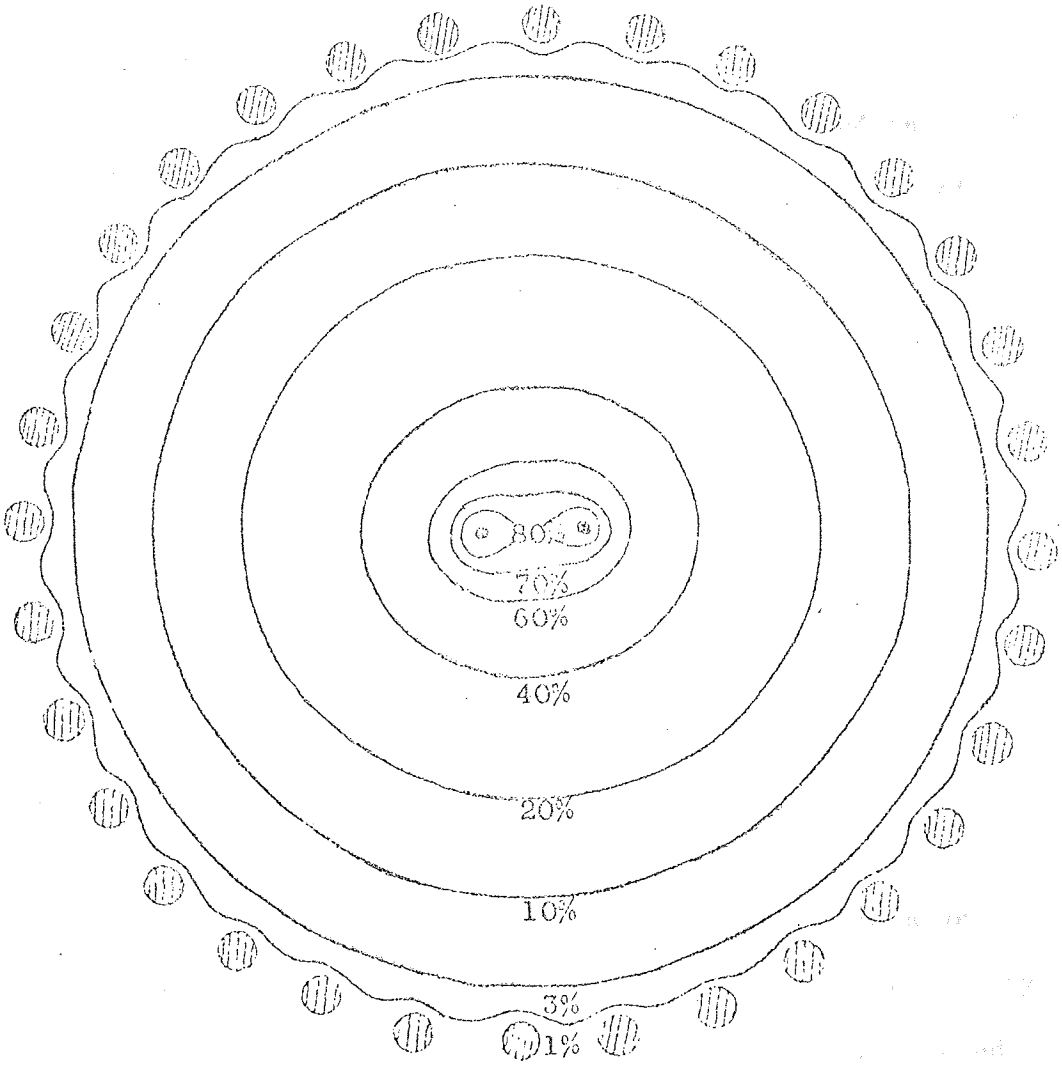

Figure 49

of the end plates.

Originally P.T.F.E. insulation bushes were used in the centre of the end plates, but the operation of the gauge at high anode voltages caused sufficient heating of the anode wires to melt these bushes. Subsequently ceramic bushes were used. Each bush required careful baking procedure before being fitted into the locating holes. The commercial ceramics used were either 'Ceramtec' or 'Aremco' both of which, the manufacturers claimed, had a resistivity of 10^{14} ohms cm^{-1} in air at $20^{o}c$. It will be shown later that, with the gauge constructed as described above, leakage currents across this insulator could be a limiting factor to the use of the device.

The anode wires were held under tension by drawing the end plates apart along the four 6 B.A. stainless steel rods as shown in Figure 48. The collector cage was held under tension by the same process. Tungsten anode and collector wires were used since it had been shown by Lawson [22] Hartmann [23,24] and others that tungsten can exhibit less positive ion desorption than most other high melting point metals. This will be discussed in more detail later.

It was expected that the 16 collector wires used to simulate the electrostatic field previously produced by a solid cylinder would produce some distortion of the field in the region of the collector wires. However Figure 49 shows in a field plot drawn to simulate a 32 wire collector cage the electrostatic field remains undisturbed within the 5% equipotential. Furthermore

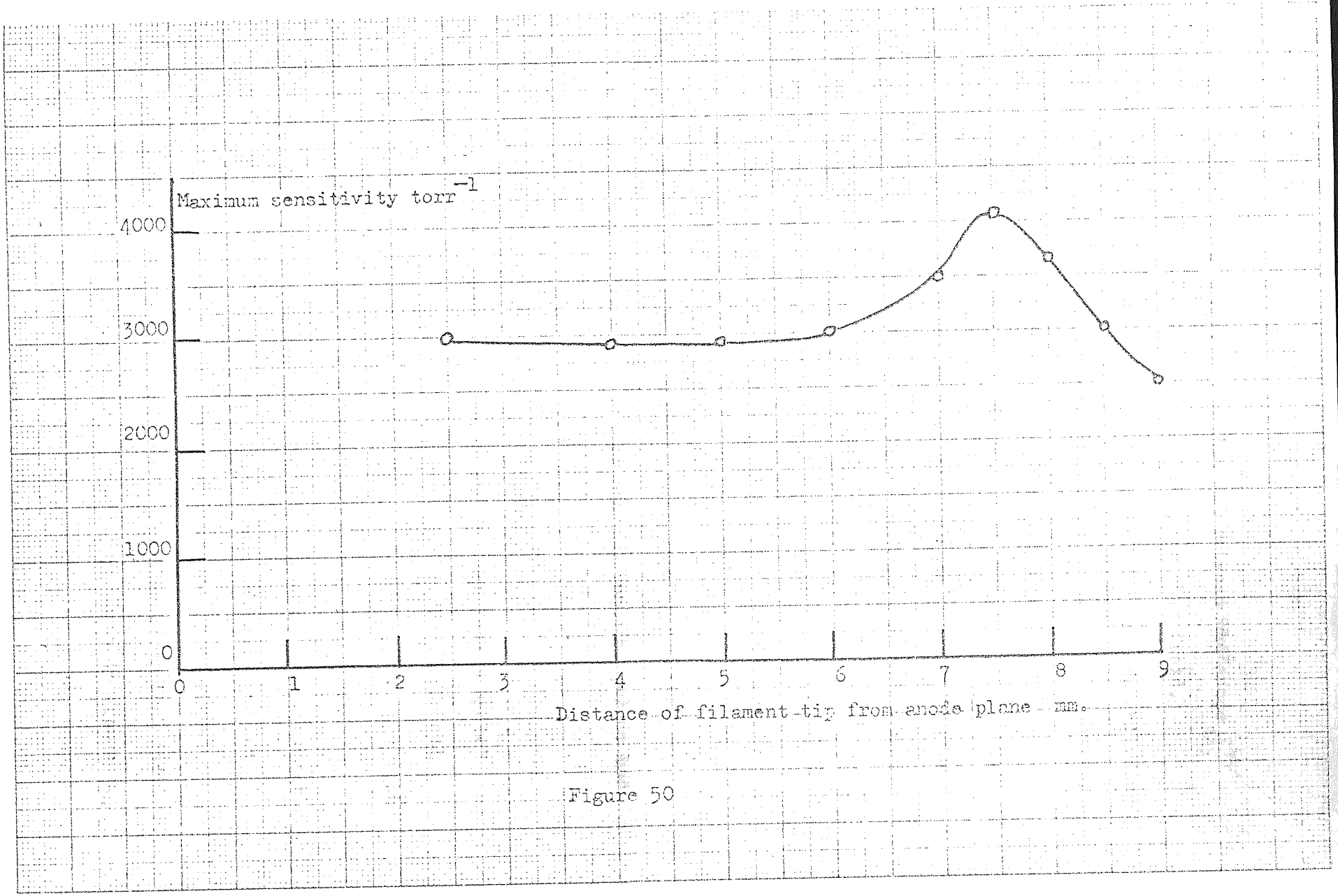
Maximum sensitivity torr^{-1}
4000
3000
2000
1000
0
0
1
2
3
4
5
6
7
8
9
Distance of filament tip from anode plane - mm.

Figure 50

it was expected that electrons oscillating between the anode wires would experience very little of the disturbed field.

A number of filaments were designed and tested, including a small electron gun mounted outside the collector cage. However it was decided that the simplest and most effective method of injecting the electrons was by means of a small hairpin filament, made from 0.010 cm tungsten mounted as shown in Figure 48. The filament in this form could be raised or lowered into the volume contained within the cage, and could be moved in the axial direction to within 0.5 cm of either end of the oscillator.

In the nude form described above it was anticipated that the oscillator would be more suitable for use as a U.H.V. gauge than in the form described in section 5.4., since the conductance between the vacuum system and the ionizing volume had been improved.

5.6. Preliminary tests in high vacuum

The nude gauge was mounted in the high vacuum system and some preliminary experiments carried out. The electrical circuit was the same as that described in section 5.3 except that dry batteries were used to supply the anode voltage and as mentioned earlier the anode current was measured and the filament centre tapped. The sensitivity of the gauge was measured for different positions of the filament tip from the anode wires. In each measurement the bias voltage V_B was altered so that the maximum ion current was recorded. The result shown in Figure 50, reveals a distinct optimum position about 0.7 cm from the plane

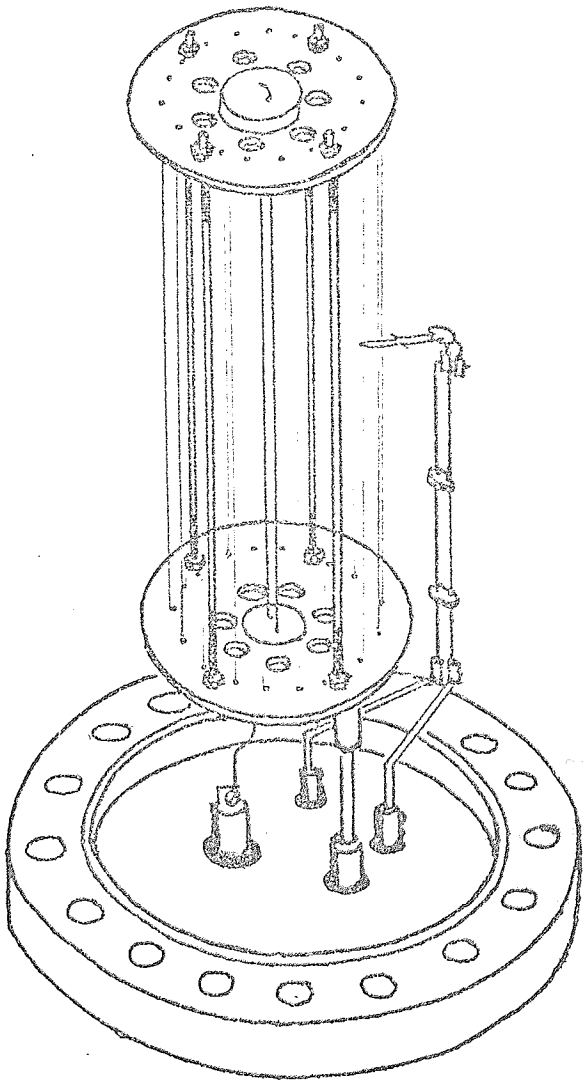

Figure 51

of the anode wires, that is with the filament inserted to a depth of about 0.5 cm inside the cage. A possible explanation will be advanced in order to explain this optimum condition at a later stage, but at the time the experiment was conducted no obvious explanation was apparent. With the filament tip at a position of 0.8 cm from the anode wires the filament was moved parallel to the cylinder or 'z' axis with a constant insertion depth and with a bias voltage V_B of 120 volts. The sensitivity remained constant at about 3500 $torr^{-1}$ at an anode voltage of 1kV, for the length of the oscillator provided that the filament was at least 0.5 cm from either end plate. This result was expected since it has been shown in chapter 2 that the equipotential distribution in the axial direction did not alter rapidly until it was very close to the end plates.

The nude gauge was rebuilt with a rigid filament assembly mounted, together with the cylindrical cage, on a 6" O.D. conflat flange. The filament was mounted centrally in the axial direction with the tip approximately 0.8 cm from the anode wires. The gauge assembly mounted on the flange is shown in Figure 51.

5.7. The U.H.V. system

A schematic diagram of the U.H.V. system is shown in Figure 52. The system was roughed out by a liquid nitrogen cooled zeolite sorption pump with both isolation valves open and the air admittance valve closed. The backing pressure was measured by a thermocouple gauge mounted in the backing line. When a backing pressure of about 10 microns was reached the two

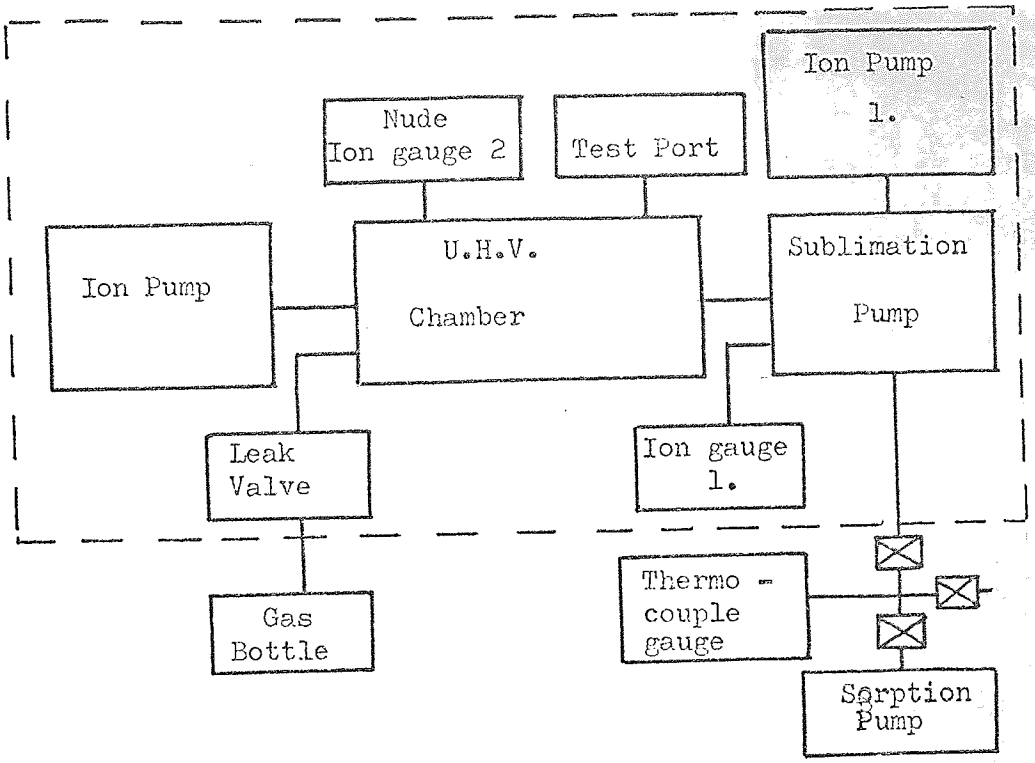

Figure 52.

15 litre per second ion pumps were struck, and after a few minutes when the initial outgassing of the ion pumps had subsided the U.H.V. isolation valve and the sorption pump isolation valve were closed.

Total gas pressure in the system was measured by a Mullard I.O.G. 12 ion gauge mounted on the sublimation pump and a nude Mullard I.O.G. 20N modulator gauge mounted on a 4" O.D. flange and inserted into the U.H.V. chamber.

Extra pumping speed was obtained by a water cooled 200 l/s sublimation pump as shown. The sublimation pump could be operated manually or with an automatically controlled sublimation period and cycling rate. In the unbaked state

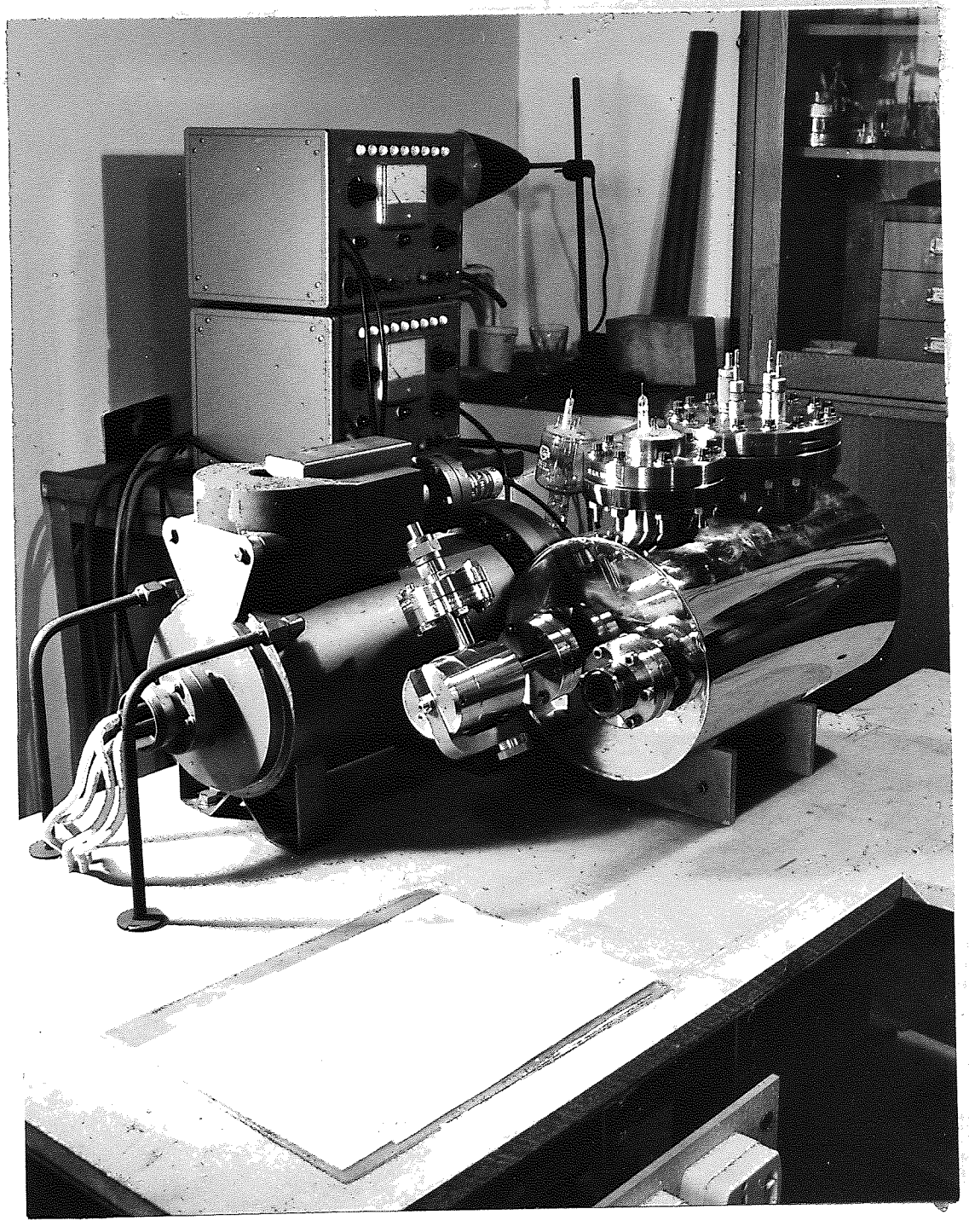

Figure 53

pressures in the region of 10^{-8} to 10^{-9} torr could be achieved. The gas pressure in the U.H.V. chamber could be controlled by pumping against a continual leak via a U.H.V. leak valve. The leak valve had a vernier adjustment screw and it was found experimentally that leaks between 10^{-9} torr litres/sec and 10^{-5} torr litres/sec could be controlled.

The system could be baked to a temperature of about 300°C with the oven extending over the region shown by the dotted line in Figure 52, however if a higher bake-out temperature was required it was necessary to remove the magnets from the ion pumps.

Figure 53 is a photograph of the U.H.V. system prior to the addition of ion pump 2. The twin wire gauge shown in Figure 51 was mounted in the test port.

5.8. Experimental investigations under U.H.V. conditions

Initial results showed that the sensitivity of the gauge shown in Figure 51 was only about 1000 $torr^{-1}$ at 1 kV - rather lower than the gauges with demountable filament assemblies investigated in the high vacuum system. It was discovered that when the U.H.V. chamber was partially screened from the magnetic field of ion pump 1, by placing a large sheet of μ-metal between the pump and the chamber, the sensitivity of the twin wire gauge doubled. The necessity of screening the magnetic field from the ion pump was expected on consideration of the discussion in chapter 2. Although it was not possible to screen the U.H.V. chamber from stray fields completely, the large sheet of μ-metal was used in all subsequent experiments so that the gauge sensitivity

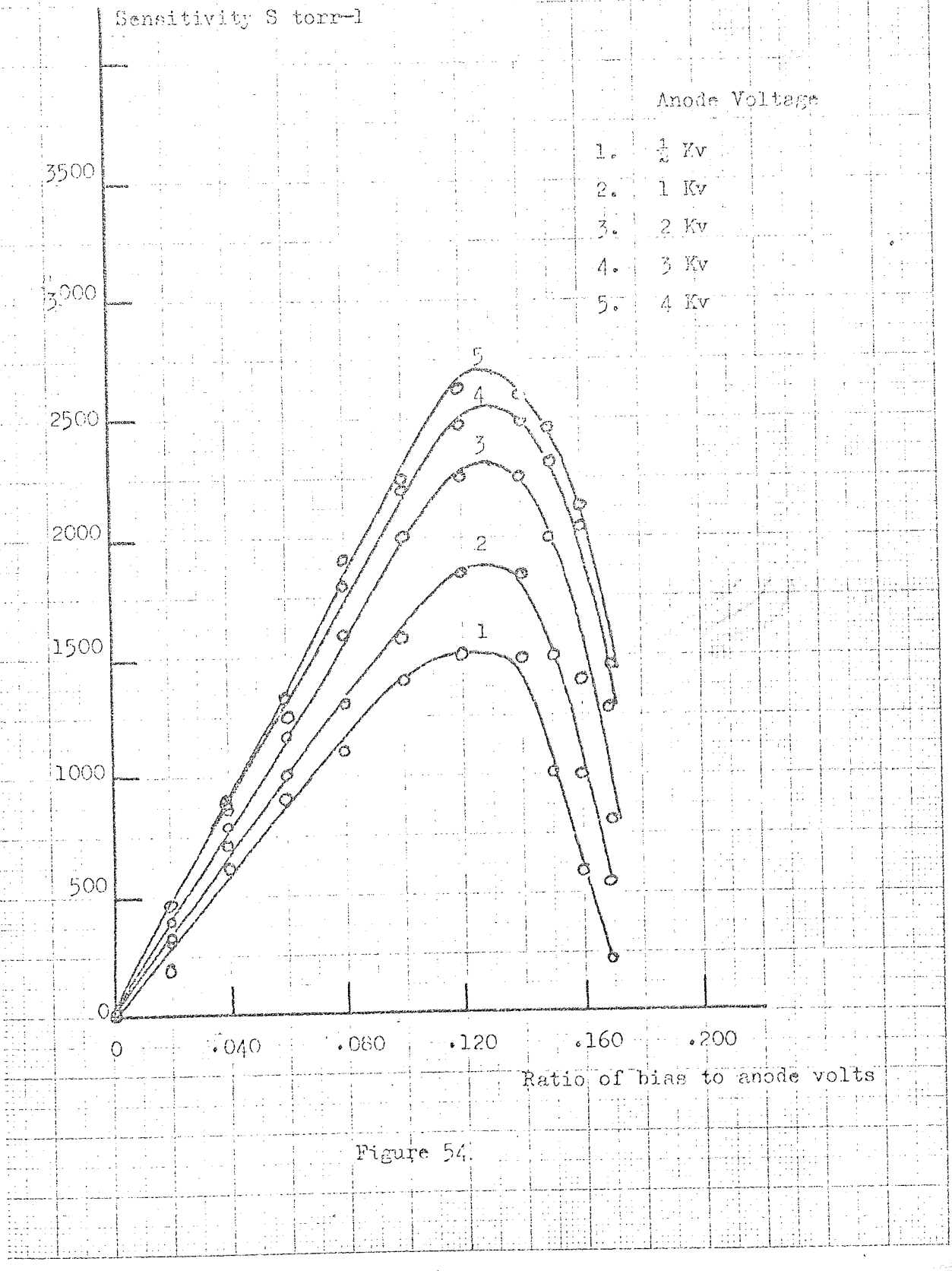
Sensitivity S torr⁻¹
Anode Voltage
1. ½ Kv
2. 1 Kv
3. 2 Kv
4. 3 Kv
5. 4 Kv
3500
3000
2500
2000
1500
1000
500
0
0
.040
.080
.120
.160
.200
Ratio of bias to anode volts

Figure 54.

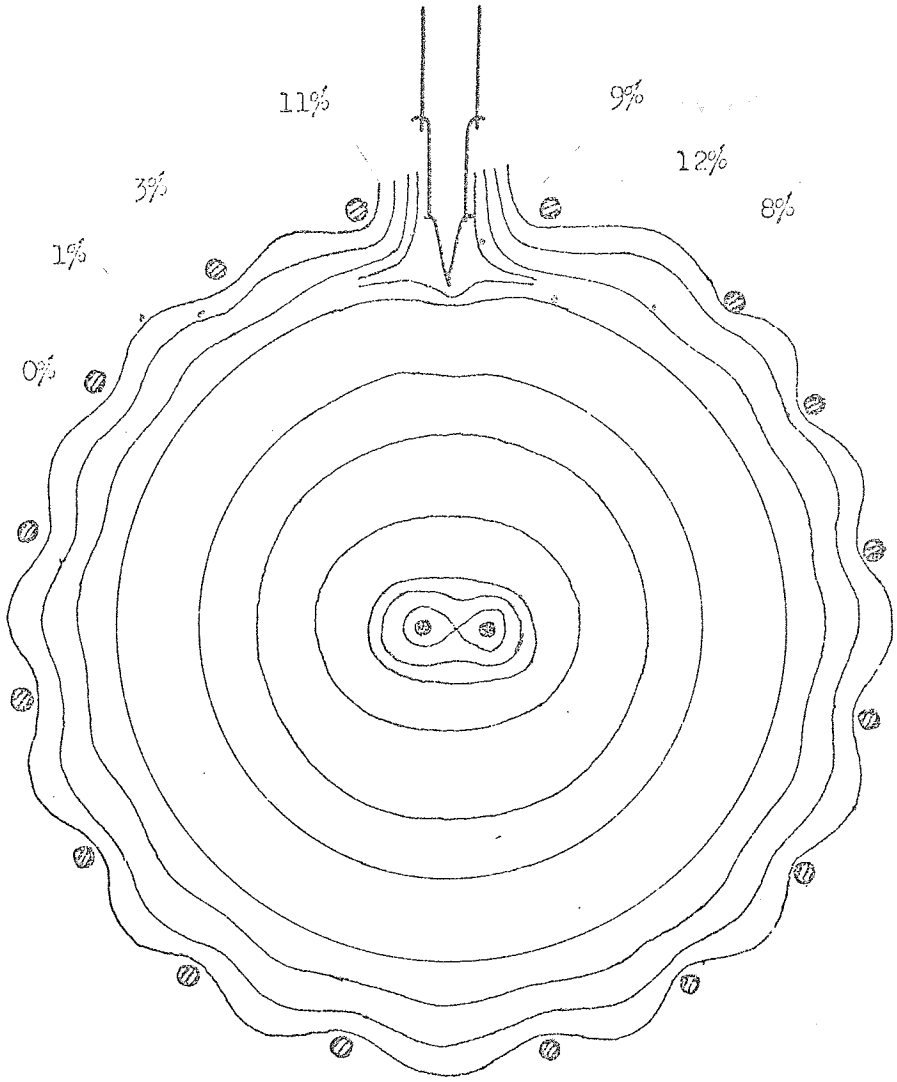

Anode wires at 100%

Saddle point approximately 80%

Figure 55

was as high as possible.

Figure 54 shows the variation of the sensitivity of the nude gauge with the ratio of bias to anode voltage. A distinct maximum occurred when this ratio was equal to 0.13, for anode voltages between ½ and 4kV. The reason for the maximum can be explained in terms of the matching of the electrostatic field produced by the anode wires with the bias applied to the filament tip. Figure 55 shows a field plot of the potential disturbance caused by the insertion of the filament into the volume contained within the collector cage. It was apparent from Figure 54 that the sensitivity of the twin wire gauge was critically dependent on the focussing of the electrons between the anode wires and consequently on the ratio of V_B/V_t. It was assumed that the focussing would be optimised when the potential disturbance in the region of the filament tip was as small as possible. With the tip of the filament a distance 'p' from the plane of the anode wires it has been shown in Appendix V that the condition of minimum disturbance occurs when

$$\frac{V_B}{V_t} = 1 - \frac{\ln\left(\frac{a^2 + p^2}{2ab}\right)}{\ln\left(\frac{a^2 + R^2}{2ab}\right)}$$

V_B, V_t, a , b , and R have their usual meaning. From the above expression it has been shown in Appendix V that when the dimensions of a , b , and R pertaining to the nude gauge were inserted into the equation the ratio of V_B/V_t was about 0.13. This result was in good agreement with the experimental results

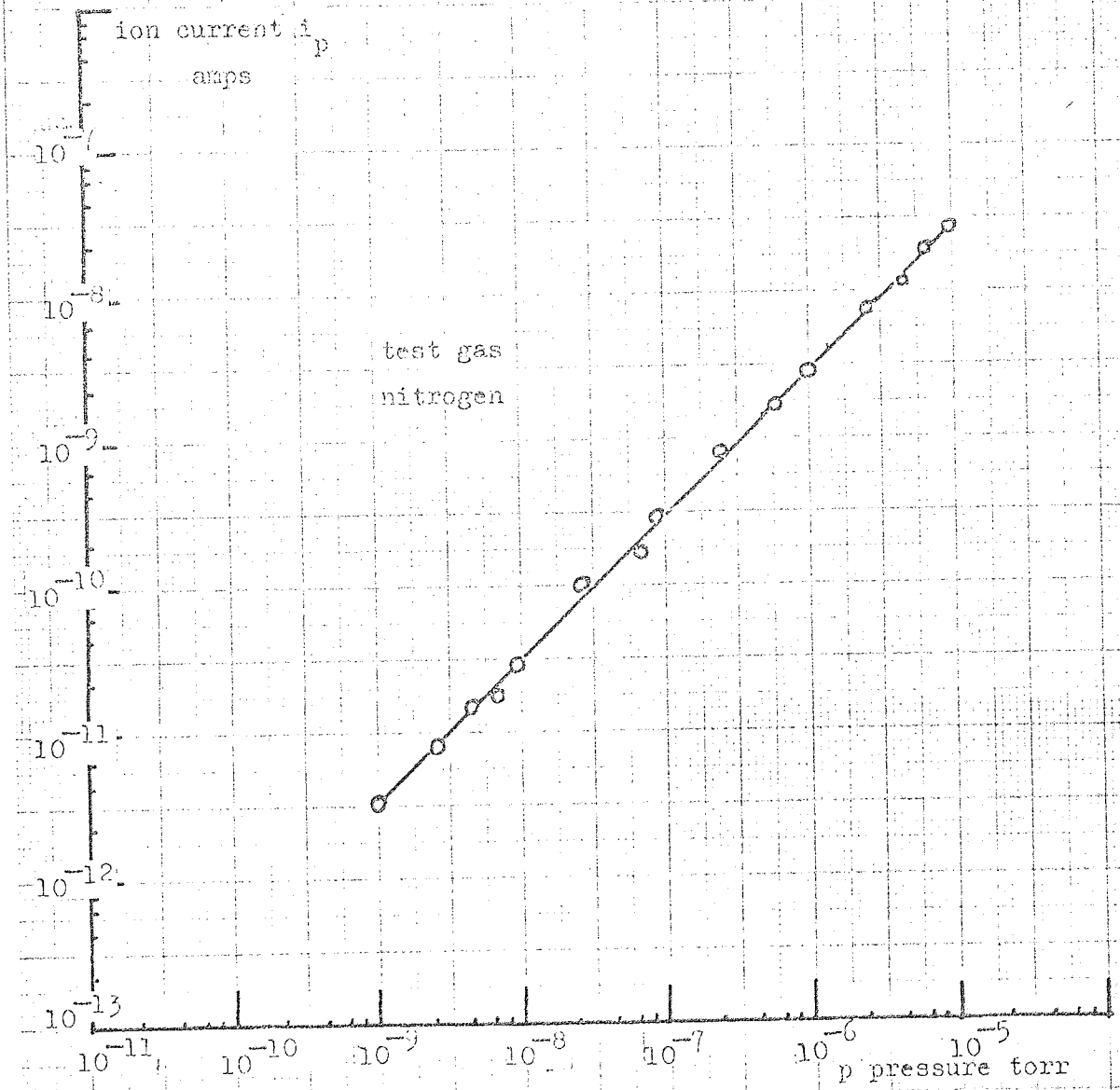
ion current i_p
amps
10^{-7}
10^{-8}
10^{-9}
10^{-10}
10^{-11}
10^{-12}
10^{-13}
test gas
nitrogen
10^{-11}
10^{-10}
10^{-9}
10^{-8}
10^{-7}
10^{-6}
10^{-5}
p pressure torr

Figure 56(a)

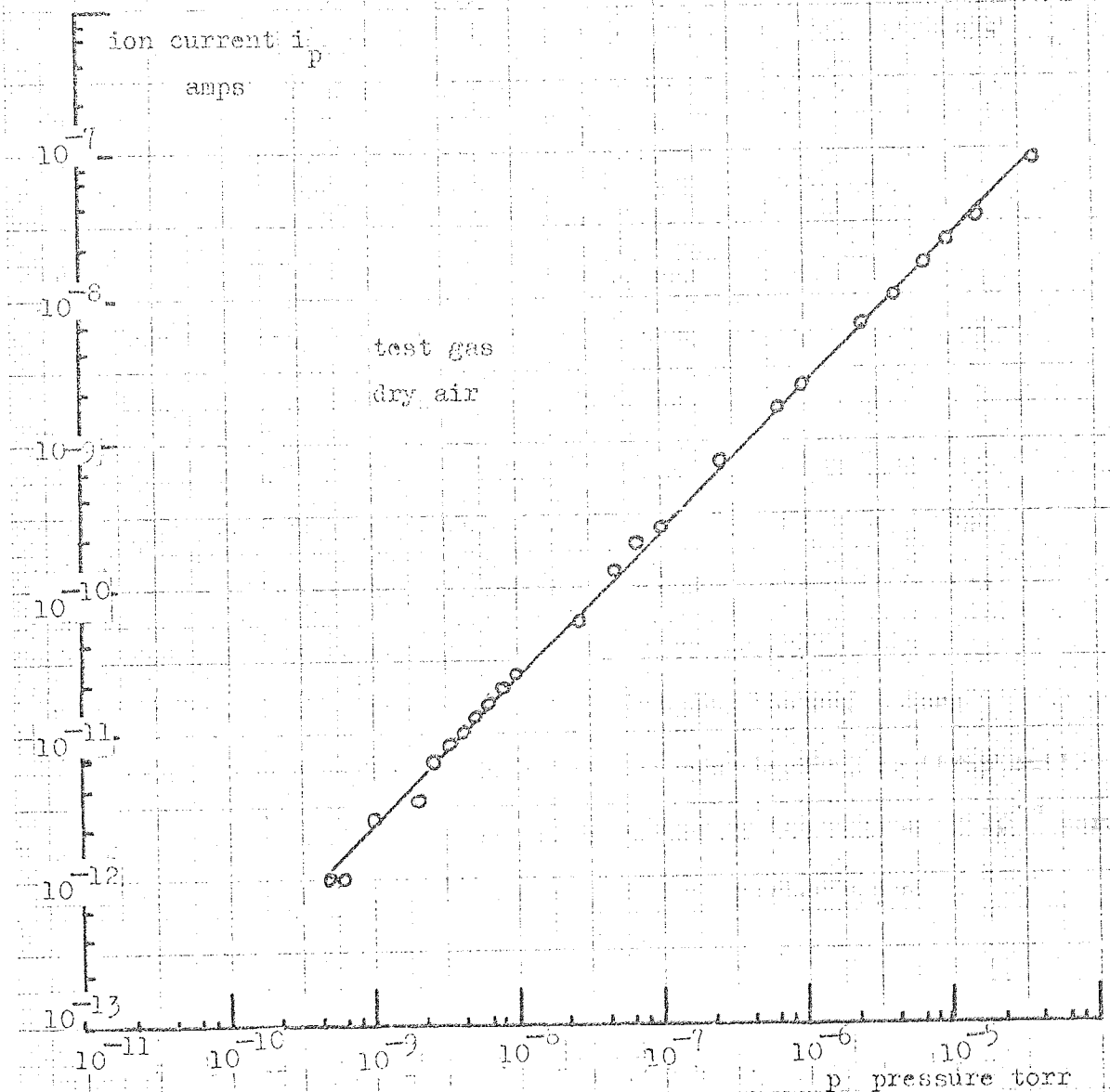
ion current i_p
amps
10^{-7}
10^{-8}
10^{-9}
10^{-10}
10^{-11}
10^{-12}
10^{-13}
test gas
dry air
10^{-11}
10^{-10}
10^{-9}
10^{-8}
10^{-7}
10^{-6}
10^{-5}
p pressure torr

Figure 56(b)

shown in Figure 54.

The twin wire gauge was subsequently compared with two Mullard I.O.G. 12 gauges. Comparisons were made with air and also with nitrogen. In order to attain the low pressures recorded it was found necessary to bake the system as described earlier, for about 1 week at 300°C.

Figure 56 (a) shows a comparison made between an I.O.G. 12 mounted in the U.H.V. chamber and the twin wire gauge. The test gas used was nitrogen. With the anode voltage at 1 kV and a bias of 120 volts applied to the filament the twin wire gauge showed a linear variation of ion current over the range 5×10^{-10} torr to about 10^{-4} torr. The emission current was only 1 μA. The gauge in this form was exhibited in the 1969 Physics Exhibition at Alexandra Palace, London. Some difficulty was experienced with the ion pump tending to 'trip out' at 10^{-4} torr and so pressure measurements in the region of 10^{-4} torr and above were difficult until the pump was stripped and reconstructed at a later date.

Figure 56(b) shows a comparison made under the same conditions as above but with air used as the test gas. There was no apparent difference in sensitivity although some deviation from linearity of ion current with pressure was observed at a pressure of about 5×10^{-5} torr recorded by the I.O.G. 12. The reason for this has been explained in section 5.4. and the theoretical high pressure limit derived as 5×10^{-5} torr in

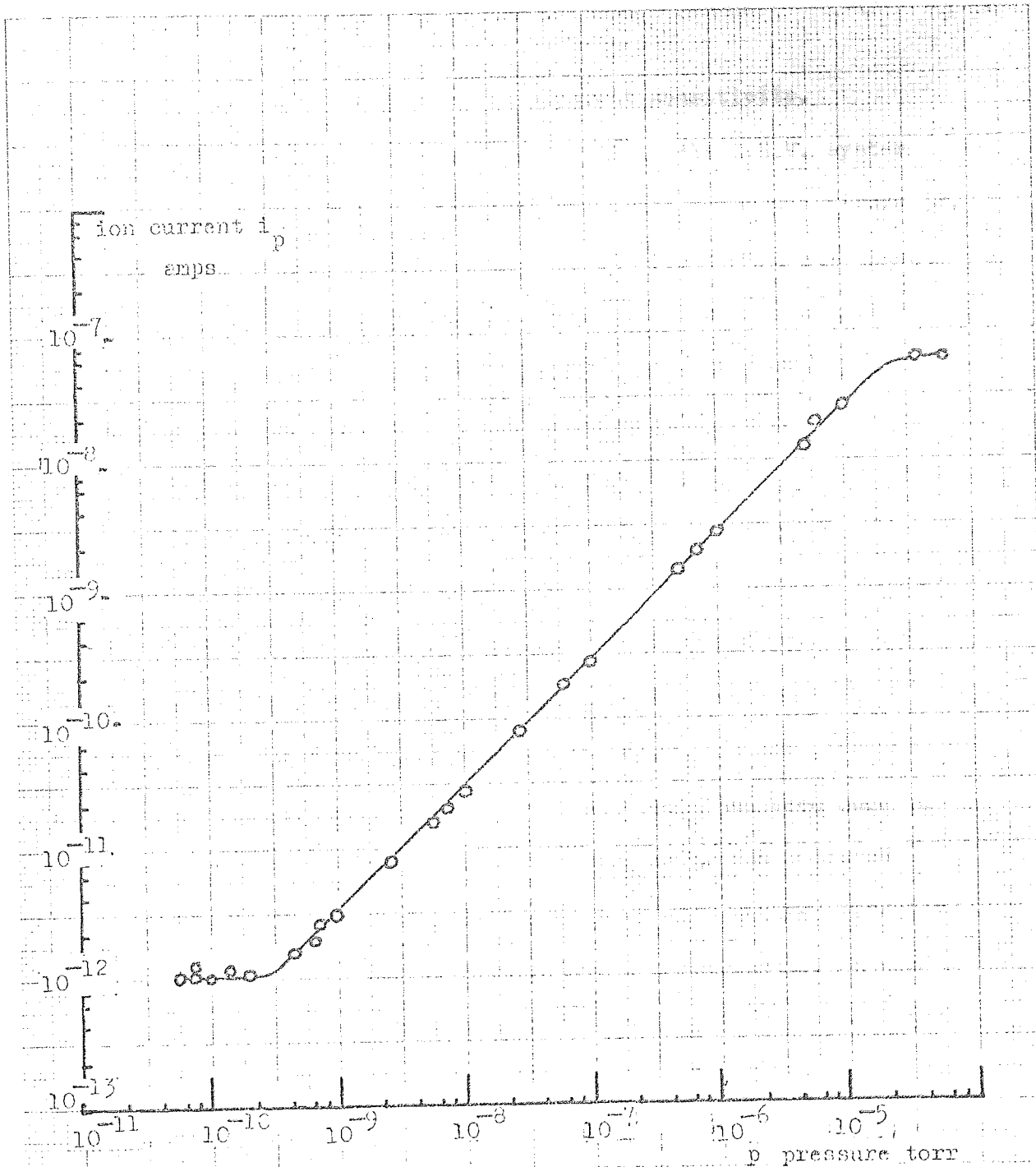
ion current i_p
amps
10^{-7}
10^{-8}
10^{-9}
10^{-10}
10^{-11}
10^{-12}
10^{-13}
10^{-11}
10^{-10}
10^{-9}
10^{-8}
10^{-7}
10^{-6}
10^{-5}
p pressure torr

Figure 56(c)

Appendix VI, for a 10% reduction in apparent sensitivity.

In order to investigate the low pressure limit the U.H.V. system shown in Figure 53 was modified as shown in the schematic Figure 52. The system was baked to a temperature of 300°C into the sorb pump initially and then into the two ion pumps. Bakeout lasted for a period of two weeks and the system allowed to cool gradually with the sublimation pump operated at the correct cyling rate for a further week. All the gauges were outgassed including the anodes of the twin wire gauge. This was achieved by applying about 5 kV to the anode wires and bombarding them with a 100 μA beam of electrons from the filament until the anode wires were observed to reach a cherry red colour. The anodes were not raised to a higher temperature because it was feared that a further increase might cause them to evaporate. No arrangements had been made to outgas the collector wires. The twin wire gauge was compared with a Mullard IOG 20N (modulator) ion gauge also mounted directly into the chamber, as shown in Figure 56(c). The comparison was made under the same conditions as that of Figure 56(b) except that the bias voltage was increased to 130 volts. The modulator gauge indicated a pressure of 5×10^{-11} torr in the chamber whereas the twin wire gauge exhibited a low pressure limit in the region of 2×10^{-10} torr. The low pressure limit of most ion gauges is usually due to two main factors as explained in chapter 1, that is the presence of residual currents due to positive ion desorption from the anode or the presence of residual currents due to the production of X-rays from the anode wires.

In the twin wire gauge the presence of both types of residual current is possible. However since the positive ion desorption characteristics depend on the material of the anodes, whether or not the anodes had been outgassed, the gas in the system and the number of incident electrons, it can be seen that the problem of ion desorption can be reduced by correct choice of materials and processing. In the case of the twin wire gauge tungsten anodes were used because according to Hartmann [23,24] and Lawson [22] tungsten does not show the tendency to absorb oxygen which certain other metals do, and subsequently desorb oxygen ions. Oxygen been shown by Redhead [25] and others to be the most readily desorbed ions. The tungsten anodes were outgassed at a very low pressure, and the emission current used with the twin wire gauge was only 1 μA. Thus it was expected that the major constituent of the residual current was due to X radiation from the anodes. The residual current due to X-ray production has been calculated as approximately 2×10^{-10} in Appendix VII and supports this hypothesis since the calculated residual is in good agreement with the experimental residual.

One other cause of an apparent low pressure limit in the twin wire gauge designed as shown, could be the presence of electrical leakage currents between the collector cage and the anode wires at 1 kV. For example a leakage current of 1×10^{-12} amps would give an apparent low pressure limit of just below 2×10^{-10} torr. This source of error was eliminated since no leakage currents greater than 1×10^{-13} amps were obtained when the oscillator filament was

switched off. It should be noted that any electrical leakage which does occur would do so across the ceramic end bush which is also inside the U.H.V. chamber. The electrical lead throughs which passed through the 6" O.D. steel flange did not present any leakage problem since the flange was at earth potential and therefore acted as a guard ring.

5.9. Conclusions and Future Work

5.9.1 Effects of a potential disturbance

One feature of the work described above was the relatively low sensitivities obtained with the twin wire nude gauge. It was noticed that at an anode voltage of 5 kV, the nude oscillator exhibited a sensitivity of only 3000 $torr^{-1}$ whereas at the same anode voltage and pressure the solid collector thermionic oscillators both large and small were exhibiting sensitivities of the order of 70,000 $torr^{-1}$.

From consideration of the design of the 16 wire nude gauge it was realized that a proportion of the total ion current would be lost because of ions which would escape through the gaps between the collector wires. The effective collecting area of the nude gauge was about 1/10th of the area subtended by the solid cylinder collector of equal diameter. Even if the number of ions lost were in proportion to the collector area the decrease in sensitivity would not be accounted for. Another possible reason for the loss of sensitivity is the distortion of the electrostatic field by the collector wires as shown in Figures 49 and 55. Such a distortion could influence the electron trajectories. This

remark has been supported by experimental work carried out in this laboratory by Rushton [60], in which the gauge sensitivity and therefore presumably the electron trajectories were influenced by changes in the form of the collector cylinder.

5.9.2. Advantages of the twin wire gauge

As described in sections 5.6 and 5.8 the twin wire gauge offers some advantages over conventional commercial gauges. Firstly the fairly high sensitivities obtained enabled emission currents of the order of 10^{-6} amps to be used - rather less than those used by commercial variations of the B.A. gauges. The advantages of low emission currents have been discussed in earlier chapters. Secondly no magnetic field was required with the oscillator. Since magnets are both bulky and expensive, and magnetic fields highly undesirable in most electron and ion optical experiments, the oscillator has considerable advantage over the magnetron and Penning gauges.

The real advantage that the oscillator exhibits over the orbitron gauges described earlier however is that no ion current instabilities have ever been observed with any of the oscillators. The presence of the potential disturbance in the orbitron is regarded as the principal limiting factor of this device. It follows that since the oscillator does not require a potential disturbance to inject the electrons it should in theory be capable of higher sensitivities than the orbitron gauge.

5.9.3. Future work on the twin wire gauge

In order to realise the full potential of the oscillator as an ion gauge it is apparent that future experimental work should

be directed towards obtaining higher sensitivities. Possible methods of achieving this include the use of a double grid to return ions which escape from the collector cage. Such a method has been used with a moderate degree of success with other types of ion gauge. Alternatively it may prove advantageous to revert to the use of the solid collector cylinder. However any such design would have to make a compromise between necessary apertures required for adequate conductance to the vacuum system and the consequent distortion of the field that such apertures would inevitably produce.

Increasing the sensitivity would have the effect of reducing the residual current limit due to both X-rays and ion desorption. The X-ray limit could be further reduced by insulating all the collector wires (including the end plates) except those directly above and below the plane of the anode wires corresponding to the shaded regions in Figure 22. Thus the effective area for collecting X-rays would be substantially reduced without any appreciable reduction in the ion current collected. By making use of the techniques described above it is envisaged that the oscillator - even with a sensitivity of only 2000 $torr^{-1}$ - could exhibit an X-ray limit as low as 10^{-11} torr. If the sensitivity of the oscillator could be increased by a further two orders of magnitude, provided the problem of ion desorption could be overcome it should be possible to reduce the low pressure limit to 10^{-13} torr or less. Such a gauge would be a valuable addition to the existing total pressure measuring devices at these very low pressures.

CHAPTER 6

THE OSCILLATOR AS AN ION PUMP

6.1 Introduction

In recent years interest in ion pumps has centred around the pumping of inert gases, in particular argon, because of the problems associated with argon instability [4,5]. In particular, interest has been shown in the electrostatic 'orb-ion' pumps described for example by Bills [10] and Denison [11]. These have shown a pumping speed for nitrogen as high as 1700 litres per second and for argon of 25 litres per second, or about 1.5% of the pumping speed for nitrogen. Since the oscillator has a high ionizing efficiency it therefore follows that it also has a possible application as an electrostatic ion pump.

It has been shown in chapter 5 that the oscillator can be used in the U.H.V. region only if it is constructed as a thermionic device, because of the observed extinction of the cold cathode discharge at 10^{-6} torr. Consequently, in order that the oscillator could be operated as a U.H.V. ion pump it was necessary to construct it as an ionizer for an evaporation ion pump. Evaporation ion pumps have been described for example by Herb [8], and rely on the pumping of the active gases by the process of gettering, and the burial of the inert gases - in the form of

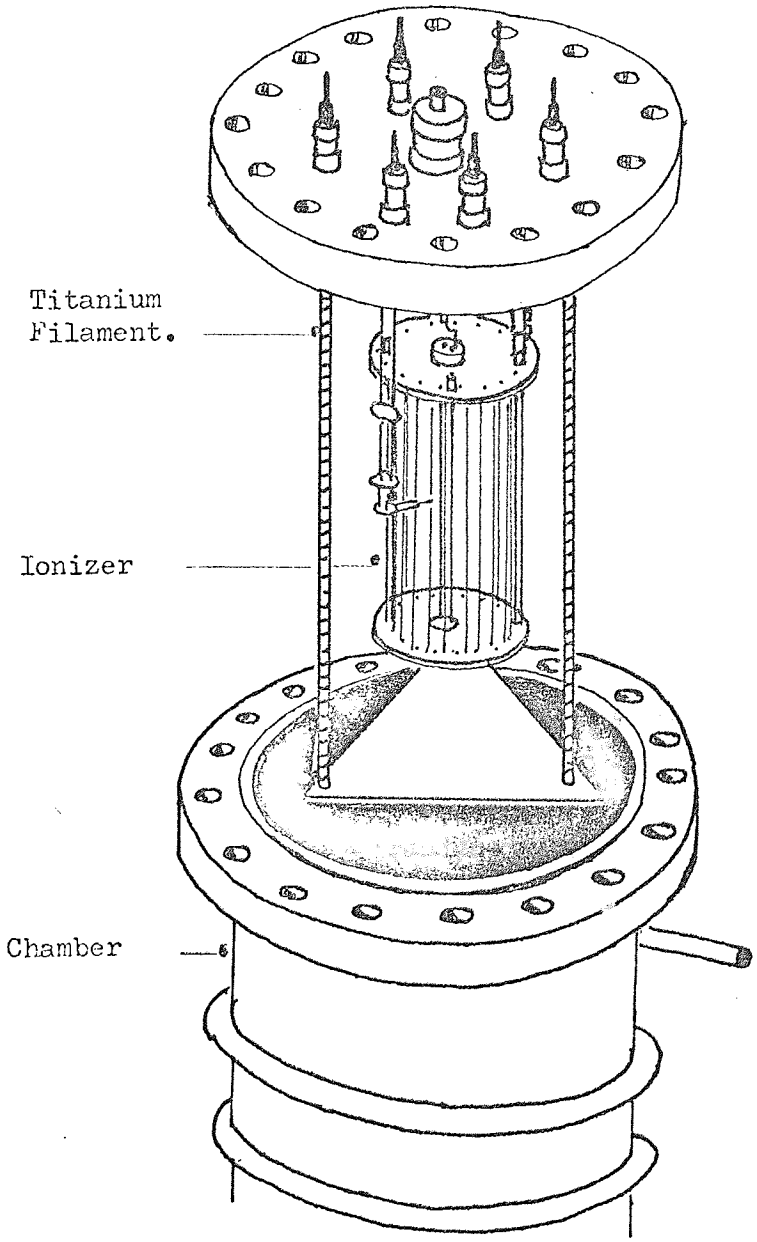

Figure 57

ions - at the pump walls. Since the oscillator may be constructed as an efficient ionizer it was considered that fairly high pump speeds for the inert gases should be possible.

6.2. Construction of a U.H.V. twin wire ion pump

The ion pump consisted essentially of an ionizer and titanium evaporation assembly mounted on a 6" O.D. "conflat" flange and inserted into a water cooled chamber as shown in Figure 57.

The ionizer was constructed as a 16 wire nude gauge identical in all dimensions to the gauge shown in Figure 51. The sublimation assembly consisted of two 'Varian' sublimation pump filaments mounted on the flange either side of the ionizer. These filaments consisted of titanium and tungsten wire twisted together, and required a current of 40 amps at 5 volts in order to deposit the required amount of titanium on the chamber wall. Experiments on filament construction carried out by the author in this laboratory confirmed the necessity of using 'stranded' filaments if a reasonable filament life is required.

The pump body consisted of a 4" diameter stainless steel cylinder with 6" O.D. 'conflat' flanges at either end. This was water cooled using copper piping wound round the steel cylinder. The overall length of the cylinder was 9" and was mounted onto the U.H.V. chamber shown in Figure 53.

6.3. The Electrical Circuit

The circuit consisted of two parts, firstly for the ionizer and secondly for the evaporation assembly. The circuit

used for the ionizer was identical to that used for the thermionic gauge and is shown in Figure 41. The titanium filament supply was a commercial 'Varian' sublimation pump control unit which enabled the sublimation time and cycling rate to be controlled automatically.

6.4. Experimental Results and Discussion

6.4.1. Experimental Technique

The technique used to measure the speed of the twin wire pump was a constant flow method in which the pump was operated against a known leak rate Q_L. The pump speed, S_T, was calculated from the measurement of the equilibrium pressure, P_e, since:-

$$S_T = \frac{Q_L}{P_e}$$

The experimental measurements were therefore separated into two parts, firstly the determination of Q_L and secondly the measurement of P_e.

6.4.2. Measurement of the leak rate Q_L

The U.H.V. system shown in Figure 52 was equipped with a bakeable U.H.V. leak valve with a vernier scale which gave reproducible leak rates between 10^{-9} and 10^{-5} torr litres per second. After bakeout the outgassing rate of the system was reduced to about 5×10^{-8} torr litres per second. The leak valve was adjusted to give leak rates (for nitrogen) about two orders of magnitude greater than this value so that the leak rates should not

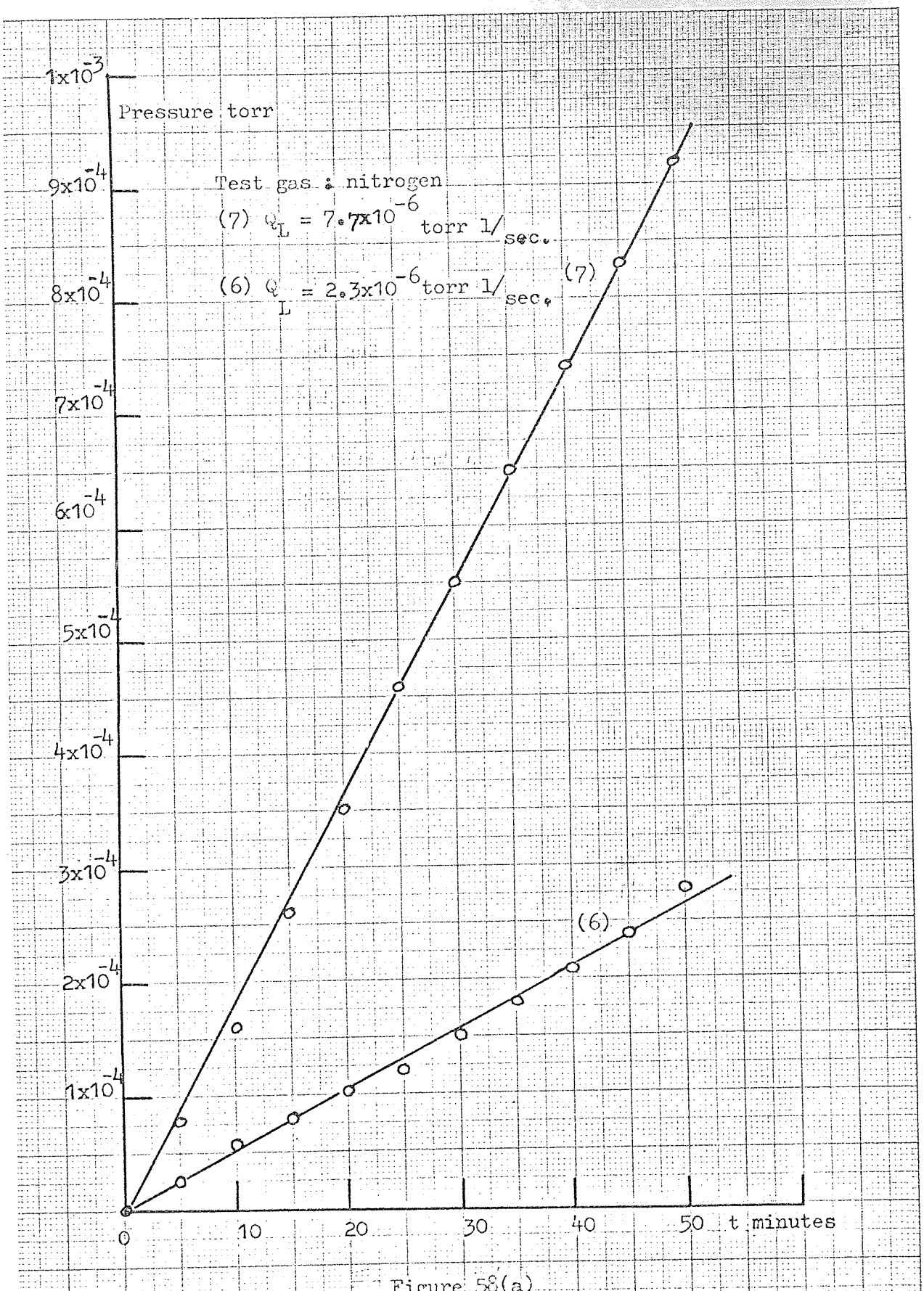
1x10^-3
Pressure torr
9x10^-4
8x10^-4
7x10^-4
6x10^-4
5x10^-4
4x10^-4
3x10^-4
2x10^-4
1x10^-4
Test gas : nitrogen
(7) $Q_L = 7.7 \times 10^{-6}$ torr l/sec.
(6) $Q_L = 2.3 \times 10^{-6}$ torr l/sec.
(7)
(6)
0
10
20
30
40
50
t minutes

Figure 58(a)

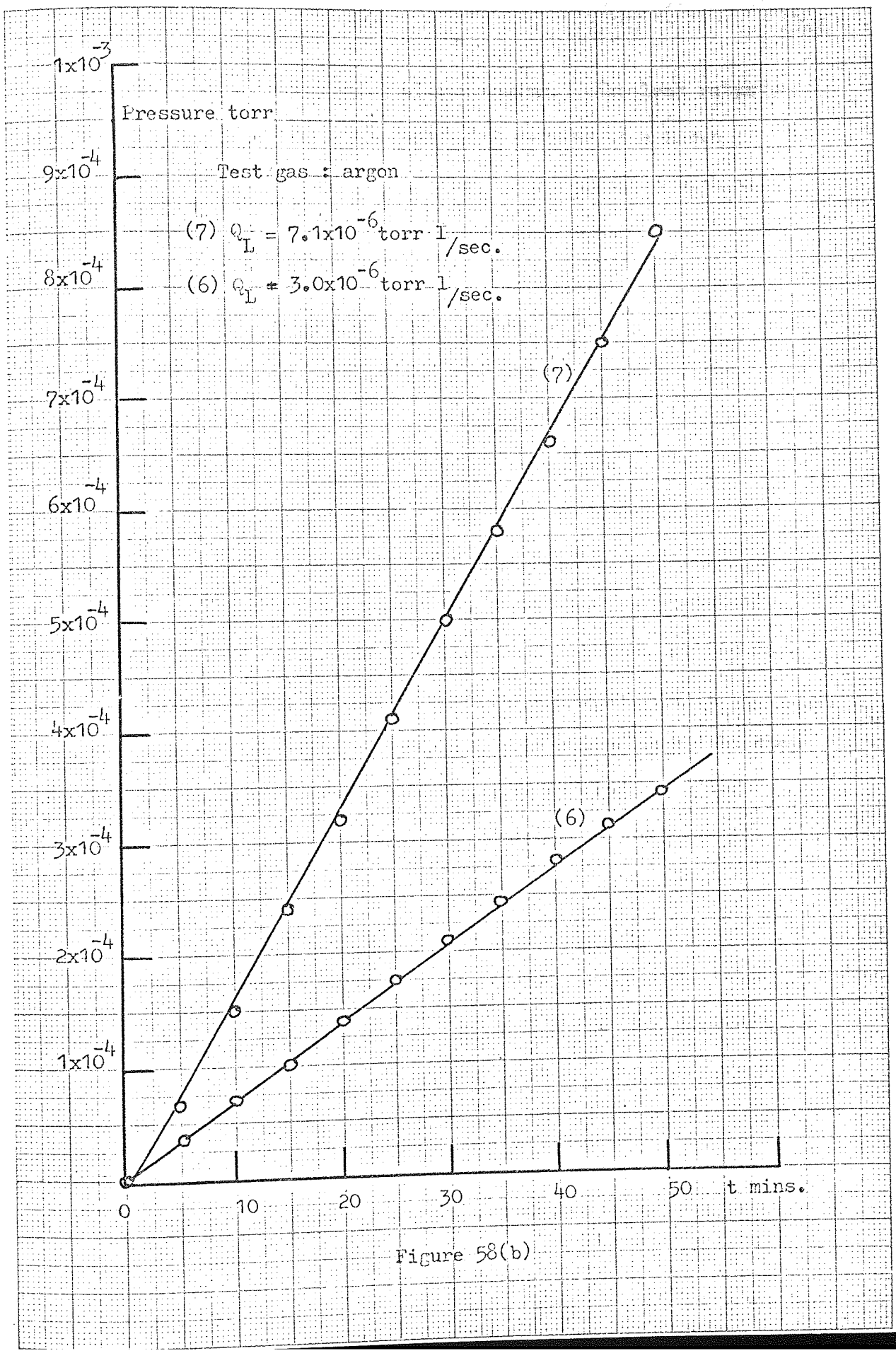
1x10^-3
Pressure torr
9x10^-4
Test gas : argon
(7) Q_L = 7.1x10^-6 torr l/sec.
8x10^-4
(6) Q_L = 3.0x10^-6 torr l/sec.
7x10^-4
(7)
6x10^-4
5x10^-4
4x10^-4
(6)
3x10^-4
2x10^-4
1x10^-4
0
10
20
30
40
50
t mins.

Figure 58(b)

be confused with the outgassing of the system. The leak rates were calculated by setting the leak valve vernier at a known position and measuring the rate of rise of the pressure with all the pumps off. Typical pressure rise plots are shown in Figures 58(a) and (b).

6.4.3. Measurement of the Penning pump speeds

With the leak valve set at positions (6) and (7) the ultimate pressures attainable with the two commercial 15 litre per second slotted cathode Penning pumps were found. Pumping together these sputter ion pumps exhibited a combined speed between 20 and 25 litres per second when nitrogen was leaked into the system. The above experiment was repeated using argon gas and the pumps gave a combined speed of about 3 litres per second, that is about 10% of their rated speed for nitrogen. This is in reasonable agreement with the published data which has established experimentally that slotted cathode, triode and magnetron ion pumps may exhibit pump speeds for argon between 8 - 20% of the speed for nitrogen.

6.4.4. Measurement of the Twin Wire pump speeds

The experiments described in section 6.4.3. were repeated using the twin wire pump. The titanium filament was operated at 40 amps continuously and the ionizer with an emission current of 7 mA. At a pressure of 2×10^{-7} torr the speed for nitrogen was calculated to be between 19 and 21 litres per second, and for argon the speed was about 2.2 litres per second at 10^{-6} torr.

The twin wire pump therefore exhibited a speed for argon slightly greater than 10% of the speed obtained using nitrogen. It can be shown that, operating at the leak rates and ionizer emission described above, an excess of positive ions are produced by the ionizer. For a leak rate of 3×10^{-6} torr litres per second 9×10^{13} molecules enter the system via the leak valve every second. A pessimistic estimate of the number of positive argon ions collected can be made by calculating the number or argon ions collected by the ionizer. With the leak rate at the above value the twin wire pump held an equilibrium pressure of 1×10^{-6} torr. Since the ionizer was operated with an emission current of 7 mA the ion current collected by the ionizer was:-

$$i_p = S.p.i_e$$ where the symbols have their usual notation.

$$i_p = 2{,}500 \times 1 \times 10^{-6} \times 7 \times 10^{-3} \text{ amps}$$

$$= 17.5 \times 10^{-6} \text{ amps}$$

This is equivalent to 1.1×10^{14} ions per second arriving at the collector. Thus 9×10^{13} molecules enter the system per second and 1.1×10^{14} ions arrive at the collector - that is an excess of positive ions are produced. The excess is even greater than the above estimate since many ions escape between

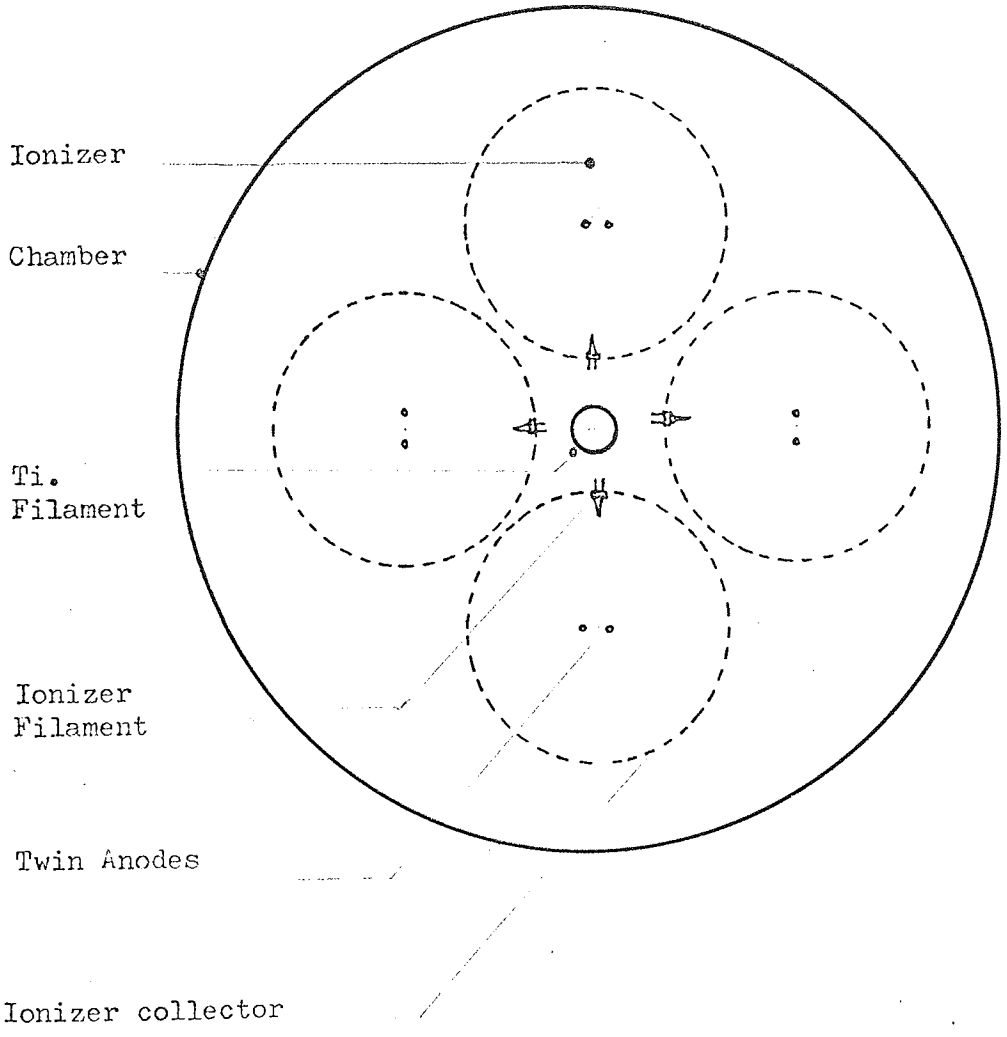
Ionizer
Chamber
Ti.
Filament
Ionizer
Filament
Twin Anodes
Ionizer collector

Figure 59

the collector wires and are buried on the chamber walls.

6.5. Conclusions

The preliminary investigations discussed in this chapter have shown that the oscillator may be successfully applied as an ionizer for an evaporation ion pump, with an argon to nitrogen pump speed ratio of about 10%, which is comparable to the Penning pumps also used, and higher than the ratio exhibited by the pump described by Bills [10]. This could be due to the production of more energetic ions from the twin wire ionizer than from the orbitron ionizers [10].

It is expected that future work with the oscillator applied as an ionizer in an evaporation ion pump would lead to an arrangement as shown in Figure 59. It appears that the filament life of both the ionizer and titanium evaporator in the present design of the twin wire pump is necessarily limited in just the same way as any other evaporation ion pump. Indeed the arrangement described in section 6.2 proved particularly fragile. However the oscillator exhibits a fundamental advantage over the orbitron devices in that ions can be produced with sufficiently high energy to cause sputtering. It follows that if the cold cathode discharge could be maintained to pressures below 10^{-6} torr, the oscillator could be designed as a sputter ion pump which would be robust and simple, as well as free from magnetic fields.

CHAPTER 7

CONCLUSIONS AND SUGGESTIONS FOR FUTURE WORK

This investigation has shown that the oscillator has application as an ultra high vacuum gauge, pump and ion source. Of these the ion source appears particularly promising since it exhibits several advantages over existing sources. Firstly the twin wire source can be used at pressures of 10^{-5} torr or less which, as far as the author is aware, is not possible with any other device. It also has the advantage of being entirely electrostatic thus avoiding the limitations associated with the Penning type ion sources. Furthermore the construction of the oscillator is extremely simple and the emergent ion beam does not require focussing in order to produce a beam density sufficiently high to cause cleaning, polishing and thinning of metallurgical specimens. This ion source can also be used for etching alloys and ceramics and would be particularly useful in the field of electron microscopy, since it could be built into the specimen stage of an electron microscope in order to maintain a clean surface on the specimen. Future work on the ion source should be directed at increasing the ion beam density and maintaining the discharge to lower pressures since any improvements in either of these directions would extend the useful operating range of

the device. It is believed that the ion beam density cannot be greatly increased with the source designed in its present form because of the evaporation of the anode wires when very high discharge currents are used. One further possible development of the ion source is the use of an electrostatic ion lens to focus the emergent ion beam and consequently increase the beam density. However, such a modification would inevitably sacrifice some of the simplicity of the device.

The twin wire ultra high vacuum gauge has also shown several advantages over most existing ionization gauges. For example in one particular gauge specifically designed for U.H.V. operation a sensitivity of about 2600 $torr^{-1}$ was obtained. This enabled an emission current of 1 μA to be used - at least two orders of magnitude less than the emission current of a typical B.A. gauge. Furthermore the absence of magnetic fields allowed the twin wire gauge to be used in situations where the use of a Penning or magnetron type of gauge would be undesirable. The performance of the existing twin wire gauges show some advantage over the orbitron ionization gauge since no ion current instabilities have ever been observed with the twin wire gauge. Two experimental gauges constructed by the author, but not designed for ultra high vacuum use, exhibited sensitivities in the region of 10^5 $torr^{-1}$. With further development it should be possible to combine the high sensitivity with ultra high vacuum construction. The residual current limit of the twin wire gauge can be reduced by suitable design of the collector.

It has not been possible in the present work to investigate the full potential of the ion pump. Preliminary investigations however have shown that the oscillator can be successfully applied as an evaporation ion pump. Pump speeds of 20 litres per second for nitrogen and 2 litres per second for argon have been obtained. Since the performance of any evaporation ion pump is limited by the evolution of gas from the source of titanium it is concluded that future work should be directed towards the problem of sustaining a glow discharge in order that the oscillator could be re designed as a cold cathode sputter ion pump. Such an investigation should study the influence of the electrode surfaces on the discharge, in particular the nature and state of the cathode surface, as it is believed that such an investigation could lead to a better understanding of the discharge process and a subsequent improvement in both the ion pump and ion source.

Finally it is interesting to note that the oscillator principle has been used to acount for the radio sources first discovered by Hewish et al [61] and known as pulsars. McIlraith [62] has shown that by means of a model based on a pair of rotating neutron stars the constancy of the pulse repetition frequency and the shape of the signal received can be interpreted.

APPENDIX I

For an infinitely long cylinder of radius 'b' metres and charge +q coulombs per metre the electric displacement D_r at some radius r when r> b is given by:-

$$D_r = E_r \epsilon \epsilon_o = \frac{q}{2\pi r} \quad \ldots\ldots\ldots \quad (i)$$

when E_r = field at radius r

ϵ = dielectric constant = 1 (vacua) . . dimensionless.

ϵ_o = permitivity of free space = $\frac{1}{36\pi} \times 10^{-9}$ farads metre^{-1}

$$\text{hence } E_r = \frac{-q}{2\pi\epsilon\epsilon_o r} = \frac{-dVr}{dr} \quad \ldots\ldots\ldots\ldots \quad (ii)$$

when V_r is the potential at any radius r, in volts.

thus:-

$$V_r = \frac{-q}{2\pi\epsilon\epsilon_o} \ell n\ r + \text{constant} \quad \ldots\ldots\ldots \quad (iii)$$

Referring to Figure 7. At some point P (x,y) for a cylinder of radius R meters, anode radius 'b' metres, anode separation 2a metres, it follows that the potential at P, from equation (iii), due to a charge +q coulombs per metre on each anode is:-

$$V_p = \frac{-q}{2\pi\epsilon\epsilon_o} \ell n\ r_1 - \frac{q}{2\pi\epsilon\epsilon_o} \ell n\ r_2 + k'_o \qquad k_o \text{ is a constant}$$

$$V_p = \frac{-q}{2\pi\epsilon\epsilon_o} \ell n\ r_1 r_2 + k_o \text{ volts} \quad \ldots\ldots \quad (iv)$$

At the saddle point O, the potential is:-

$$Vo = \frac{-q}{2\pi\epsilon\epsilon_o} \ln a^2 + k_o \quad \text{volts}$$

The potential at P relative to that at O is:-

$$V_{xy} = V_p - V_o$$

$$= \frac{-q}{2\pi\epsilon\epsilon_o} [\ln r_1 r_2 - \ln a^2]$$

$$= \frac{q}{2\pi\epsilon\epsilon_o} \ln \frac{a^2}{r_1 r_2} \quad \ldots\ldots\ldots\ldots \text{(v)}$$

$$= \frac{q}{4\pi\epsilon\epsilon_o} \ln \frac{a^4}{(r_1 r_2)^2}$$

since:-

$$r_1^2 = (x^2+a^2) + y^2$$

$$r_2^2 = (x^2-a^2) + y^2 \quad \text{then:-}$$

$$V_{xy} = \frac{q}{4\pi\epsilon\epsilon_o} \ln \frac{a^4}{(y^2+(x-a)^2)(y^2+(x+a)^2)} \quad \text{(vi)}$$

Differentiating with respect to x and y gives the field in the x and y directions respectively:-

$$E_x = \frac{-\partial V_{xy}}{\partial x} = \frac{-q}{4\pi\epsilon\epsilon_o} \cdot \frac{4x(x^2+y^2-a^2)}{(y^2+(x+a)^2)(y^2+(x-a)^2)} \quad \text{(vii)}$$

$$E_y = \frac{-\partial V_{xy}}{\partial y} = \frac{-q}{4\pi\epsilon\epsilon_o} \cdot \frac{4y(x^2+y^2+a^2)}{(y^2+(x+a)^2)(y^2+(x-a)^2)} \qquad \text{(viii)}$$

$$[E_x] = \frac{\partial V_{xy}}{\partial x} \quad \text{and} \quad [E_y] = \frac{\partial V_{xy}}{\partial y}$$

From (wii) $E_x = 0$ if $x = 0$ or $x^2+y^2-a^2=0$

i.e. $E_x = 0$ at the saddle point and on a circle passing through the poles and with the poles as a diameter. Inside this circle $x^2+y^2<a^2$ hence $[E_x]$ is negative. The force on an electron in the x direction is eE_x when 'e' is the electron charge, and this will be directed away from the y axis inside the circle.

Converseley if $x^2+y^2>a^2$ $[E_x]$ is positive and electrons are attracted towards the y axis. The force $F_y = eE_y$ is always directed towards the x axis since $(x^2+y^2+a^2)$ is always positive;

It can be seen that $\frac{E_y}{E_x} \rightarrow \frac{y}{x}$ if $x^2+y^2>>a^2$

The equation of motion of an electron on the y axis can be obtained from equation (viii). The accelerating force on an elcctron towards the saddle point is:-

$$F_y = + (E_y)_x = o$$

Hence the equation of motion of such an electron is:-

$$m\ddot{y} = +e(E_y)_x = o \qquad \text{when}$$

$$\ddot{y} = \frac{d^2y}{dt^2}$$

t = time in seconds

m = mass of electron in Kgm

$$\therefore \quad \ddot{y} = + \frac{e}{m} (E_y)_{x=o}$$

From equation (viii) when x = o

$$(E_y)_{x=o} = \frac{-qy}{\pi\epsilon\epsilon_o} \cdot \frac{1}{(y^2+a^2)}$$

$$= \frac{-q}{\pi\epsilon\epsilon_o} \cdot \frac{y}{y^2+a^2}$$

hence:-

$$\ddot{y} + \frac{e}{m}\left(\frac{q}{\pi\epsilon\epsilon_o}\right)\frac{y}{y^2+a^2} = 0 \quad \ldots\ldots \quad (ix)$$

Equation (ix) can be written in a more practical form by evaluating 'q'. Suppose the superposition of the outer electrode radius R at earth potential is such that the electrostatic field is not significantly different from the field with an infinite boundary i.e. assume R is large compared with 'a' then:-

$$r_1^2 = r_2^2 = R^2+a^2$$

The potential at the cylinder wall is:-

$$V_R = \frac{-q}{4\pi\epsilon\epsilon_o} \ln (R^2+a^2)^2 + k_o$$

The potential at the surface of the anode wires is:-

$$V_a = \frac{-q}{4\pi\epsilon\epsilon_o} \ln (b^2(2a-b)^2) + k_o$$

If the potential of the anodes with respect to the outer collector (which is at earth potential) is V_A

$$V_A = V_a - V_R$$

$$= \frac{-q}{4\pi\epsilon\epsilon_o} [\ln(b^2(2a-b)^2) - \ln (R^2+a^2)^2]$$

$$= \frac{2q}{4\pi\epsilon\epsilon_o} \ln \frac{R^2+a^2}{b(2a-b)}$$

hence

$$q = \frac{4\pi\epsilon\epsilon_o V_A}{2\ln\left(\frac{R^2+a^2}{b(2a-b)}\right)} \quad \ldots\ldots\ldots\ldots (x)$$

Thus the equation of motion may be written as:-

$$\ddot{y} + \frac{e}{m}\frac{1}{\pi\epsilon\epsilon_o}\frac{4\pi\epsilon\epsilon_o V_A}{2\ell n\left(\frac{R^2+a^2}{b(2a-b)}\right)}\frac{y}{y^2+a^2} = 0$$

or

$$\ddot{y} + \frac{4eV_A}{2m\ell n\left(\frac{R^2+a^2}{b(2a-b)}\right)}\frac{y}{y^2+a^2} = 0 \quad \ldots\ldots (xi)$$

writing

$$k_1 = \frac{2eV_A}{m\ell n\left(\frac{R^2+a^2}{b(2a-b)}\right)}$$

$$\ddot{y} + k_1\frac{y}{y^2+a^2} = 0 \quad \ldots\ldots\ldots\ldots (xii)$$

It can be seen that if $y<a$ i.e. $y^2<<a^2$

$$\ddot{y} + \frac{k_1}{a^2}\cdot y = 0$$

However in most cases $y^2 \not< a^2$ hence the motion is not S.H.M. Unfortunately equation (ix) is not soluble for y analytically in terms of t, but can be solved for $\dot{y}$.

$$\dot{y} = \frac{dy}{dt} \qquad \frac{d}{dt}(\dot{y}) = \frac{-k_1 y}{y^2+a^2}$$

hence

$$\frac{dy}{dt}\int d(\dot{y}) = -k_1\int\frac{ydy}{y^2+a^2}$$

$$\therefore \quad (\dot{y})^2 = -\frac{k_1}{2} \ln (y^2+a^2) + \text{constant } k_2$$

when $\frac{dy}{dt} = 0 \quad y = y_o$ when y_o describes the distance from the saddle point at the time when the particle is momentarily at rest.

$$\therefore \quad 0 = -\frac{k_1}{2} \ln(y^2+a^2) + k_2$$

$$\therefore \quad \dot{y}^2 = \frac{k_1}{2} [\ln(y_o^2+a^2) - \ln(y^2+a^2)]$$

$$\dot{y} = \left[\frac{k_1}{2}\right]^{\frac{1}{2}} \left[\ln \frac{y_o^2+a^2}{y^2+a^2}\right]^{\frac{1}{2}}$$

$$dt = \left[\frac{2}{k_1}\right]^{\frac{1}{2}} \left[\ln \frac{y_o^2+a^2}{y^2+a^2}\right]^{-\frac{1}{2}} dy$$

The period T_n is given by:-

$$T_n = 4 \left[\frac{2}{k_1}\right]^{\frac{1}{2}} \int_o^{y_o} \left[\ln \frac{y_o^2 + a^2}{y^2 + a^2}\right]^{-\frac{1}{2}} dy \quad \ldots \quad \text{(xiii)}$$

This expression is not soluble analytically but may be solved by numerical techniques, assuming the following values.

V_A = 10 kV

e/m = 1.76×10^8 coulombs/gm = 1.76×10^{11} coulombs/kgm

R = 0.027 metres

a = 0.0025 metres

b = 0.0001 metres all of which values have been used in practice.

Inserting these figures into equation (xiii) and solving numerically, yields the following table.

Table 1

y_o	Period T_n (seconds)	Frequency f_n (c.p.s.)
2a	1.38×10^{-9}	7.27×10^{8}
4a	2.42×10^{-9}	4.15×10^{8}
6a	3.50×10^{-9}	2.86×10^{8}
8a	4.73×10^{-9}	2.11×10^{8}
10a	5.75×10^{-9}	1.74×10^{8}

If we had assumed the particle performed S.H.M.

i.e. $$\frac{d^2y}{dt^2} = \frac{-4\pi^2}{T^2} \cdot y$$

and:- $$e\frac{dV_{xy}}{dy} = e(E_y)_{x=o} = m\frac{d^2y}{dt^2}$$

gives $$T^2 = \frac{4\pi^2 y^2}{2e/m \cdot V_{xy}}$$

then the simple harmonic frequency is given by

$$f_{SHM} = \frac{1}{2\pi y_o} \sqrt{\frac{2eV_{xy}}{m}}$$

substituting for V_{xy} yields

$$f_{SHM} = \frac{1}{2\pi y_o} \sqrt{k_1 \ell n \frac{y_o^2 + a^2}{a^2}}$$

substituting the values for k_1, y_o, a, assumed above it is possible to make a comparison between the S.H.M. frequency and the oscillator frequency.

TABLE 2

y_o	$f_{SHM.}$ (C.P.S.)	$f_{oscillator}$ (c.p.s.) = f_n
2a	8.75×10^8	7.27×10^8
4a	5.80×10^8	4.15×10^8
6a	4.37×10^8	2.86×10^8
8a	3.52×10^8	2.11×10^8
10a	3.02×10^8	1.74×10^8

It can be seen from the above table that if $y_o \leq 2a$ the approximation to S.H.M. is within 12%. When y_o is large the approximation to S.H.M. becomes increasingly less valid confirming predictions made from equation (ix).

APPENDIX II

In order to simplify the analysis of axial reflection consider the oscillator as consisting of a cylinder radius R length 2L, with a single central pole of radius a, along the Z axis. Assuming the cylinder at earth potential and the central pole at a potential V_o with respect to earth, i.e. the saddle point potential, Figure 9 shows that, by the method of images, the cylinder with plane end plates is equivalent to an infinitely long cylinder at earth potential containing a set of wires running along the Z axis each of length 2L and potential alternatively $\pm V_o$. By Fourier analysis, the potential of the central electrode at some position Z is:-

$$V_Z = \frac{4V_o}{\pi}\left[\sin\frac{\pi Z}{2L} + \frac{1}{3}\sin\frac{3\pi Z}{2L} + \cdots\right]$$

that is:-

$$V_Z = \frac{4V_o}{\pi}\sum_{n=0}^{n=\infty}\frac{1}{2n+1}\sin\frac{(2n+1)\pi Z}{2L} \quad \cdots \quad (i)$$

Suppose V is the potential at some arbitrary point (r,z) when $a < r < R$. V must satisfy Laplaces equation in this space. Since the field is symmetrical about the Z axis, Laplaces equation may be reduced to:

$$\frac{\partial^2 V}{\partial r^2} + \frac{1}{r}\frac{\partial V}{\partial r} + \frac{\partial^2 V}{\partial Z^2} = 0 \quad \ldots\ldots \text{(ii)}$$

The solution V can be expressed as a function of r, and z, thus:-

$$V = R(r)\, Z(z) \quad \ldots\ldots \text{(iii)}$$

Using equation (ii)

$$R^{11}(r)\, Z(z) + \frac{1}{r} R^{1}(r) Z(z) + R(r)\, Z^{11}(z) = 0$$

Dividing by R(r) Z(z)

$$\frac{R^{11}(r)}{R(r)} + \frac{1}{r}\frac{R^{1}(r)}{R(r)} + \frac{Z^{11}(z)}{Z(z)} = 0$$

Separating the variables

$$\frac{R^{11}(r)}{R(r)} + \frac{1}{r}\frac{R^{1}(r)}{R(r)} = -\frac{Z^{11}(z)}{Z(z)} = -k^2$$

Hence

$$\frac{R^{11}(r)}{R(r)} + \frac{1}{r}\frac{R^{1}(r)}{R(r)} + k^2 = 0$$

This can be re-written

$$r^2 R^{11}(r) + r R^{1}(r) + r^2 k^2 R(r) = 0 \quad \ldots \text{(iv)}$$

The general Bessel equation is:-

$$r^2 R^{11}(r) + r\, R^{1}(r) + (r^2 - n^2)\, R(r) = 0$$

when n is not an integer, as in equation(iv) we have a modified Bessel equation. Hence solving Laplaces equation for each component of equation(i) using the solution to the modified Bessel function (iv) yields on adding

$$V = \Sigma \left[A_n I_o(\alpha_n r) + B_n K_o(\alpha_n r) \right] \frac{\sin \alpha_n z}{n} \quad \ldots\ldots (v)$$

when I_o and K_o are modified Bessel functions of $(\alpha_n r)$ and:-

$$\alpha_n = \frac{n\pi}{2L} \quad : \quad A_n = \frac{1}{I_o(\alpha_n a) - I_o(\alpha_n R) K_o(\alpha_n a) \Big/ K_o(\alpha_n R)}$$

$$B_n = - \frac{A_n I_o(\alpha_n R)}{K_o(\alpha_n R)}$$

R = radius of outer cylinder

a = radius of central pole

Assuming values of a: R: L = 1 : 100 : $1000\ ^{\pi}/_{2}$ then

$\alpha_1 a = 0.001$; $\alpha_1 R = 0.1$; $a_1 L = {}^{\pi}/_{2}$

McIlraith [46] shows expression (v) to be slowly convergent, hence it proved necessary to use thirty terms in the summation. It can

be seen that $\alpha_1 z = \frac{\pi z}{2L}$

Values of $\alpha_1 z$ were taken for $\alpha_1 z = 4.5^\circ$ and 90° i.e. for $z = 0.786\ R$ and for $z = L$. The variation in V for these two values of $\alpha_1 z$ were found for different values of r/R. Table 3 summarises the results.

Table 3

r/R	$V_z = L$	$V_z = 0.786R$	δV (expressed as a percentage)
0.1	0.3922	0.3855	- 1.7%
0.3	0.2053	0.1884	- 8.2%
0.5	0.1177	0.1025	- 12.9%
0.7	0.0608	0.0508	- 16.5%
0.9	0.1780	0.0147	- 17.3%
1.0	0.0000	0.0000	-

As to be expected, the greatest percentage change in the field occurs at the outer electrode. It is reasonable to suppose that if this central wire were to be displaced from the axis of the cylinder a small distance the field due to it would vary with z in a manner similar to that found above. As far as the termination of the field is concerned, Table 3 gives a good approximation to the case of the twin wire oscillator.

Since the value of R has been taken as $\frac{100}{1000} \cdot \frac{2}{\pi} L$

it follows that when $z = 0.786\ R$

$$z = \frac{0.78 \times 2L}{10\pi}$$

i.e. the fractional length of the length $z = 0.786\ R$ from the end of the oscillator is

$$= \frac{0.78}{10\pi} \times 100\% = 2.5\%$$

Consequently even at the walls of the cylinder, the field remains uniform within an error of 17.3% for 95% of the length of the oscillator, and this is the largest degree of non uniformity of the field over this length of tube. When r/R is only 0.1 the degree of non uniformity is only 1.7% over 95% of the oscillators length.

It follows that the arrangement described by Figure 9 utilizing flat end plates makes effective use of the volume of the oscillator.

Appendix III

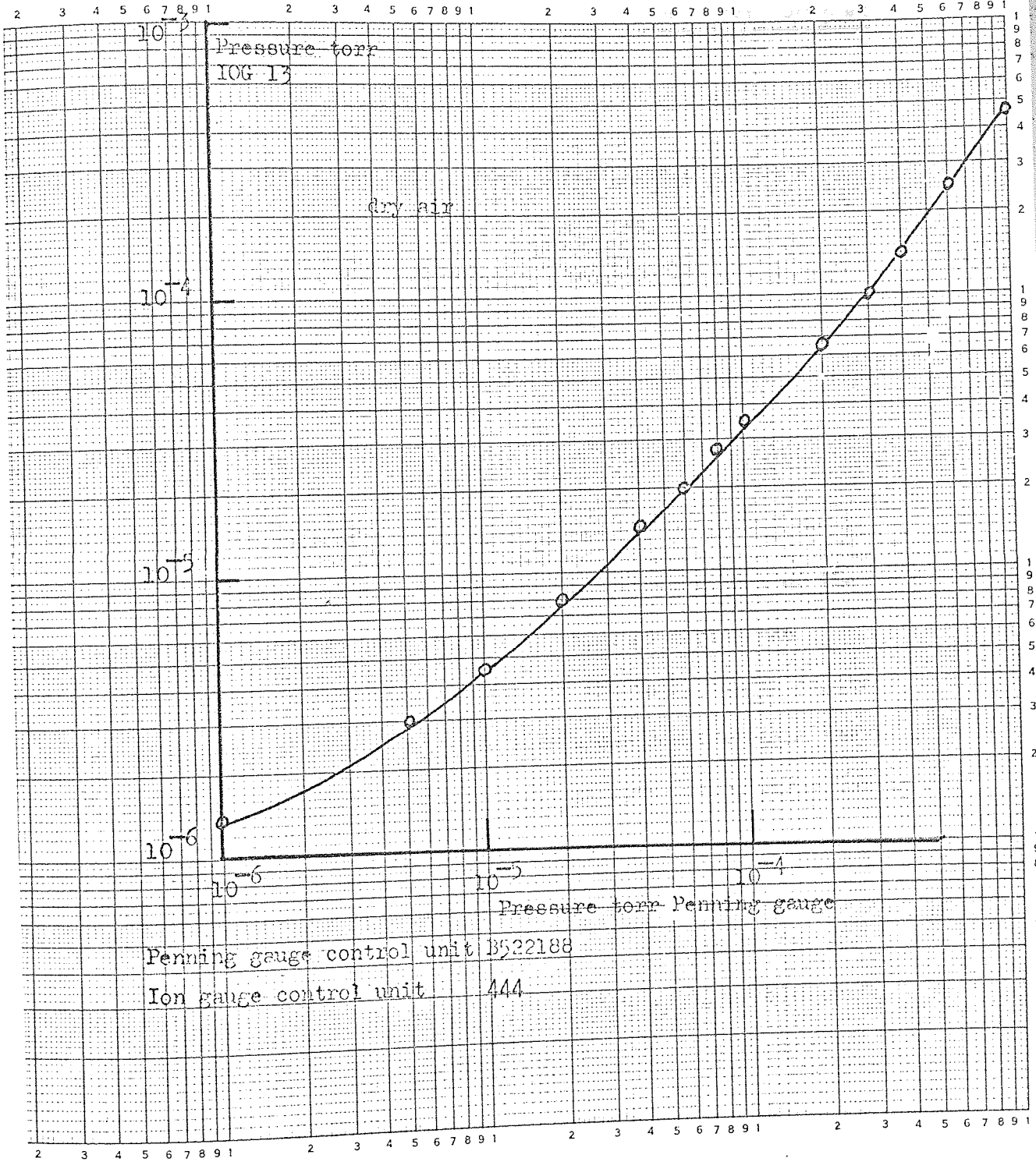

APPENDIX IV

CALCULATION OF ION SOURCE ENERGIES FROM ETCH WIDTH CONSIDERATIONS

Introduction

It is well known that a slot or aperture can have a focussing effect on a beam of ions or electrons. Such a phenomena is utilized for example in 3 electrode electrostatic lenses. The slot in the ion source has a divergent effect on the ions leaving the oscillator. The effective focal length of the slot depends upon the electrostatic field at the slot and the energy of the ions passing through it.

It was noticed during the experimental investigation of sputtering of copper that the width of the etched region of the specimen was dependent upon the voltage applied across the oscillator. It became apparent that if the focal length of the slot were known for the particular ions under consideration the starting point of the ions within the oscillator - and consequently the ion energies - could be estimated from a measurement of this etched width.

Correspondingly the technique used to estimate the ion energies is set out below. This requires an initial estimate of the ion energies and application of the method of successive approximations.

It should be noted that the method is NOT considered accurate and is intended to give a rough approximation only to the ion energy. Several drastic approximations are made which lead to results that are accurate only to within a few kV.

SUMMARY OF METHOD

1. For a given applied voltage across the tube V_t it was assumed that the ions were born on average at some equipotential ϕ This value was estimated with some previous information from sputtering yield data. It was assumed that any ion born on the equipotential ϕ had zero initial kinetic energy - consequently that ϕ represents the energy of the ion emerging from the slot. This assumption is reasonable since the interchange of momentum of an electron in collision with an atom imparts little momentum to tne resultant positive ion.

2. The corresponding focal length of the slot f (ϕ) was calculated corresponding to each value of ϕ and V_t.

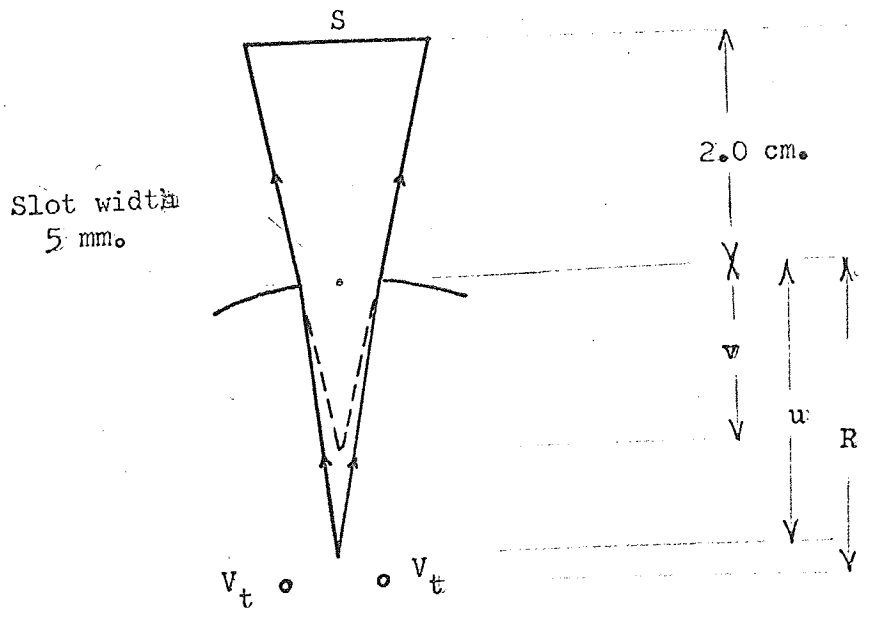

3. Using the above figure the position v was calculated from measurements of the etch width S (i.e. the total angular spread of the beam) - accurate only to 10%

4. The lens formula $\frac{1}{u} + \frac{1}{v} = \frac{1}{f(\phi)}$ was applied to <u>each</u> value of $f(\phi)$, and corresponding values of u obtained. This is justifiable only if individual values of $f(\phi)$ are considered.

5. From the position u the corresponding starting point of the ion was known. By using field plots obtained in chapter 2 the corresponding equipotential ϕ_1 was estimated.

6. If the value of ϕ_1 was not reasonably close to the predicted value of ϕ for the ion energy the process was repeated with ϕ_1 as the approximation.

<u>CALCULATION</u>

It can be shown from Appendix II that the field on the y axis of the oscillator is given by

$$E_y = \frac{-q}{\pi\epsilon\epsilon_0} \cdot \frac{y}{y^2+a^2} \quad \ldots\ldots (i)$$

where the symbols have the same meanings as before. It has also been shown that

$$q = \frac{2\pi\epsilon\epsilon_0 V_t}{\ell n\left(\frac{R^2+a^2}{b(2a-b)}\right)} \quad \ldots\ldots\ldots (ii)$$

when V_t is the P.D. across the tube with radius R. It follows

that

$$E_y \simeq \frac{2V_t}{\ell n\left(\frac{R^2+a^2}{2ab}\right)} \cdot \frac{y}{y^2+a^2} \quad \ldots \text{(iii)}$$

at the cylinder wall

$$y = R \qquad R^2 >> a^2 \quad :-$$

$$E_{wall} \simeq \frac{2V_t}{\ell n\left(\frac{R^2}{2ab}\right)} \cdot \frac{1}{R} \quad \ldots\ldots\ldots \text{(iv)}$$

if $R = 10a = 100b$

$$E_{wall} \simeq \tfrac{1}{3} \cdot \frac{V_t}{R} \qquad \text{from equation (iv)}$$

The focal length of the slot which acts as a cylindrical lens is given by

$$f(\phi) \simeq \frac{2\phi}{E_{wall} - E_{outside\ wall}} \quad \ldots\ldots \text{(v)}$$

(Bull, S.C. J.I.E.E. Part III 1945)

when ϕ is the energy of the ion passing through the slot and $f(\phi)$ is dependent on this energy as described previously.

Since $E_{\text{outside wall}} = 0$ from equations (iv) and (v)

$$f(\phi) \simeq \frac{\phi}{V_t} \cdot R \cdot \ln \frac{R^2}{2ab} \quad \ldots\ldots\ldots \text{(vi)}$$

$$\simeq \frac{152\phi}{V_t} \text{ mm.}$$

Since R = 25.4 mm.

At this point it is necessary to assume values for ϕ corresponding to the applied voltage V_t. The values of ϕ were estimated from sputtering data. It should be recognised that in all probability the actual spread of energies of the ions produced is very large with the consequence that the meaning of such a value ϕ becomes rather dubious. However estimating ϕ leads to a crude approximation of the ion energies as follows.

V_t(kV)	1st approximation of ϕ (kV)	$\frac{\phi}{V_t}$	$f(\phi)$
8.0	6.6	0.8	~ 127 mm
7.0	5.5	0.78	117 mm
6.0	2.0	0.33	50 mm
5.0	1.3	0.20	30 mm
4.0	0.5	0.13	20 mm

Now by measuring the width of the etched region S shown in the above diagram, the value of v may be determined

$$\text{since } v = \frac{100}{S-5} \quad \ldots\ldots\ldots\ldots \text{(viii)}$$

TABLE 4

V_t(kV)	S(mm)	v(mm)
8.0	9.5 ± 0.5	22.3
7.0	11.0 ± 0.5	16.7
6.0	14.0 ± 1.0	11.1
5.0	17.0 ± 2.0	8.3
4.0	19.0 ± 3.0	7.1

By using the well known lens equation

$$-\frac{1}{u} + \frac{1}{v} = \frac{1}{f(\phi)}$$

$$u = \frac{vf(\phi)}{[f(\phi)-v]} \quad \ldots\ldots\ldots \text{(viii)}$$

TABLE 5

V_t(kV)	v(mm)	U(mm)
8.0	22.3	≈ 26
7.0	16.7	19.5
6.0	11.1	14.4
5.0	8.3	10.4
4.0	7.1	11.0

Finally by comparing the position of U on a field plot the second approximations ϕ_1 and where necessary third approximations ϕ_2 are obtained

TABLE 6

V_t(kV)	U(mm)	% field line	ϕ (kV)	from ϕ ϕ_1 (kV)	from ϕ_1 ϕ_2 (kV)
8.0	~ 26	80	6.6	6.4	-
7.0	19.5	50	5.5	3.5	4.2
6.0	14.4	32	2.0	1.9	-
5.0	10.4	18	1.3	0.9	0.9
4.0	11.0	~ 18	0.5	0.7	-

It can be seen that by using this method the ion energies ϕ_1 and ϕ_2 can be estimated to within a few kV.

APPENDIX V

MATCHING THE FILAMENT POTENTIAL IN THE TWIN WIRE GAUGE

From Appendix I suppose the filament tip lies at some position 'p' on the y axis as shown below

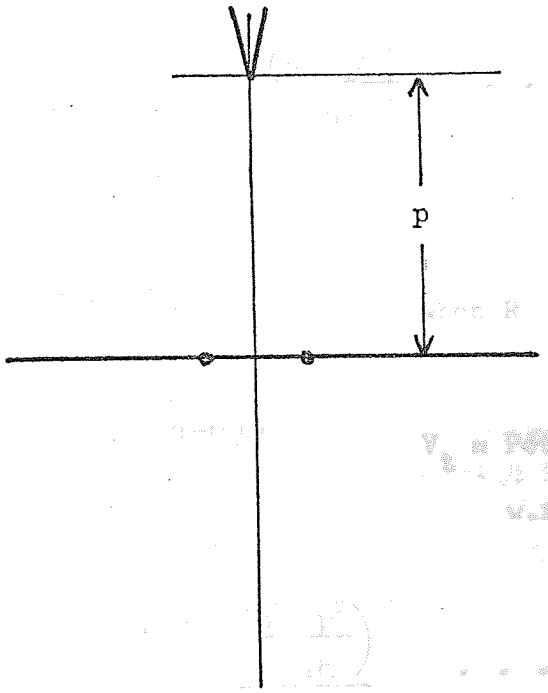

If the potential at the surface of the anode wires is V_a then the p.d. (due to the potential on the anode wires) between the position of the filament tip and the anode wires is given by

$$V_f = V_p - V_a \quad \ldots\ldots\ldots\ldots \quad (i)$$

now

$$V_p = \frac{-q}{2\pi\epsilon\epsilon_o} \ln (a^2+p^2) + k_o$$

from Appendix I equation(iv)

where the symbols have their usual meanings.

Similarly

$$V_a = \frac{-q}{2\pi\epsilon\epsilon_o} \ln b(2a-b) + k_o$$

thus

$$V_f = \frac{-q}{2\pi\epsilon\epsilon_o} \ln \frac{(a^2+p^2)}{b(2a-b)} \quad \ldots\ldots\ldots \text{(ii)}$$

but from Appendix I equation (x)

$$q = \frac{2\pi\epsilon\epsilon_o V_t}{\ln\left(\frac{R^2+a^2}{b(2a-b)}\right)}$$

when R = radius of collector cage

V_t = Potential of anode wires w.r.t. the collector

thus

$$V_f = -V_t \frac{\ln\left(\frac{a^2+p^2}{2ab}\right)}{\ln\left(\frac{a^2+R^2}{2ab}\right)} \quad \ldots\ldots\ldots \text{(iii)}$$

In practice V_t = 1000 volts (say)

2a = 2.5 mm

2b = 0.1 mm

R = 12.5 mm

p = 8.0 mm

potential difference between anode wires and filament tip is:-

$$V_f \simeq 1000 \frac{\ln\left(\frac{1.56 + 64}{0.125}\right)}{\ln\left(\frac{1.56 + 156}{0.125}\right)}$$

$$\simeq \quad 870 \text{ volts}$$

potential difference between filament tip and collector cage is therefore

$$V_t - V_f = 130 \text{ volts} = V_t \left(1 - \frac{\ln\left(\frac{a^2+p^2}{2ab}\right)}{\ln\left(\frac{a^2+R^2}{2ab}\right)}\right) \qquad \text{(iv)}$$

Thus for minimum disturbance of the electrostatic field, the bias at the filament tip should be $V_B = V_t - V_f = 130$ volts i.e. the ratio

$$\frac{V_B}{V_t} = 0.13$$

It can be seen from Figure 54 that the above hypothesis agrees very well with the experimental results.

APPENDIX VI

THEORETICAL HIGH PRESSURE LIMIT OF TWIN WIRE NUDE GAUGE

The high pressure limit of any ion gauge occurs when the secondary currents are of the same order as the primary ionizing beam (Leck [18]). Below this limit the equation given below defines the ion current

$$i_p = S.p.i_e \quad \ldots\ldots\ldots\ldots \quad (i)$$

Suppose that 10% of the electrons collected at the anode wires are from sources other than the primary beam i.e. electrons resulting fro m the primary ionization processes. In this case there is an apparent increase in the emission current of 10% with no further increase in the ion current, i_p. This occurs when $\frac{i_p}{i_e} = \frac{1}{10}$, so that the pressure at which this occurs is given by:

$$p = \frac{1}{S} \frac{i_p}{i_e} = \frac{1}{10} \times \frac{1}{2000} \text{ torr}$$

$= 5 \times 10^{-5}$ in the case of the nude twin wire gauge, which is in good agreement with Figure 56(c).

APPENDIX VII

RESIDUAL CURRENTS DUE TO X-RAYS

If the emission current $i_e = 10^{-6}$ amps and the anode voltage 1000 volts then the rate of energy loss to the anode wires is

$$10^{-6} \times 10^{3} \text{ watts}$$

$$= 10^{-3} \text{ watts}$$

The electrons strike the anode wires producing soft X-rays. The efficiency of producing X-rays is

$$\epsilon = kzV_t = \frac{\text{energy/}_{\text{sec}} \text{ X-rays emitted}}{\text{energy/}_{\text{sec}} \text{ electrons collected}} \qquad \text{(i)}$$

when

z = atomic No. = 74 for Tungsten

k = Konstant = 10^{-9} volts

V_t = Anode volts = 10^{3} volts

From equation (i) the energy/$_{\text{sec.}}$ of the emitted X-rays is given by W when

$$W = \text{energy/}_{\text{sec}} \text{ electrons collected} \times kzV_t$$

$$W = 10^{-3} \times kzV_t$$

$$W = 7.4 \times 10^{-8} \text{ watts}$$

If the X-rays strike the collector, assuming each X-ray reaches the collector the number of electrons liberated per second is given by:

$$n = Q \times \text{no. of X-ray photons arriving per second} \quad \ldots\ldots\ldots\ldots\ldots\ldots \text{(ii)}$$

when Q is the quantum efficiency and depends on the photon energy and target material.

The number of X-ray photons arriving per second is:-

$$= \frac{W}{\text{X-ray energy per photon}}$$

$$= \frac{7.4 \times 10^{-8} \text{ watts}}{1.6 \times 10^{-19} \times 10^{3} \text{ joules}}$$

$$= 4.6 \times 10^{8} \text{ photons/sec.}$$

Hence if the quantum efficiency Q for 1000 volt photons striking tungsten is 10^{-2} , from equation (ii)

$$n = 10^{-2} \times 4.6 \times 10^{8} \text{ electrons/sec.}$$

and this is equivalent to a residual current of

$$i_r = 1.6 \times 10^{-19} \times 4.6 \times 10^{8} \times 10^{-2} \text{ amps}$$

when the charge on one electron is 1.6×10^{-19} coulombs.

$\therefore \quad i_r = 7.4 \times 10^{-13}$ amps

if the twin wire oscillator has an effective collection area of about $\frac{1}{10}$ of that of the solid cylinder, the residual current becomes

$$i_r = \frac{7.4}{10} \times 10^{-13} \text{ amps}$$

$$i_r \simeq 1 \times 10^{-13} \text{ amps (say)}$$

In practice the effective area of the 16 wire nude gauge is about $\frac{1}{10}$ of the total area presented by a solid cylinder, consequently the residual current due to X-rays is of the order of 10^{-13} amps with the nude gauge. If the nude gauge has a sensitivity of ~ 2500 torr^{-1}, the ion current due to gas ionization at a pressure of 2×10^{-10} torr would be

$$i_p = S.p.i_e$$

$$= 2.5 \times 10^3 \times 2 \times 10^{-10} \times 10^{-6} \text{ amps}$$

$$= 5 \times 10^{-13} \text{ amps}$$

Thus at 2×10^{-10} torr the residual current is about $\frac{1}{5}$ of the ion current i_p. Consequently an X-ray limit in the region of 2 or 3×10^{-10} torr is expected.

List of Figures

List of main symbols

a	=	Half the anode centre to centre separation
$B, B_x \ldots$	=	Magnetic field
b	=	Anode wire radius
D_r	=	Electric displacement
e	=	Electron charge
$E, E_x \ldots$	=	Electrostatic field
$F, F_x \ldots$	=	Force on an electron or ion
$f(\phi)$	=	Focal length
f_n	=	Frequency
I_t	=	Tube current
i_a	=	Anode current
i_e	=	Emission current
i_f	=	Filament current
i_p	=	Positive ion current; collector current.
$K, k, k_o \ldots$	=	Konstants
m	=	Mass of an electron
P, p	=	Pressure
q	=	Charge per unit length
R	=	Radius of collector cylinder
T_n	=	Period of oscillation
t	=	Time
V	=	Volume
V_A, V_t	=	Anode voltage

V_B	=	Filament bias voltage
V_x.....	=	Potential in x direction
v_x	=	Velocity in x direction
x,X	=	Co-ordinate axes
y,Y	=	
z,Z	=	
ϵ	=	Dielectric constant
ϵ_o	=	Permitivity of free space
ϕ	=	Potential
θ	=	Angular rotation from the Y axis
$\ddot{y}$	=	Acceleration
$\dot{y}$	=	Velocity

References

1.	Anderson, P.A.	Phys.Rev.115, 553, 1959.
2.	Pirani, M. and Yarwood, J.	Principles of Vacuum Engineering. p.56 Chapman and Hall 1963
3.	Holland, L. and Harte, A.	Vacuum. 10, 133, 1960.
4.	Holland, L.	J. Sci.Inst. 36, 105, 1959.
5.	Jepsen, R.L.	Proc. Fourth International Vacuum Congress. Part 1. p 317 I.P.P.S. Conference Series No.5.1968.
6.	Stout, V.L. and Gibbons, M.D.	J. App. Phys. 26, 1488, 1955.
7.	Gabor, D.	British Patent 887, 251, 1962.
8.	Herb, R.G.	Vacuum 9, 97, 1960.
9.	Herb, R.G., Paulty, T. Welton, R.D. and Fisher, K.J.	Rev. Sci.Inst. 35, 573, 1964.
10.	Bills, D.G.	J. Vac.Sci.Tech. 4, 149, 1967.
11.	Denison, D.R.	J. Vac.Sci.Tech. 4, 156, 1967.
12.	Douglas, R.A. Zabritski, J. and Herb, R.G.	Rev.Sci.Inst. 36, 1, 1965.
13.	Maliakal, J.C., Limon, P.J.	J. Vac. Sci. Tech. 1, 54, 1964.
14.	Steinherz, H.A. and Redhead, P.A.	Sci. American. 206, 78, 1962.
15.	Carr, P.H.	Vacuum, 14, 37, 1964.
16.	Fletcher, B. and Watts, J.F.	Vacuum, 17, 445, 1967.

17.	Bayard, R.T. and Alpert D.	Rev. Sci.Inst. 21, 571, 1950.
18.	Leck, J.H.	Pressure Measurement in Vacuum Systems. p.100 2nd Ed. Chapman and Hall 1964.
19.	Cobic, B., Carter, G. and Leck, J.H.	Vacuum 11, 247, 1961.
20.	Freytag, J.P. and Schram, A.	Nuovo Cimento Suppl. Series 1, 1, 405, 1963
21.	Comsa, G.	Vacuum, 17, 373, 1967.
22.	Lawson, R.W.	Brit.J.App.Phys. 18,1763, 1967.
23.	Hartman, T.E.	Rev. Sci.Inst. 34, 281, 1963.
24.	Hartman, T.E.	Rev.Sci.Inst. 34, 1190, 1963.
25.	Redhead, P.A.	J.Vac.Sci.Tech. 3, 173, 1966.
26.	Steckelmacher, W.	J.Sci.Inst. 42, 2, 1965.
27.	Helmer, J.C. and Hayward, W.H.	Rev.Sci.Inst. 37, 1652, 1966.
28.	Redhead, P.A. and Hobson, J.P.	Brit.J. App.Phys. 16, 1555, 1965.
29.	Schuemann, W.C.	Rev. Sci.Inst. 34, 700, 1963.
30.	Redhead, P.A.	Rev.Sci.Inst. 31, 343, 1960.
31.	Penning, F.M.	U.S. Patent 2146025, 1936.
32.	Young, J.R. and Hessian, F.P.	Trans.Nat.A.V.S. symposium No.10. p.234. McMillan. (New York) 1963.
33.	Redhead, P.A.	Canad. J. Phys. 37, 1260, 1959.
34.	Barnes, G., Gaines J., and Kees, J.	Vacuum 12, 141, 1962.
35.	Lafferty, J.M.	Rev.Sci.Inst. 34, 467, 1963.
36.	Hooverman, R.H.	J.App.Phys. 34, 3505, 1963.

37.	Herb, R.G., Pauly, T., and Fisher, K.J.	Bull. Am. Phys.Soc. 8,336, 1963.
38.	Mourad, W.G., Pauly T, and Herb, R.G.	Rev.Sci.Inst. 35, 661, 1964
39.	Gammon, R.B.	Vacuum, 17, 379, 1967.
40.	Fitch, R.K. and Thatcher, W.J.	J.Sci.Inst. 1, 317, 1968.
41.	Meyer, E.A. and Herb, R.G.	J.Vac.Sci.Tech. 4,63, 1967.
42.	Fitch, R.K., Norris, T.J. and Thatcher, W.J.	Vacuum 19, 227, 1969.
43.	McIlraith, A.H.	Nature, 212, 1422, 1966.
44.	McIlraith, A.H.	British Patent 20592/65
45.	White, A.D. and Perry, D.L.	Rev. Sci.Inst. 32, 730, 1961.
46.	McIlraith, A.H.	Notes on a charged particle oscillator (unpublished)
47.	McIlraith, A.H.	Notes on the initiation of a self sustained discharge (unpublished) June, 1969.
48.	Guseva, L.G.	from 'Investigations into electrical discharges in gases', edited by B.N. Klyarfel'd. p.21. Pergammon Press. 1964.
49.	McLure, G.W.	App. Phys. Letters, 12, 233, 1963.
50.	Penning, F.M. and Moubis, J.H.A.	Proc. K. Ned. Akad. Wetensch. 43, 41, 1940.
51.	Wehner, G.K.	'Advances in electronics and electron physics', Vo. VII p.239. Academic Press Inc. 1955.
52.	Barnes, B.T.	J.App.Phys. 37, 2679, 1966.
53.	Laegreid, N. and Wehner, G.K.	J.App.Phys. 32, 365, 1961.

54. Laegreid, N., Wehner, G.K. and Meckel, J. — J. App.Phys. 30, 374, 1959.

55. Hagstrum, H. and D'Amico, C. — J.App.Phys. 31, 715, 1960.

56. Almèn, O. and Bruce, G. — Nuclear Inst. Methods, 11, 257, 1961.

57. Keywell, F. — Phys.Rev. 97, 1611, 1955.

58. Wear, K.B. — J.App.Phys. 38, 1936, 1967.

59. Holland, L. — 'Vacuum Deposition of Thin Films' p.412 Chapman and Hall, 1963.

60. Rushton, G.J. — Thesis for degree of M.Sc. Physics Department, University of Aston. September, 1969.

61. Hewish, A., Bell, S.J. Pilkington, J.D.H., Scott, P.F. and Collins, R.A. — Nature 217, 709, 1968.

62. McIlraith, A.H. — Nature, 461, 5166, 1968.